Addis Ababa University
Addis Ababa Institute of Technology
Department of Electrical and Computer Engineering

DESIGN AND EVALUATION OF HIGH VOLTAGE TRANSMISSION SYSTEM FOR THE GRAND RENAISSANCE HYDRO ELECTRIC POWER PLANT IN ETHIOPIA

A thesis Submitted to Addis Ababa Institute of Technology, School of Graduate Studies, Addis Ababa University

In partial Fulfillment of the Requirement for the Degree of

Master of Science in Electrical Engineering (Electrical Power Engineering)

By MELAKU DESTA

Advisor: Dr.-Ing. GETACHEW BIRU WORKU

December 2012, Addis Ababa

Addis Ababa University
Addis Ababa Institute of Technology
Department of Electrical and Computer Engineering

DESIGN AND EVALUATION OF HIGH VOLTAGE TRANSMISSION SYSTEM FOR THE GRAND RENAISSANCE HYDRO ELECTRIC POWER PLANT IN ETHIOPIA

By MELAKU DESTA

APPROVED BY BOARD OF EXAMINERS

_____	_____
Chairman, Department of Graduate Committee	Signature
_____	_____
Advisor	Signature
_____	_____
Internal Examiner	Signature
_____	_____
External Examiner	Signature

Declaration

I, the undersigned, declare that this thesis is my original work, has not been presented for fulfillment of a degree in this or any other university, and all sources and materials used for the thesis have been acknowledged.

All examiners' comments are duly incorporated.

Name: Melaku Desta

Signature: _____

Place: Addis Ababa

Date of submission: _____

This thesis has been submitted for examination with my approval as a university advisor.

Dr.-Ing Getachew Biru _____

Advisor's Name Signature

Dedication

... to my beloved brother

Zelalem Desta

and

to my beloved sister

Genet Desta

... for their incomparable support in all of my academic achievements!

Acknowledgement

First of all, I would like to thank the Almighty God for his provision of Grace to complete the entire work.

Secondly, I wish to express my deepest gratitude to my advisor, Dr.-Ing Getachew Biru for his patience, guidance, encouragement and support in shaping the outlook of this thesis. He provided invaluable insights that have guided my thinking and understanding.

And also, I would like to thank EEPCo, especially to Planning Department respective officials for their sincere cooperation in providing me the necessary data and information.

Finally to those who encouraged me and showed me great affection throughout this thesis work, my sincere thank is here, Thank you all.

Melaku Desta

Abstract

The Ethiopian Electric Power Corporation (EEPCo) is, currently, undertaking a huge electric power generation expansion plan. The generation capacity under construction is about 7757 MW. This huge expansion demands new transmission line installations. Among the Electric power Generations that are under construction is the Grand Renaissance Hydro Electric Power Plant. This project takes the lion share which accounts about 5250 MW.

To transmit this huge power EEPCo planning department designed two dual circuit 500 kV HVAC transmission lines. The length of these transmission lines from GRHEPP to Menagesha substation (Main Grid) is about 574 km. Estimates showed that the break even distance is around to 500 km. the range of this value vary depending on the range of power transmitted and cost of equipments incurred.

The intention of this thesis work is to develop two 500 kV bipolar HVDC transmission system and compared with the HVAC transmission system in terms technical performance and costs incurred for each transmission systems. In technical performance: transmission line efficiency, voltage regulation, corona losses are considered and in cost analysis: investment cost and power loss cost over the entire life cycle (i.e. 35 years) of the transmission lines are considered.

From the technical performance it can be saved 133 MW power, if two bipolar HVDC transmission line is implemented, the HVDC line is more regulated than HVAC line and the HVAC line is less friendly to the environment than the HVDC line. From the cost analysis the break even distance obtained is around 400 km i.e. below 574 km. So the bipolar HVDC transmission system is less costly than HVAC transmission system for distances above the break even distance.

And the dynamic performance of the HVDC transmission system during transient states is analyzed and observed obtained that during three phase short circuit faults applied on ac side of both transmission lines, the HVDC line reached its steady state condition after 4 cycles (EEPCo standard).

The designed HVDC transmission system has better technical performance and also cheaper in investment cost when compared with the HVAC transmission system.

KEY WORDS: HVDC, HVAC, Break even distance, Transmission line efficiency, corona loss, Loss cost, Current controller, Gamma angle controller.

Table of Contents

List of Tables

List of Figures

List of Appendices

List of Annexes

Nomenclatures

ac	alternate current
A	Ampere
CC	Capacitor Commutation
CIGRÉ	Conseil International des Grands Réseaux Électriques (International Council for Large Electric Systems)
CSC	Current Source Converter
dc	direct current
EEPCo	Ethiopian Electric Power Corporation
ESIA	Environment and Social Impact Assessment
F	Farad
GERD	Grand Ethiopian Renaissance Dam
GRHEPP	Grand Renaissance Hydro Electric Power Project
H	Henry
HD	Harmonic Distortion
HVAC	High Voltage Alternate Current
HVDC	High Voltage Direct Current
ICS	Inter Connected System
k	kilo
km	kilo meter
LC	Line Commutation
LCC	Line Commutated Converters
MW	Mega Watt
MVAR	Mega Volt Ampere Reactive
OH	Over Head
pu	per unit
PV	Present Value
RAP	Resettlement Action Plan
RoW	Right of Way
SCS	Self Contained System
THD	Total Harmonic Distortion

V	Volt
VSC	Voltage Source Converter
A	Cross sectional area of conductor (Sq. cm)
C_c	annual average cost of capacity ($/kWh)
d	Conductor Diameter (mm)
D	Bundle Diameter (m)
d_{eq}	Equivalent bundle diameter (m)
D	Overall diameter of conductor (m)
d	Discount rate
E	Modulus of Elasticity (final) of conductor (kgf/Sq. cm)
E	Conductor Surface Voltage Gradient (kV/cm)
E_c	annual average cost of energy ($/kWh)
f_1	Initial stress in conductor at temperature t_1 kgf/ sq. m (Tension per unit area)
f_2	Final stress in conductor at temperature t_2 (kgf/Sq. cm)
G_{av}	Average Conductor Gradient (kV/cm)
G_{max}	Max. Conductor Gradient (kV/cm)
H	Mean height of conductor (m)
I	annual average current (amps)
I_{dn}	The rated dc current of a smoothing reactor, kA.
K	Stress Constant
L	Span (m)
L	dc side inductance in mH
L_T	Converter transformer inductance
L_d	Smoothing reactor inductance
LC	cost of losses ($/km/year)
L_D	annual load factor
L_o	annual loss factor
N	Economic life time of the transmission line
n	Number of Conductor

P_1	Maximum wind pressure on conductor (kgf/ sq. m)
P_2	Wind load on conductor at minimum temperature, per meter length (kgf/m)
P_3	Wind load on conductor at 32 °C per meter length (kgf/m)
P	Barometric pressure in kilo-Pascal's
PV	Present value of an annually recurring loss cost
P	Pole to Pole spacing (m)
q_1	Still wind loading factor (1)
q_2	2/3 Maximum wind loading factor
q_3	Maximum wind loading factor
R	Outside radius of bundle (cm)
Re	Equivalent Radius of bundle conductor (cm)
R	Conductor resistance (ohms/phase/km)
S	Conductor Spacing (m)
S_1	Sag at initial condition T_1 (m)
S_2	Sag at final condition T_2 (m)
t_1	Initial conductor temperature (°C)
t_2	Final conductor temperature (°C)
T_1	Initial tension in conductor at temperature $t_1 = f_1 \times \alpha$ (kgf)
T_2	Final tension in conductor at temperature $t_2 = f_2 \times \alpha$ (kgf)
T	Temperature in centigrade
U	Ultimate tensile strength of conductor (kgf)
U_d	The rated dc voltage, pole- to- ground, of a smoothing reactor kV.
W	Linear mass of conductor (kgf/m)
δ	Linear mass of conductor per meter per unit sectional area, kgf/Sq.cm/m.

CHAPTER ONE
INTRODUCTION

1.1 Background

Electric power system is the system of equipments and controls dedicated for the generation, transmission and consumption of electrical power. Electrical energy is the most suitable form of energy for transmission and distribution. Due to this important behavior it is being intensively utilized as a means of energy transfer. This in turn resulted in the appearance of huge electric power transmission systems. Electric power transmission systems play the role of transporting electrical energy for a wide range of distances ranging from few kilometers up to hundreds even thousands of kilometers. They connect energy generating parts and energy consuming parts of a power system. These transmission systems operate under carefully designed and controlled conditions in order to achieve the energy transmission tasks.

Ethiopia's widely distributed population has led to the development of an extensive transmission network. The Ethiopian electric grid system consists of five principal levels of transmission voltages: 400, 230, 132, 66 and 45 kV. The existing transmission system comprises a total of about 10,397 km of transmission lines, 687 km of which are at the 400 kV level, 3286 km are at the 230 kV, 4316 km are at the 132 kV level, 1835 km are at the 66 kV and 273 km are at the 45 kV voltage level in the ICS system and the rest 245 km in SCS [1].

As per the Growth and Transformation Plan (GTP) (2010-2015) of Ethiopian Government, the electricity demand growth is estimated to reach 32%. Due to this the Ethiopian Federal government is now undertaking extensive generation and transmission system expansions. Among the generation expansion the Grand Millennium (Heddasie) Hydro Power Generating Plant Project (GMHPGPP) is expected to come to the power system in to 2017. There is also a transmission system expansion, as part of this project.

The new HVAC transmission line designed by the EEPCo Planning Department is a two 500 kV ac double circuit transmission line, consisting of 344 km long two 500 kV double circuit transmission line from Grand Renaissance switchyard to Dedesa substation and 230 km long two 500 kV ac. double circuit transmission line from Dedesa substation to Menagesha substation (EEPCo Main grid) [1].

Alternating current became very familiar for the industrial and domestic uses, but still for the long transmission lines, ac has some limitations which have led to the use of dc transmission in some projects. Current and voltage limits are the two important factors of the high voltage transmission line. The ac resistance of a conductor is higher than its dc resistance because of skin effect, and eventually loss is higher for ac transmission. The switching surges are serious transient over voltages for the high voltage transmission line, in the case of ac transmission the peak values are two or three times normal crest voltage but for dc transmission it is 1.7 times normal voltage [2].

HVDC transmission has less corona and radio interference than that of HVAC transmission line the long HVAC overhead lines produce and consume the reactive power, which is a serious problem. The reactance of the line is proportional to the length of the line, and thus power per circuit of an operating voltage is limited by steady-state stability, which is inversely proportional to length of line. For the reason of stability the load angle is kept at relatively low value under normal operating condition (about 30°) because power flow disturbances affect the load-angle very quickly. In an uncompensated line the phase angle varies with the distance when the lines operating at natural load and puts a limit on the distance. On the other hand dc transmission has no reactance problem, no stability problem, and hence no distance limitation. In ac links the phase angle between sending end and receiving end should not exceed 30^{o} at full-load for transient stability. The phase angle change at the natural load of a line is thus 0.6^{o} per 10 km [4].

But for the long transmission, dc is still more favorable than ac because of its economical, technical, and environmental advantages. Economic considerations call for a certain minimum transmission distance (break-even distance) before HVDC can be considered competitive purely on cost. Estimates for the break even distance of overhead lines are around 500 km [3] with a wide variation about this value depending on the magnitude of power transfer and the range of costs of lines and equipment.

In this thesis a study has been conducted to evaluate the HVDC transmission in terms of technical and financial parameters and an alternative design has been presented for further considerations.

1.2 Problem Statement

The total capacity of the Grand Ethiopian Renaissance Dam which is going to generate from 15 units is 5250 MW. Each unit has 350 MW generation capacities. The transmission line needed to transmit this huge power from the generation to the main grid elongates 574 km. This power can be transmitted using two modes of transmission line options (i.e. ac or dc). EEPCo Planning Department designed two double circuit 500 kV HVAC transmission line. EEPCo didn't consider an HVDC transmission system as a candidate option for the proposed transmission line. These modes of transmission line options have got their own advantage and disadvantage depending on the length and voltage level of the transmission line. The aim of this thesis is to show the comparative advantages and disadvantages of the two transmission line options i.e. HVDC or HVAC by making a thorough analytical analysis of both systems.

1.3 Motivation

EEPCo's Planning Department finished working on the designing of HVAC Transmission line for the Grand Renaissance Hydro Electric Power Plant. After that this project has been given to Chine's Consulting Company to conduct the feasibility study of an HVDC as a candidate option for HVAC as being said by EEPCo Planning Department officials.

According to [28], there is an HVDC (±500 kV and 3000 MW) transmission line in China having distance coverage of 574 km from Sichuan to Shanxi, has been in operation since October 2009, which is equal to the distance from Grand Renaissance Hydro Electric Power Plant to the EEPCo Main Grid (Menagesha) [16].

According to ATCOelectic, the Eastern Alberta HVDC Transmission Project launched on May 2010 includes a new ±500 kV conventional HVDC bipolar transmission line would be built between the Gibbons-Redwater area northeast of Edmonton and the Brooks area southeast of Calgary. Depending on the final route, the line will be approximately 500 km in length and will be finalized on December 2013 [29].

From the above paragraphs and other studies, it is advantageous to look at the possibility of using HVDC as a potential means of transmission for GRHEPP project.

1.4 Objectives of the Thesis

In this thesis work, the general objective is to evaluate the technical performance and cost effectiveness of HVAC and HVDC transmission line systems so as to identify the best option for the transmission system of Grand Renaissance Hydro Electric Power Plant of Ethiopia.

Specific objectives:

The specific objectives of the thesis work include:

- Study and analysis of the designed HVAC system
- Modeling and design of main components of an HVDC transmission system.
- Evaluation of HVDC vs. HVAC transmission systems in terms of investment cost, operational cost and technical performance parameters.
- Modeling of the HVDC transmission system in DigSILENT.
- Analysis of the model in terms of load flow and harmonics.
- Draw conclusions and recommendations which can be implemented in the GRHEPP.

1.5 Thesis Outline

This thesis is organized into six chapters.

Chapter 1 is an introductory part giving background of the study. The basic problem to be investigated is described. The objectives of the thesis work are stated. Finally the Methodologies are described briefly.

Chapter 2 deals with the theoretical back ground of the thesis work. Under this chapter comparison of HVDC and HVAC is discussed in terms of cost and technical performance. Organization and operation of HVDC is discussed and definition of system components is stated. The power factor and reactive power management of HVDC transmission line is explained. Analysis of harmonic filters is discussed. Mathematical modeling of the Line Commutated Converter (LCC) is also discussed.

Chapter 3 deals with modeling of main components of the HVDC system based on Cigré HVDC benchmark model (or, power system modeling) followed by design of the network components which are transmission line conductor, converters, converter transformer, Ac filters and smoothing

reactors. Beside to this, designing of the controllers based on Cigré HVDC Benchmark model (or, control system modeling) is also presented.

Chapter 4 deals with economical and technical comparison of HVDC with HVAC. In the economical aspect the investment and loss cost of each transmission line is covered and the break even distance is calculated to choose which transmission system is better to implement. In the technical aspect, performance parameters like transmission line efficiency, voltage drop, and corona loss are calculated to find out which transmission system has better performance.

Chapter 5 covers the steady state and dynamic (transient) state simulation studies of the HVDC system based on RMS and Harmonic load flow simulations on the DigSILENT software environment.

Chapter 6 deals with the relevant conclusions and recommendations.

1.6 Methodology

Data Collection: The data collection is the basis for this study. Relevant data's has been collected from the power company EEPCo. These data's include generation, transmission and the receiving end bus bar (or National grid) data's. Investment cost of HVAC is also collected from EEPCo's Planning Department.

Modeling of HVDC: Based on Cigre Bench mark model, the power circuit model consists of converter model, converter transformer model, Transmission line model, smoothing reactor model and Harmonic filter models. For the transient analysis of the HVDC line the controllers needed at the Rectifiers and Inverters are modeled based on the Cigre bench mark controller models. Using these models, the bipolar HVDC transmission system is developed using DigSILENT software tool.

Design of main components of HVDC: Design of system components listed in the bench mark model has been held for the HVDC transmission system. After all, the bipolar line fulfills the *N-1 contingency criteria*. The converters and converter transformers are designed based on the data's obtained from EEPCo. The transmission line conductor is designed based on IEEE Standard for Calculating the Current-Temperature of Bare Overhead Conductors. And the smoothing reactor is designed based on IEEE Standard General Requirements and Test Code for Dry-Type and Oil-Immersed Smoothing Reactors for DC Power Transmission. The harmonic filters are designed to fulfill the standards set by ABB group which is the worldwide HVDC equipment supplier.

Comparison of HVDC with HVAC: Comparison of the two transmission line options is carried out based on the investment cost, loss cost and technical performance parameters i.e. Transmission line efficiency, voltage drop and corona loss. The loss cost is made based on the life cycle cost over 35 year's period. The break even distance is calculated using Mathlab/M-file code to identify whether HVDC or HVAC transmission system is economical.

Simulation Studies: Steady state and Dynamic state simulation studies are made on the HVDC system model developed on the DigSILENT software. The dynamic state simulation is done by creating disturbances at different location of the HVDC system and the Harmonic load flow is done to see the performance of the harmonic ac filters connected at the Generation and Menagesha bus bars. The simulation results have been compared with the standards that are stated in each section of the thesis work.

CHAPTER TWO

THEORETICAL BACK GROUND AND LITERATURE REVIEW

Many researchers and scholars have made comparison of HVDC and HVAC transmission systems based on cost and technical performance criteria's. Some of the studies done in the area of HVDC and HVAC comparisons are described below and theoretical back ground of an HVDC system is also discussed.

2.1 Overview of an HVDC System

HVDC transmission refers when ac power generated at a power plant is transformed into dc power before its transmission. At the inverter (receiving side), it is then transformed back into its original ac power. Such power transmission method makes it possible to transmit electric power in an economic way through up-conversion of voltage, which is an advantage in existing ac transmission technology and to overcome many disadvantages associated with ac power transmission as well.

2.1.1 Classification of HVDC Links

HVDC links may be broadly classified into the following categories:

- Monopolar links
- Bipolar links
- Homopolar links

The basic configuration of a **monopolar** link is shown in Figure 2.1 [3]. It uses one conductor, usually of negative polarity. The return path is provided by ground or water. Cost considerations often lead to the use of such systems, particularly for cable transmission. This type of configuration may also be the first stage in the development of a bipolar system.

Instead of ground return, a metallic return may be used in situations where the earth resistivity is too high or possible interference with underground/underwater metallic structure is objectionable. The conductor forming the metallic return is at low voltage.

The bipolar link configuration is shown in Figure 2.2 [3]. It has two conductors, one positive and the other negative. Each terminal has two converters of equal rated voltage, connected in series

on the dc side. The junction between the converters is grounded. Normally, the currents in the two poles are equal, and there is no ground current. The two poles can operate independently. If one pole is isolated due to fault on its conductor, the other pole can operate with ground and thus carry half the rated load or more by using the overload capabilities of its converters and the line.

The homopolar link, whose configuration is shown in Figure 2.3 [3], has two or more conductors, all having the same polarity. Usually a negative polarity is preferred because it causes less radio interference due to corona (in negative polarity many of the electrons are concentrated in the outer, lower-field areas i.e. a region of lower potential-gradient). The return path for such a system is ground. Homopolar configuration offers an advantage in this regard in situations where continuous ground current is acceptable.

The ground current can have side effects on gas or oil pipe lines that lie within a few miles of the system electrodes. Pipelines act as conductors for the ground current which can cause corrosion of the metal. Therefore, configurations using ground return may not always be acceptable.

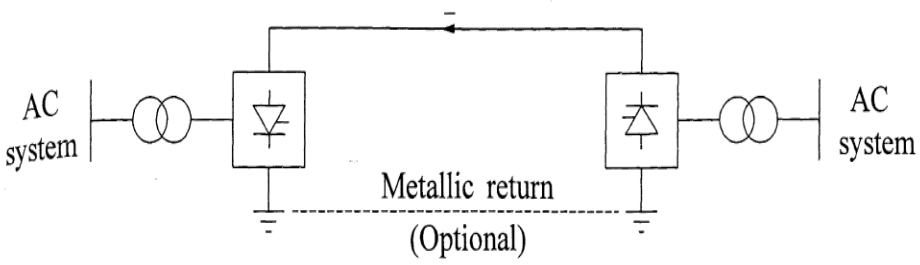

Figure 2.1 Monopolar HVDC link

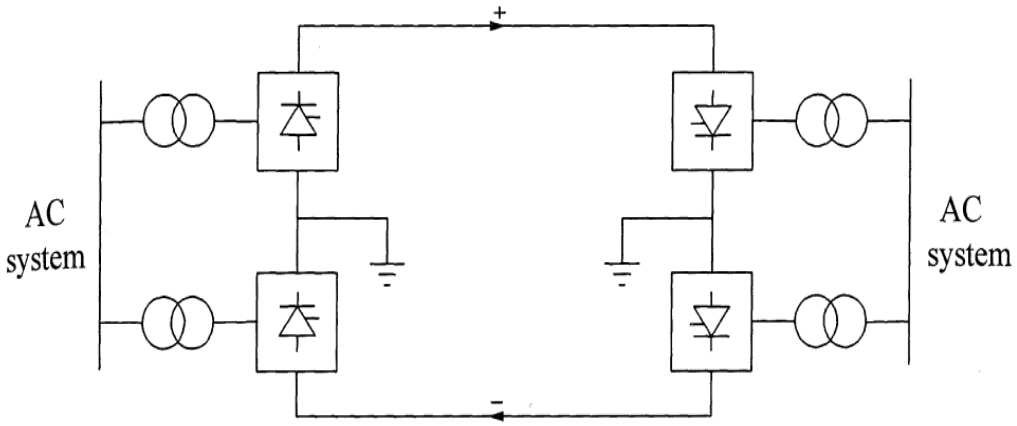

Figure 2.2 Bipolar HVDC link

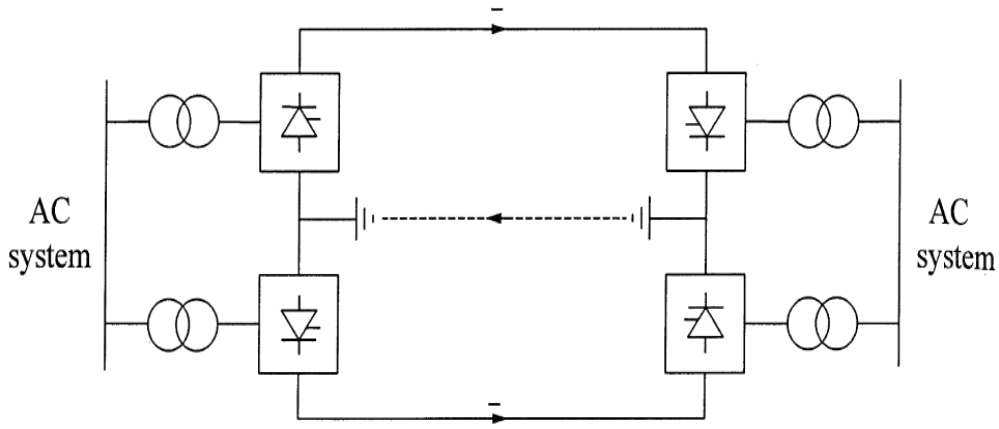

Figure 2.3 Homopolar HVDC link

Each of the above HVDC system configurations usually has cascaded groups of several converters, each having a transformer bank and a group of valves. The converters are connected in parallel on the ac side (transformer) and in series on the dc side (valve) to give the desired level of voltage from pole to ground.

Back-to-back HVDC systems (used for asynchronous ties) may be designed for monopolar or bipolar operation with a different number of valve groups per pole, depending on the purpose of interconnection and the desired reliability.

Most point-to-point (two-terminal) HVDC links involving lines are bipolar, with monopole operation used only during contingencies. They are normally designed to provide maximum independence between poles to avoid bipolar shutdowns

2.1.2 Core HVDC Technologies

An HVDC system requires an electronic converter for its ability of converting electrical energy from ac-dc or vice versa. There are basically two configuration types of three-phase converters possible for this conversion process (Figure 2.4 [16]) that are used in modern HVDC transmission systems.

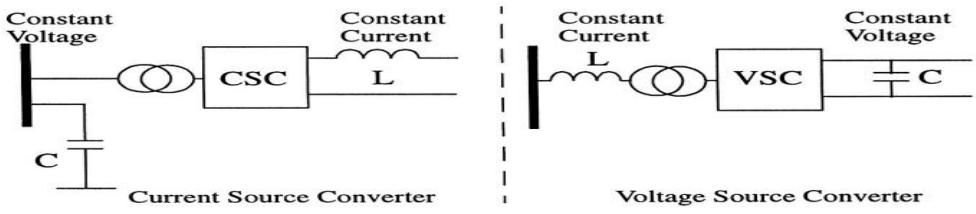

Figure 2.4 Core HVDC technologies

Line-Commutated Current Source Converter

Conventional HVDC transmission employs line-commutated CSCs with thyristor valves. Such converters require a synchronous voltage source in order to operate. The basic building block used for HVDC conversion is the three phases, full-wave bridge referred to as a six-pulse or Graetz bridge. The term six-pulse is due to six commutations or switching operations per period resulting in a characteristic harmonic ripple of six times the fundamental frequency in the dc output voltage. Each six-pulse bridge is comprised of six controlled switching elements or thyristor valves. Each valve is comprised of a suitable number of series-connected thyristors to achieve the desired dc voltage rating.

The dc terminals of two six-pulse bridges with ac voltage sources phase displaced by 30^o can be connected in series to increase the dc voltage and eliminate some of the characteristic ac current and dc voltage harmonics. Operation in this manner is referred to as 12-pulse operation. In 12-pulse operation, the characteristic ac current and dc voltage harmonics have frequencies of 12n± 1 and 12n, respectively. The 30^o phase displacement is achieved by feeding one bridge through a transformer with a wye-connected secondary and the other bridge through a transformer with a delta-connected secondary.

Most modern Line Commutated CSC HVDC transmission schemes utilize 12-pulse converters to reduce the harmonic filtering requirements required for six-pulse operation; e.g., fifth and seventh on the ac side and sixth on the dc side. This is because, although these harmonic currents still flow through the valves and the transformer windings, they are 180^o out of phase and cancel out on the primary side of the converter transformer.

Line-commutated converters require a relatively strong synchronous voltage source in order to commutate. Commutation is the transfer of current from one phase to another in a synchronized firing sequence of the thyristor valves. Line commutated CSCs can only operate with the ac current lagging the voltage, so the conversion process demands reactive power. Reactive power is supplied from the ac filters and shunt capacitors.

To date, the vast majority of HVDC links employ 12-pulse, two-bridge, line commutated (sometimes also referred to as naturally commutated) converters. At the sending end, the ac is converted by a converter to dc, which is reconverted at the receiving end by a second converter

(inverter) to ac. The intermediate dc overhead line of a line commutated power converter system usually contains a smoothing reactor.

Line-commutated current-source converters (CSCs) using thyristor. This technology is well established for high power, typically around 1000MW, with the largest project being the Itaipu system in Brazil at 6300MW power level [4].

Self-Commutated Voltage Source Converter

HVDC transmission using VSCs with pulse-width modulation (PWM), commercially known as HVDC Light, was introduced in the late 1990s. Since then the progression to higher voltage and power ratings for these converters has roughly paralleled that for thyristor valve converters in the 1970s.These VSC-based systems are self-commutated with insulated-gate bipolar transistor (IGBT) valves and solid-dielectric extruded HVDC cables.

HVDC transmission with VSCs can be beneficial to overall system performance. VSC technology can rapidly control both active and reactive power independently of one another. Reactive power can also be controlled at each terminal independent of the dc transmission voltage level. This control capability gives total flexibility to place converters anywhere in the ac network since there is no restrictions on minimum network short-circuit capacity. However, due to the voltage limitations in the presently used PWM technology an IGBT high-power switches, the VSC rating can be extended to about ±150 kV, 300 MW in a bipolar link, although larger ratings are under development [16].

It is well established technology for medium power levels thus far, with the largest size project being named Estlink at 350 MW levels [4].

2.1.3 D.C Converter Operation

The six pulse converter bridge of Figure 2.5 as the basic converter unit of HVDC transmission is used equally well for rectification where electric power flows from the ac side to the dc side ~~and~~ inversion where the power flow is from the dc side to the ac side. Thyristor valves operate as switches which turn on and conduct current when fired on receiving a gate pulse and are forward biased. A thyristor valve will conduct current in one direction and once it conducts, will only turn off when it is reverse biased and the current falls to zero. This process is known as line commutation.

An important property of the thyristor valve is that once it's conducting current falls to zero when it is reverse biased and the gate pulse is removed, too rapid an increase in the magnitude of the forward biased voltage will cause the thyristor to inadvertently turn on and conduct.

Commutation

Rectification or inversion for HVDC converters is accomplished through a process known as line or natural commutation. The valves act as switches so that the ac voltage is sequentially switched to always provide a dc voltage. With line commutation, the ac voltage at both the rectifier and inverter must be provided by the ac networks at each end and should be three phase and relatively free of harmonics as depicted in Figure 2.5 [16]. As each valve switches on, it will begin to conduct current while the current begins to fall to zero in the next valve to turn off. Commutation is the process of transfer of current between any two converter valves with both valves (same row) carrying current simultaneously during this process. Once current is transferred to the incoming valve, the reverse voltage across the outgoing valve is maintained for a time period t_{off} (equivalent to gamma angle); the outgoing valve must be reverse biased for a period greater than the turn-off time of the device The time difference between t_{off} and t_q is required to provide a margin of security for the device to achieve its voltage blocking capability. Typical valves of t_q and t_{off} are $350\ \mu S$ and $700\ \mu S$ respectively [16].

Consider the rectification process. Each valve will switch on when it receives a firing pulse to its gate and its forward bias voltage becomes more positive than the forward bias voltage of the conducting valve. The current flow through a conducting valve does not change instantaneously as it commutates to another valve because the transfer is through transformer windings. The leakage reactance of the transformer windings is also the commutation reactance so long as the ac filters are located on the primary or ac side of the converter transformer. The commutation reactance at the rectifier and inverter is shown as an equivalent reactance X_c in Figure 2.5. The sum of all the valve currents transferred the dc side and through the dc reactor is the direct current and it is relatively flat because of the inductance of the dc reactor and converter transformer.

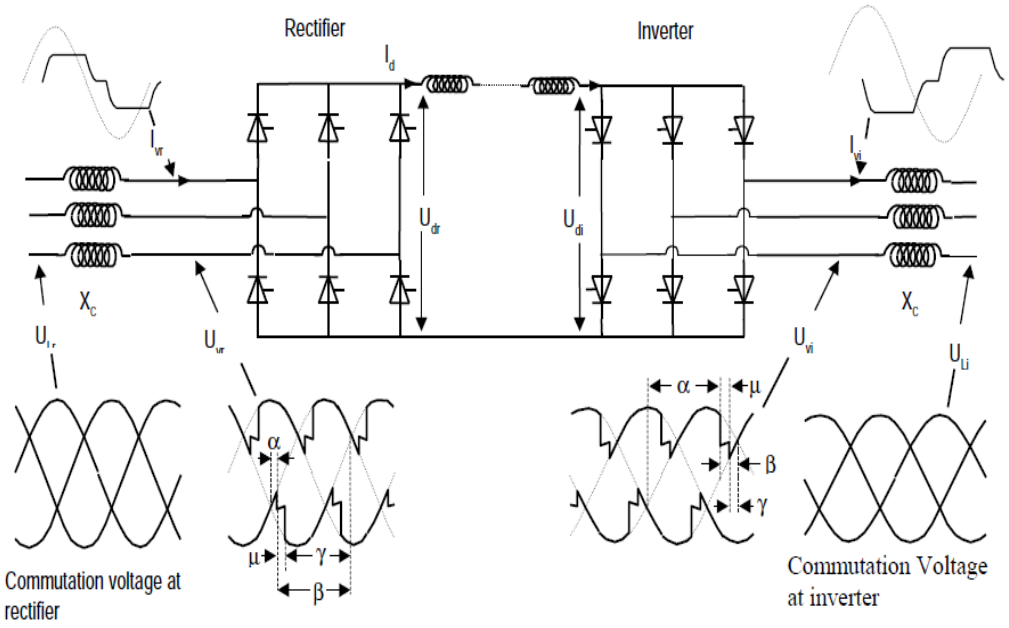

Figure 2.5 Voltage and current wave shapes associated with dc converter bridges.

At the inverter, the three phase ac voltage supplied by the ac system provides the forward and reverse bias conditions of each valve in the converter bridge to allow commutation of current between valves the same as in the rectifier. The inverter valve can only turn on and conduct when the positive direct voltage from the dc line is greater than the back negative voltage derived from the ac commutation voltage of the ac system at the inverter.

Due to the line commutation valve switching process, a non-sinusoidal current is taken from the ac system at the rectifier (I_{vr} in Figure 2.5.) and is delivered to the ac system at the inverter (I_{vi} in Figure 2.5). Both I_{vr} and I_{vi} are lagging to the alternating voltage. This non-sinusoidal current waveform consists of the fundamental frequency ac component plus higher harmonics being taken from, and injected into, each ac system. The ac filters divert the harmonics from entering the ac system by offering a low impedance bypass path allowing the commutation voltage to be relatively harmonic free (U_{Lr} and U_{Li} in Figure 2.5).

Reversal of power flow in a line commutated dc link is not possible by reversing the direction of the direct current. The valves will allow conduction in one direction only. Power flow can only be reversed in line commutated dc converter bridges by changing the polarity of the direct

voltage. The dual operation of the converter bridges as either a rectifier or inverter is achieved through firing control of the grid pulses.

Regions of Converter Operation

From converter theory, the relationship between dc voltage V_d and the firing angle alpha is

$$V_d = V_{do}\cos\alpha - \left(\frac{3X_C}{\pi}\right)I_d \qquad (2.1)$$

where,

V_d = dc voltage

V_{do} = no load direct voltage

X_c = commutating reactance

I_d = dc current

α = alpha firing angle

Converter operating regions are shown in Figure 2.6 as a polar plot of V_d versus alpha [16]. These 4 regions are divided into four quadrants Q_1 to Q_4. Theoretical and practical limits to these regions are defined in Table 2.1 Provided an adequate ac supply is available, line commutated (LC) converter operation is possible in quadrants Q_1 and Q_2. In Q_1, the converter operates as a rectifier consuming reactive power from the supply. The practical alpha-min limit (5 degrees) is required for the valves to have a forward-bias voltage before turning on. In Q_2, the converter operates as an inverter again consuming reactive power from the supply. Generally, two limits apply in this region i.e. the alpha-min (105 degrees) and alpha-max (145 degrees) limits in inverter mode of operation; the alpha-min limit is imposed for operational reasons following recovery from dc line faults, etc., and the alpha-max limit is imposed to ensure commutation margin angle security. The practical operational region for a LC inverter is shown as region *X*. To operate beyond region *X* into quadrant Q_3 requires assistance from forced or circuit commutation. Theoretically, forced commutation permits operation in any quadrant

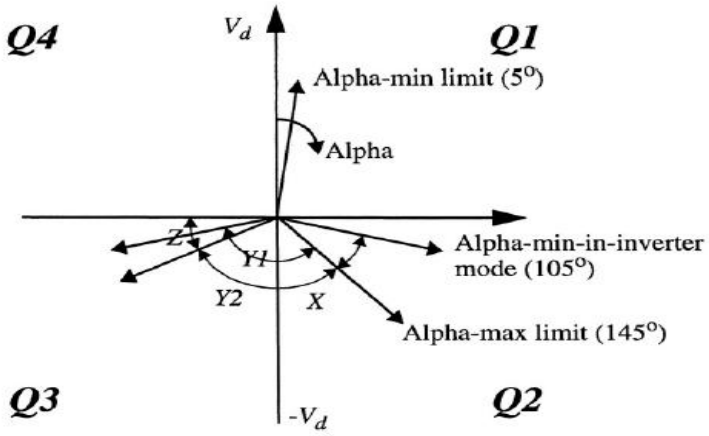

Figure 2.6 Region of Converter operations

Table 2.1 Four quadrant operation

Quadrant	Converter operate as	Alpha limits (degree)	
		Theoretical	Practical
Q1	LC rectifier	1-90	5-90
Q2	LC Inverter	90-180	105-145
Q3	CC inverter	180-270	180-240
Q4	CC rectifier	270-360	-

The ignition angle α may range from 0^o to 180^o. Outside of this range, the commutation voltage at the firing instant is negative and the commutation fails

Converter bridge angles

Figure 2.5 shows the various electrical angles which define the operation of converter bridges. These angles are measured on the three phase valve side voltages and are based upon steady state conditions with a harmonic free and idealized three phase commutation voltage. They apply to both inverters and rectifiers.

Delay angle α**.** The time expressed in electrical angular measure from the zero crossing of the idealized sinusoidal commutating voltage to the starting instant of forward current conduction. This angle is controlled by the gate firing pulse and if less than 90 degrees, the converter bridge

is a rectifier and if greater than 90 degrees, it is an inverter. This angle is often referred to as the firing angle.

Advance angle β**.** The time expressed in electrical angular measure from the starting instant of forward current conduction to the next zero crossing of the idealized sinusoidal commutating voltage. The angle of advance β is related in degrees to the angle of delay α by:

$$\beta = 180 - \alpha$$

Overlap angle μ.The duration of commutation between two converter valve arms expressed in electrical angular measure.

Extinction angle γ the time expressed in electrical angular measure from the end of current conduction to the next zero crossing of the idealized sinusoidal commutating voltage. γ depends on the angle of advance β and the angle of overlap μ and is determined by the relation:

$$\gamma = \beta - \mu$$

2.2 Line commutated converter model

In this section the conventional line-commutated converter is analyzed. Its topology is the three-phase, full-wave bridge circuit shown in Fig. 2.7 [14]. The following idealizations form the basic assumptions of the analysis used from [14]:

- The ac voltage is stiff and may be represented by an ideal sinusoidal source in series with a lossless inductance.
- The direct current is ripple-free and (in steady-state operation) constant.
- The valves are ideal switches with zero on-resistance and infinite off-resistance. They change instantaneously between these two states.
- The valves are fired at equal intervals of one-sixth cycle (60^o).

The instantaneous line-to-neutral voltages of the ac sources are taken as

$$\begin{aligned} e_a &= E_m \cos\left(\omega t + 60^o\right) \\ e_b &= E_m \cos\left(\omega t - 60^o\right) \\ e_c &= E_m \cos\left(\omega t - 180^o\right) \end{aligned} \tag{2.2}$$

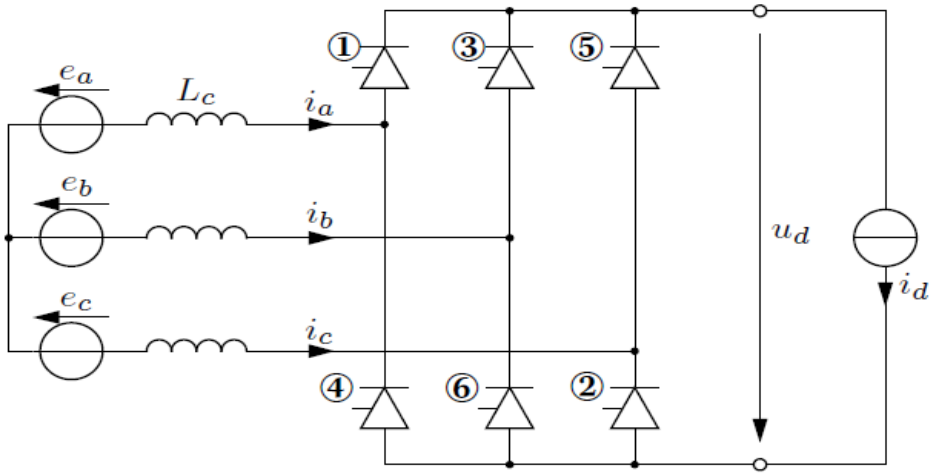

Figure 2.7: Equivalent circuit for the line commutated converter. The valves are numbered in the order of their firings.

The corresponding line-to-line voltages are then

$$\begin{aligned} e_{ac} &= e_a - e_c = \sqrt{3}E_m \cos\left(\omega t + 30^o\right) \\ e_{ba} &= e_b - e_a = \sqrt{3}E_m \cos\left(\omega t - 90^o\right) \\ e_{cb} &= e_c - e_b = \sqrt{3}E_m \cos\left(\omega t + 150^o\right) \end{aligned} \tag{2.3}$$

2.2.1 Analysis without commutation overlap

Figure 2.8 [14] shows the typical wave-forms of the converter if the ac inductance *Lc* is neglected. In the top graph the ac line-to-neutral voltages are drawn in thin lines and, in heavy lines, the potentials of the positive and negative dc terminals with respect to ac neutral. The middle graph shows the ac line-to-line voltages and, in a heavy line, the instantaneous direct voltage u_d. The bottom graph shows the constant dc current and, in a heavy line, the ac line current i_d.

At any given instant, one valve of the upper commutation group and one of the lower rows are conducting. Therefore, the instantaneous direct

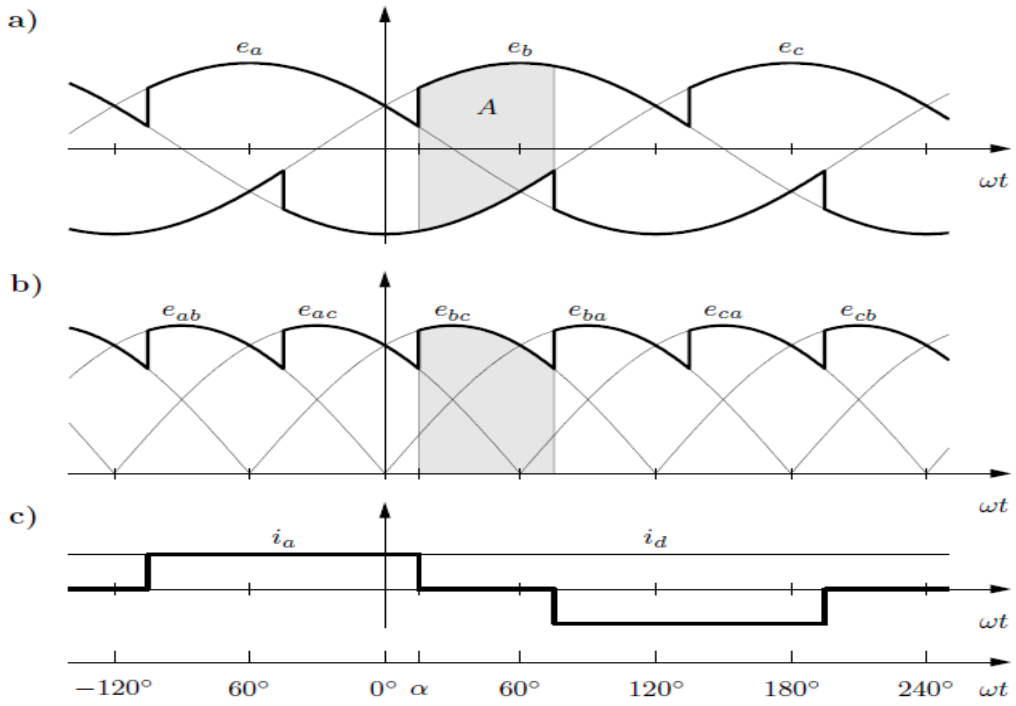

Figure 2.8: Voltage and current waveforms without overlap: (a) positive and negative dc terminal potentials, (b) instantaneous direct voltage, (c) phase a line current.

Voltage at any time equals one of the six line-to-line voltages. The instant at which the direct voltage changes to another line-to-line voltage is controlled via the firing angle α. It is assumed that the valves are fired at equal intervals. Hence, u_d consists of six identical segments of 60^o width each, and so the average direct voltage can be found by averaging the direct voltage over any 60^o interval. Considering the interval indicated by the shaded area A in Figure 2.8.

The average direct voltage is given by

$$U_d = \frac{3}{\pi} A = \frac{3}{\pi} \int_{\alpha}^{\alpha+60^o} (e_b - e_c)\, d(\omega t)$$

$$= \frac{3}{\pi} \int_{\alpha}^{\alpha+60^o} \sqrt{3} E_m \cos(\omega t - 30^o)\, d(\omega t)$$

$$= \frac{3\sqrt{3}}{\pi} E_m \int_{\alpha}^{\alpha+60^o} \cos(\omega t - 30^o)\, d(\omega t)$$

$$= U_{dio} \sin(\omega t - 30^o) \uparrow_{\alpha}^{\alpha+60}$$

$$= U_{dio} 2 \sin 30^o \cos \alpha$$

$$U_d = U_{dio} \cos \alpha \tag{2.4}$$

where,

$$U_{dio} = \frac{3\sqrt{3}}{\pi} E_m \tag{2.5}$$

E_m = the peak value of the line to neutral voltage

In terms of the RMS line to neutral E_{LN} and line to line E_{LL} voltages, the expression for V_{dio} becomes

$$U_{dio} = \frac{3\sqrt{6}}{\pi} E_{LN} = 2.34 E_{LN}$$

$$U_{dio} = \frac{3\sqrt{2}}{\pi} E_{LL} = 1.35 E_{LL}$$

Where,

U_{dio} is the so- called ideal no- load direct voltage

AC current magnitude and phase

Since the direct current i_d is constant by assumption and each valve conducts for a period of 120°, the ac currents are rectangular blocks with magnitude I_d and width 120° as shown in Fig. 2.8. The phase displacement changes with the firing angle α. The peak value of the fundamental frequency component of the alternating line current can be determined by Fourier analysis:

$$I_{peak} = \frac{2}{\pi} \int_{\frac{-2\pi}{3}}^{0} i_d \cos x$$

$$I_{peak} = \frac{2}{\pi} i_d [\sin 0^o - \sin(-120)^o] \tag{2.6}$$

$$I_{peak} = \frac{2\sqrt{3}}{\pi} i_d$$

By assumption, the converter is lossless and therefore the ac active power must equal the dc power emanating from the bridge i.e.

$$\frac{3}{2}E_m I_{peak}\cos\phi = U_d i_d$$

$$= U_{dio} i_d \cos\alpha \quad (2.7)$$

where,

ϕ denotes the angle by which the fundamental frequency component of the line current lags the line-to-neutral voltage.

Inserting Equations (2.5) and (2.6) gives:

$$\left(\frac{3}{2}E_m \frac{2\sqrt{3}}{\pi} i_d\right)\cos\phi = \left(\frac{3\sqrt{3}}{\pi} E_m i_d\right)\cos\alpha$$

$$\cos\phi = \cos\alpha \quad (2.8)$$

That is, the firing angle α shifts the fundamental frequency component of the ac current by an angle $\phi = \alpha$ with respect to the ac line-to-neutral voltage.

2.2.2 Analysis including commutation overlap

Because of the inductance *Lc* present at the ac-terminals the phase currents cannot change instantaneously. Therefore, the dc current requires a finite time to transfer from one phase to another. This phenomenon is called commutation overlap. Its effect on the voltage and current waveforms of the converter circuit is shown in Fig. 2.10 [14]. The angle corresponding to the time needed for commutation is denoted by μ. The angle $\delta = \alpha + \mu$ is called the extinction angle.

In normal operation, the overlap angle is less than 60^o; typical full-load values are in the range of $15^o\ to\ 25^o$ [36]. With $0^o < \mu < 60^o$, during commutation three valves conduct. A new commutation begins every 60^o and lasts for an angular period of μ. Therefore the angular period when two valves conduct with no ignition delay (i.e.$\alpha = 0^o$) is the $(60^o - \mu)$ as shown in Figure 2.9 [36]. During the commutation period, the current in the incoming valve increases from 0 to i_d, the current in the outgoing valve reduces from i_d to 0.

If $60^o < \mu < 120^o$, an abnormal mode of operation occurs in which alternately three and four valves conduct [36]. Here we will consider only the normal operation when $\mu < 60^o$.

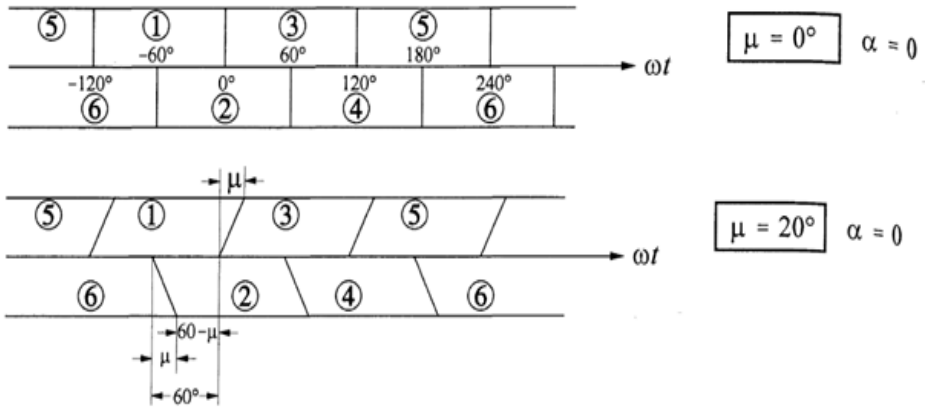

Figure 2.9 Effect of overlap angle on the periods of conduction valves.

Fig. 2.11 shows the equivalent converter circuit during commutation from valve 1 to valve 3. At the beginning of commutation (i.e. when valve 3 is fired), the phase current i_a equals the direct current while i_b is still zero. The voltage $e_b - e_a$ then drives a current through the loop containing valves 1 and 3. The commutation ends when i_a has decreased to zero and i_b has taken over the whole dc current:

$$\text{At } \omega t = \alpha : i_a = i_d \text{ and } i_b = 0$$

$$\text{At } \omega t = \delta(\alpha + \mu) : i_a = 0 \text{ and } i_b = i_d \qquad (2.8)$$

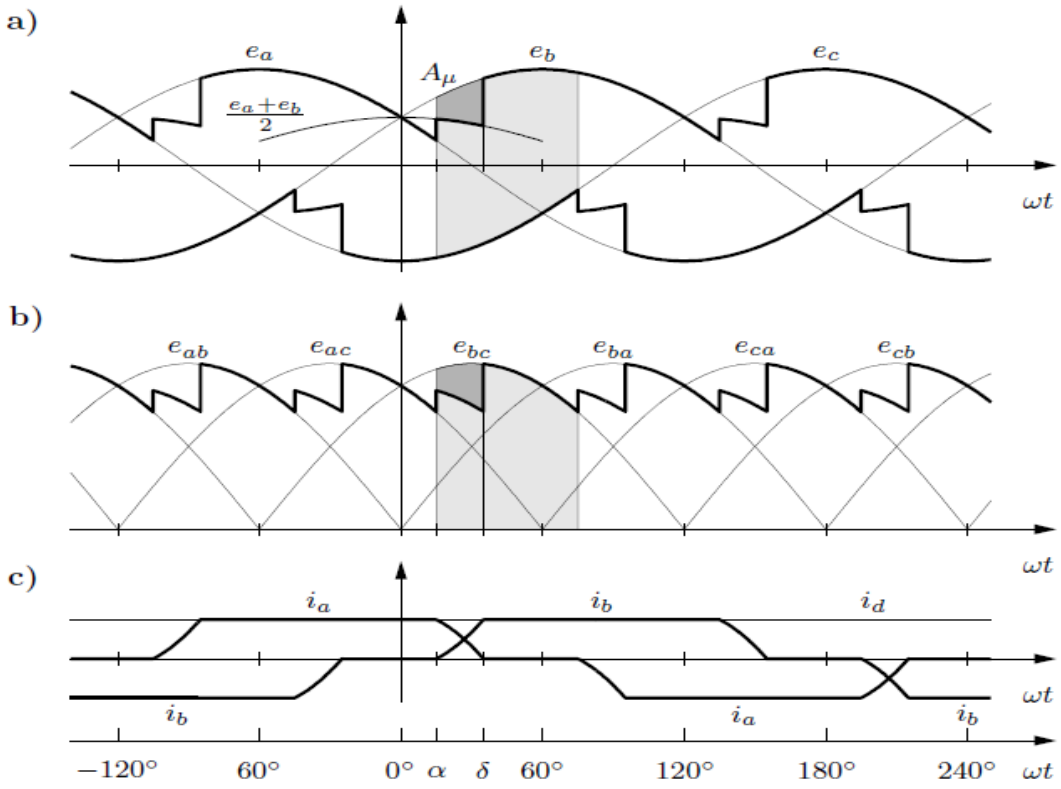

Figure 2.10: Voltage and current waveforms showing the effect of overlap: (a) Positive and negative dc terminal potentials, (b) instantaneous direct voltage, (c) phase a and b line currents.

The mesh equation for the above described loop is:

$$e_b - e_a = L_c \frac{di_b}{dt} - L_c \frac{di_a}{dt} \tag{2.9}$$

The sum of i_a and i_b during commutation equals the direct current; therefore,

$$\frac{di_a}{dt} + \frac{di_b}{dt} = \frac{di_d}{dt} = 0$$

$$\frac{di_a}{dt} = -\frac{di_b}{dt} \tag{2.10}$$

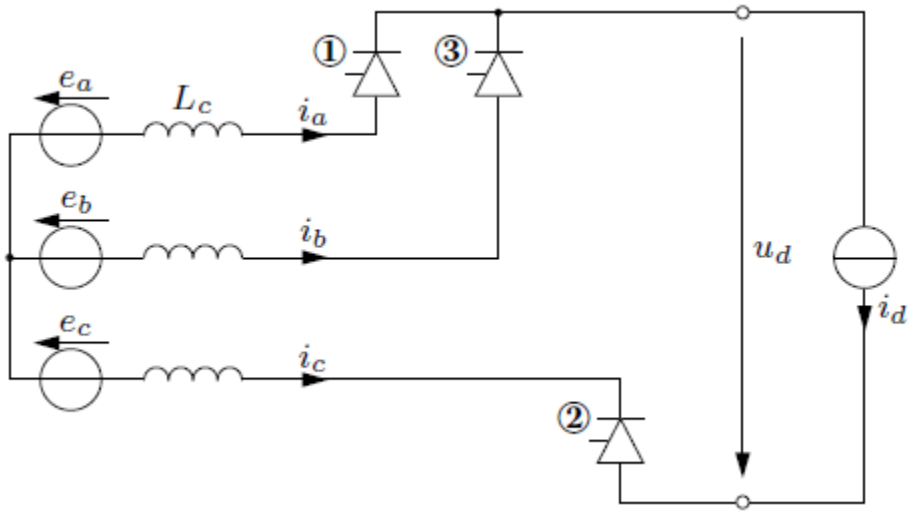

Figure 2.11: Equivalent LCC circuit during commutation from valve 1 to valve 3 (non-conducting valves not shown)

Inserting Equations (2.3) and (2.10) into (2.9) yields

$$\sqrt{3}E_m \sin \omega t = 2L_c \frac{di_b}{dt}$$

$$\frac{di_b}{dt} = \frac{\sqrt{3}E_m}{2L_c} \sin \omega t \tag{2.11}$$

Integration over the duration of the commutation gives

$$\int_{\frac{\alpha}{\omega}}^{\frac{\delta}{\omega}} \frac{di_b}{dt} dt = \frac{\sqrt{3}E_m}{2\omega L_c} (\cos \alpha - \cos \delta)$$

Finally inserting the boundary conditions (2.8) into the left-hand side:

$$i_d = \frac{\sqrt{3}E_m}{2\omega L_c} (\cos \alpha - \cos \delta) \tag{2.12}$$

Average direct voltage

During commutation the two impedances in the commutation loop act as a voltage divider that sets the potential of the positive converter terminal to the average of the two line voltages. It is

only after the commutation that the terminal potential recovers to the voltage of the on-going phase.

The consequence is that the voltage/angle-area A derived in Eq. (2.4) is decreased by an area Aμ as shown in Fig. 2.10. This results in a voltage drop ΔU_d of the average direct voltage.

$$A_\mu = \int_\alpha^\delta \left(e_b - \frac{e_a + e_b}{2} \right) d(\omega t) = \int_\alpha^\delta \frac{e_b - e_a}{2} d(\omega t)$$

$$= \frac{\sqrt{3}E_m}{2} \int_\alpha^\delta \sin(\omega t) d(\omega t)$$

$$= \frac{\sqrt{3}E_m}{2} (\cos\alpha - \cos\delta)$$

$$\Delta U_d = \frac{3}{\pi} A_\mu$$

$$= \frac{3\sqrt{3}E_m}{2\pi} (\cos\alpha - \cos\delta)$$

$$= \frac{U_{dio}}{2} (\cos\alpha - \cos\delta) \quad (2.14)$$

Comparison of Eqns. (2.12) and (2.14) shows that the voltage drop is directly proportional to the dc current:

$$\Delta U_d = \frac{3}{\pi} \omega L_c i_d \quad (2.15)$$

$$U_d = U_{dio} \cos\alpha - \Delta U_d$$

$$= U_{dio} \cos\alpha - R_c i_d \quad (2.16)$$

With

$$R_c = \frac{3}{\pi} \omega L_c \quad (2.17)$$

Rc is called the equivalent commutation resistance. It accounts for the voltage drop due to commutation. However, it is not a real ohmic resistance and thus consumes no active power. *Lc*

is the commutation reactance in Henry with Eq. (2.14) the average direct voltage could also be written as

$$U_d = U_{dio}\cos\alpha - \frac{U_{dio}}{2}\left(\cos\alpha - \cos\delta\right)$$

$$= U_{dio}\left(\frac{\cos\alpha + \cos\delta}{2}\right) \tag{2.18}$$

AC current magnitude and phase

Due to the overlap the ac currents are no longer rectangular blocks. Instead, their shape is that of a deformed trapezoidal as can be seen in Fig. 2.10. Still, Eq. (2.6) is a good approximation for the fundamental frequency component of the ac current

$$I_{peak} = \frac{2\sqrt{3}}{\pi} i_d \tag{2.19}$$

Comparing again ac active power and dc power and using Eq. (2.18) gives

$$\frac{3}{2} E_m I_{peak}\cos\phi = U_d i_d$$

$$= U_{dio} i_d \left(\frac{\cos\alpha + \cos\delta}{2}\right) \tag{2.20}$$

and after substituting from Equationss (2.4) and (2.19):

$$\left(\frac{3}{2} E_m \frac{2\sqrt{3}}{\pi} i_d\right)\cos\phi \approx \left(\frac{3\sqrt{3}}{\pi} E_m i_d\right)\frac{\cos\alpha + \cos\delta}{2}$$

$$\cos\phi \approx \frac{\cos\alpha + \cos\delta}{2} \tag{2.21}$$

With Eq. (2.18) another expression for the power factor $\cos\phi$ is

$$\cos\phi \approx \frac{U_d}{U_{dio}} \tag{2.22}$$

$$\cos\phi \approx \cos\alpha - \frac{R_c i_d}{U_{dio}} \tag{2.23}$$

and with substituting from Eq. (2.16), $U_{dio}\cos\alpha - R_c i_d$

Eq. (2.23) shows that with increasing load the power factor decreases and accordingly the phase shift between the fundamental ac current and the ac voltage increases.

The inverter operation may also be described in terms of α and δ defined in the same way as for the rectifier, but having values between 90^o *and* 180^o. However the common practice is to use ignition advance angle β and extinction advance angle γ for describing the inverter performance

$\beta = \pi - \alpha$ = ignition advance angle

$\gamma = \pi - \delta$ = extinction advance angle (or, gamma angle)

$\mu = \delta - \alpha = \beta - \gamma$ = overlap angle

δ = extinction delay angle

α = ignition delay angle

So,

$$i_d = \frac{\sqrt{3}E_m}{2\omega L_c}\left(\cos\gamma - \cos\beta\right)$$

$$U_d = \frac{dio}{2}\left(\cos\gamma + \cos\beta\right)$$

Significance of delay angle α for rectifier

The delay angle is used for control of a rectifier and hence direct voltage of rectifier U_d is controlled by means of the delay angle α as seen from the equation.

$$U_d = U_{dio}\cos\alpha$$

By varying α from zero to 90^o the direct voltage changes from maximum (at α = 0) to (at α = 90^o the following stage are rated.

α = 0, Rectifier mode maximum dc voltage.

$\alpha = 15^o$, Rectifier mode reduced dc voltage.

$\alpha = 90^0$, Rectifier mode no power transfer zero dc voltage.

$\alpha > 90^o$, Inverter mode

$\alpha = 180^o$, Full inverter mode.

In practice, the normal rectifier mode, the delay angle α is held between 15^o *to* 25^o and the choise of α has two opposite constraints [39].

1. The reactive power demand of converter valves reduced with reduction in delay angle α .Hence smaller values of α is preferred with respect to reactive power requirements (ac shunt compensation)
2. Valves needs a small voltage across them to start the commutation

Significance of Extinction angle γ for Inverter

As mentioned earlier, the converter operates in rectifier mode for $\alpha < 90^o$ and as inverter for$\alpha > 90^o$. And it is more convenient to express the angle in terms of extinction angle γ because for inverter operation, γ has nearly the same range as $(15^o \; to \; 25^o)$ as that of α for rectifier operation [39]. The direct voltage of the inverter is controlled means of the extinction angle γ.

2.3 Power Factor and Reactive Power Management

Due to the firing delay and commutation angles, the converter current in each phase always lags its voltage. The rectifier therefore absorbs lagging current (i.e. consumes reactive power) [15]. With perfect filtering, no distorting current flows into the ac system and the power factor can be approximated by the displacement factor $\cos(\phi)$, where ϕ is the phase difference between the fundamental frequency voltage and current components.

Thus under ideal conditions, with losses neglected, the active fundamental ac power (P) is the same as the dc power, i.e.

$$P = \sqrt{3}E_{LL}I_{L1}\cos(\phi) = U_d i_d \tag{2.24}$$

And

$$\cos(\phi) = \frac{U_d i_d}{\sqrt{3}E_{LL}i_{L1}} \tag{2.25}$$

Since harmonic filters are normally provided at the converter terminals, the current flowing in the ac system contains (ideally) only fundamental component frequency and its rms magnitude (obtained from Fourier analysis) is obtained from Equation 2.19.

$$I_{peak} = \frac{2\sqrt{3}}{\pi} i_d \tag{2.26}$$

$$I_{L1} = \frac{I_{peak}}{\sqrt{2}} = \frac{2\sqrt{3}}{\sqrt{2}\pi} i_d = \frac{\sqrt{6}}{\pi} i_d \tag{2.27}$$

Substituting Equation (2.27) in (2.24) yields the following expression for the dc voltage in terms of the ac side variables:

$$U_d = \frac{3\sqrt{2}}{\pi} E_{LL} \cos(\phi)$$

Also, substituting U_d and i_d from Equations (2.18) and (2.27) in (2.25), the following approximate expression results for the power factor caused by the rectification process:

$$\cos(\phi) = \tfrac{1}{2}\left[\cos(\alpha) + \cos(\alpha + \mu)\right] \tag{2.28}$$

The reactive power expressed in terms of the active power, is

$$Q = P \tan(\phi) \tag{2.29}$$

Similarly to Equation (2.28), the following approximate expression can be written for the power factor in the inversion process:

$$\cos(\phi) = \tfrac{1}{2}\left[\cos(\gamma) + \cos(\beta)\right] \tag{2.30}$$

Figure 2.12 [15] shows a typical variation of the reactive power demand versus active power of an HVDC converter; the reactive power demand is shown to be approximately 60% of the power transmitted at full load.

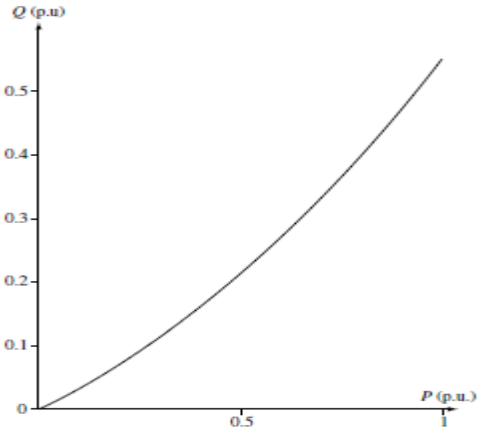

Figure 2.12 Variation of reactive power with active power

2.4 Harmonic Elimination

In the case of converters, the harmonic currents are normally prevented from entering the rest of the system by providing a shunt path of low impedance to the harmonic frequencies. This section is mainly concerned with passive filters.

2.4.1 Characteristic Harmonics

Line-commutated converters generate characteristic harmonic voltages and currents on the dc and ac sides, respectively. The orders of these harmonics are related to the pulse number of the converter configuration. A converter of pulse number *p* ideally generates only characteristic voltage harmonics of orders *pk* on the dc side and current harmonics of orders pk±1 on the ac side (where k is any integer).

The derivation of the characteristic harmonics is based on the following assumptions [15]:

- The supply voltages are displaced exactly by one-third of a cycle in time from each other and consist only of fundamental frequency.
- The dc current is perfectly constant (i.e. has no frequency components). This can only be achieved, if the dc smoothing reactor has infinite inductance.
- The valves begin conducting at equal time intervals.
- The commutation impedances are the same in the three phases (i.e. all the overlap angles are the same).

DC Side Harmonics

Fourier analysis of the voltage waveform shows that it contains harmonics of order 6n (i.e, 6^{th}, 12^{th}, 18^{th}, etc). In a bipolar system consisting of two 6-pulse bridges (one in each pole, the transformers would be connected Y-Y and Y-Δ because the 30 phase shift produces cancellation of low order harmonics on the ac bus. This would also have a beneficial effect on the dc side. The 6^{th}, 18^{th}, and 30^{th} … harmonics are out of phase in the two bridges, while the 12^{th}, 24^{th}, 30^{th} harmonics are in phase. In the case of 12 pulse bridge, the out of phase components of harmonic voltages will cancel with in 12 pulse bridge; only the in phase components will produce harmonic currents in the line.

Although the dc side voltage ripple of converters generates harmonic currents, these are rarely filtered out because they do not have a direct effect on other processes or consumers. The dc side

harmonics are reduced by the smoothing reactor this is because most of the harmonic voltages are dropped across the smoothing reactor. In general, a larger value of the smoothing reactor will require less or no dc filters [4, 15, 40].

AC Side Harmonics

With zero commutation reactance the ideal current waveform for a star/star-connected converter transformer, shown in Figure 2.13 (a) [15], is defined as follows:

$$i = I_d \text{ for } -\frac{\pi}{3} < \omega t < \frac{\pi}{3} \tag{2.31 a}$$

$$i = 0 \text{ for } -\frac{2\pi}{3} < \omega t < -\frac{\pi}{3} \text{ and } \frac{\pi}{3} < \omega t < \frac{2\pi}{3} \tag{2.31 b}$$

$$i = -I_d \text{ for } -\pi < \omega t < -\frac{2\pi}{3} \text{ and } \frac{2\pi}{3} < \omega t < \pi \tag{2.31 c}$$

The Fourier series for this current wave form is [15].

$$i_a = \frac{2\sqrt{3}}{\pi} I_d \left(\cos(\omega t) - \frac{1}{5}\cos(5\omega t) + \frac{1}{7}\cos(7\omega t) - \frac{1}{11}\cos(11\omega t) + \frac{1}{13}\cos(13\omega t) - \ldots \right) \tag{2.32}$$

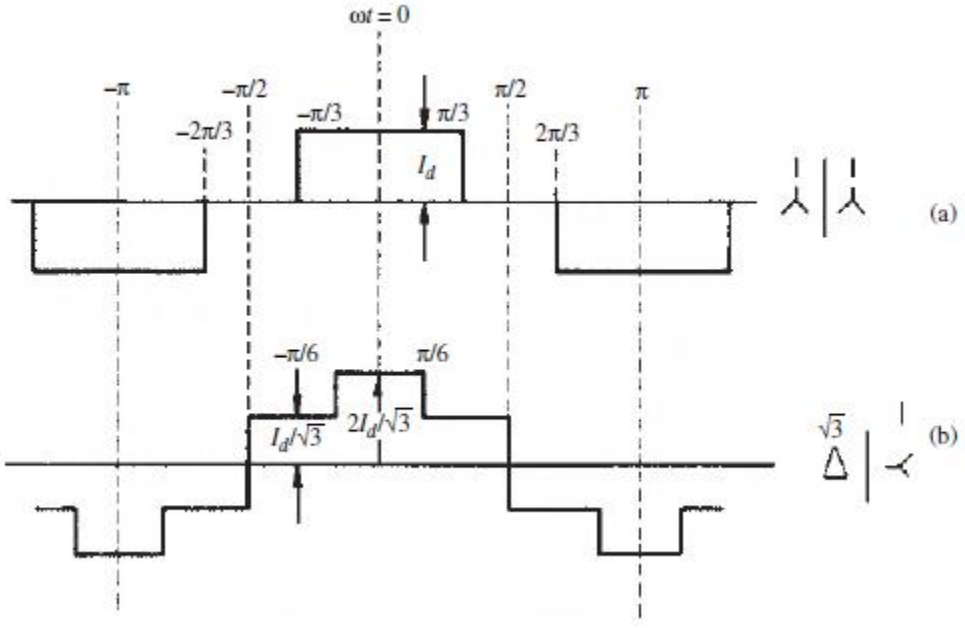

Fig 2.13 Idealized phase current wave forms on the primary side: (a) star-star transformer connection (b) delta- star transformer connection

The magnitude of the nth harmonic is given by [15]

$$I_n = \frac{\sqrt{6}}{n\pi} I_d \tag{2.33}$$

And that of the fundamental,

$$I_1 = \frac{\sqrt{6}}{\pi} I_d \tag{2.34}$$

2.4.2 Multi-Pulse Conversion

Transformer Phase Shifting

When the power rating justifies the use of more than one bridge, the need for external filtering can be reduced by appropriate phase shifting of the individual converter transformers, which can be achieved by the use of different transformer connections. The most common transformer connections are the star and delta types. A transformer consisting of star-connected primary and secondary windings does not alter the phase relationship of the input and output line-to-line voltages. However, the use of either delta–star or star–delta primary to secondary connections introduces a 30° phase shift between the input and output line-to-line voltages. The resulting current waveforms are shown in Figure 2.13 (b).

The Fourier series for the delta–star transformer connection is [15].

$$i_a = \frac{2\sqrt{3}}{\pi} I_d \left(\cos(\omega t) + \frac{1}{5}\cos(5\omega t) - \frac{1}{7}\cos(7\omega t) \right.$$

$$\left. - \frac{1}{11}\cos(11\omega t) + \frac{1}{13}\cos(13\omega t) + \ldots \right) \tag{2.35}$$

Equation (2.35) is the same as (2.32), the star–star Fourier series, with the exception that the harmonics 5, 7 (k = odd numbers) are of opposite sequence.

Double bridge configuration

Equations (2.32) and (2.35) indicate that the use of two bridges (either in parallel or series on the dc side), one with a star–star and the other with delta–star or star–delta transformer (i.e. with a 30° phase shift between them), will inject harmonic currents of orders n = 12k±1 into the ac system. The series-connected double bridge converter, shown in Figure 2.14, has become the *Standard configuration in HVDC transmission* [15]. The current waveform and harmonic spectrum of the double bridge 12-pulse configuration are illustrated in Figure 2.15 [15].

The resultant ac current is given by the sum of the two Fourier series of the star-star (equation (2.32) and delta-star (equation (2.35)) transformers, i.e.

$$(i_a)_{12} = 2\left(\frac{2\sqrt{3}}{\pi}\right) I_d \left(\cos(\omega t) - \frac{1}{11}\cos(11\omega t) + \frac{1}{13}\cos(13\omega t) - \frac{1}{23}\cos(23\omega t) + \frac{1}{25}\cos(25\omega t)... \right) \quad (2.37)$$

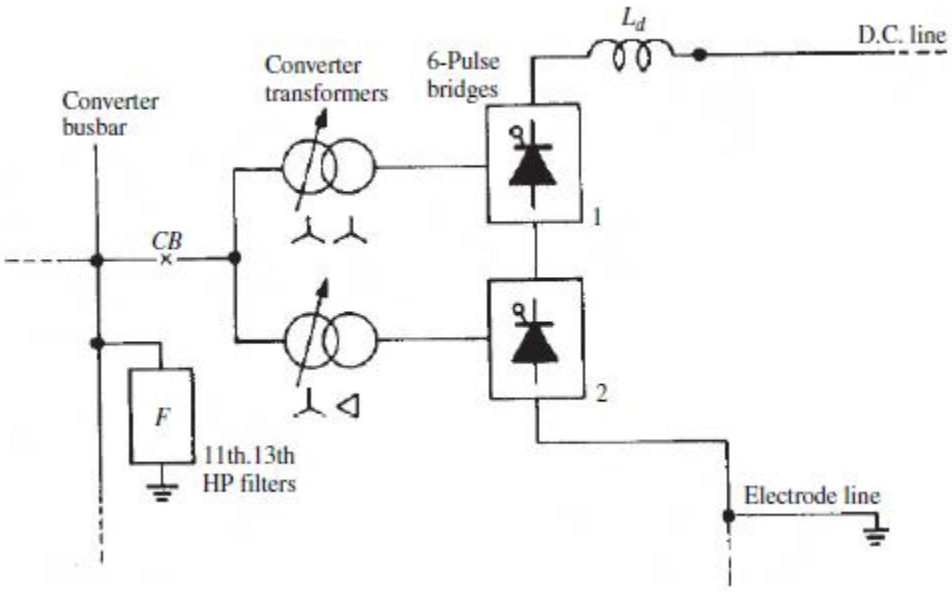

Figure 2.14 12 pulse Converter Configuration

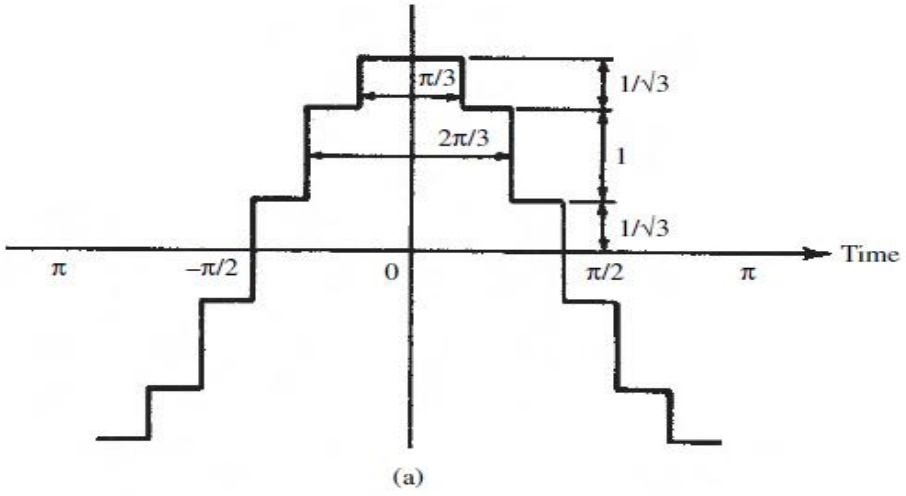

(a)

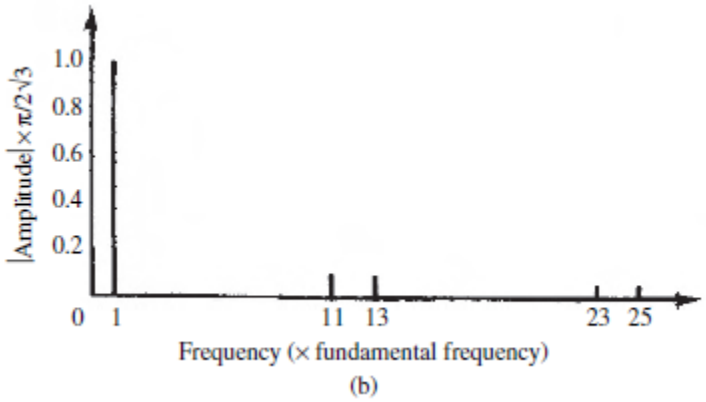

Figure 2.15 Idealized phase current wave form with 12-pulse operation: (a) current waveform; (b) frequency domain representation

2.5 Smoothing Reactor for HVDC transmission System

The main purpose of the smoothing reactor is to reduce the rate of rise of dc current following disturbances on either side of the converter. This in turn reduces the number of commutation failures following ac voltage reductions and limits the current peak seen by the rectifying station during dc line short circuits. The second task of the reactor is to provide high impedance to the flow of the harmonic currents, reduce their magnitude and thus making the dc current more smooth. The higher the reactor inductance is the smaller the remaining harmonic currents or (ripple) [36].

Smoothing reactors are available as air-cooled / air insulated reactors or as oil-immersed reactors. Air-cooled reactors are generally cheaper than oil-immersed reactors and require less maintenance, but need larger clearances to other installations [17].

Connections

Typical connections for smoothing reactors are presented in Figure 2.16 shown below [6]

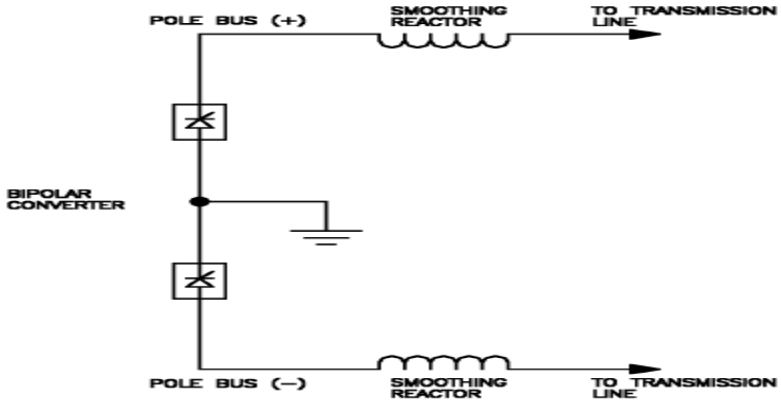

Figure 2.16 Smoothing reactor connections HVDC transmission; bipolar configuration

2.6 Literature Survey

2.6.1 Literature Reviews

Kala Meah, et al [2] made a study on comparative evaluation of HVDC and HVAC Transmission systems based on economical and environmental aspect and they have found out that the cost per unit length of an HVDC line is lower than that of an HVAC line of the same power capability and comparable reliability, but the cost of the terminal equipment of an HVDC line has much higher than that of an HVAC line. The breakeven distance of overhead lines between ac and dc line was in the range from 500 km (310 miles) to 800 km (497 miles). The HVDC has less effect on the human and the natural environment in general, which makes the HVDC friendlier to environment.

M. P. Bahrman, et al [3] made a study on HVDC Transmission and compared with HVAC based on economic comparison of capital costs and losses for different ac and dc transmission alternatives and obtained that the savings in line costs offsets the higher converter station costs due to narrower RoW, smaller transmission towers and lower line losses than with ac lines of comparable capacity. They have found that the rough approximation of the savings in line construction was 30%. In their study they showed that the long distance ac lines usually required intermediate switching stations and reactive power compensations and thus increased the substation costs for ac transmission to the point where it is comparable to that of HVDC transmission. Finally they showed that the break even distance was a typical value of 500 km.

Michael Bahrman P.E. et al [33], made a study on HVDC as economical complements to ac transmission and they have found out that the HVDC line is more economical for longer distances (>400 km) or higher ratings of power (>2000 MW).

Lars Weimers et al [22], made a study on HVDC and HVAC transmission systems based on cost and environmental effects and concluded that the break even distance calculated was around 500 km. On their study they showed that the relative cost of HVDC transmissions was reduced and become cheaper in current dollars compared with the situation 20 years ago this was due to continuing innovative technological developments made. On the environmental aspect they showed that the Corona losses of an HVDC lines were much less sensitive to variations in weather conditions when compared with HVAC lines.

2.6.2 Comparison of HVAC-HVDC transmission

An evaluation of transmission costs, technical considerations offered by the transmission alternatives is necessary to make a planning selection between either HVAC or HVDC transmission.

Advantages of dc transmission

(a) More power can be transmitted per conductor per circuit

The capabilities of power transmission of an ac link and a dc link are different.

For the same insulation, the direct voltage V_d is equal to the peak value (√2 x rms value) of the alternating voltage V_a [45].

$$V_d = \sqrt{2}V_a$$

For the same conductor size, the same current can be transmitted with both dc and ac, if skin effect is not considered.

$$I_d = I_a$$

Thus the corresponding power transmission using 2 conductors with dc and ac are as follows.

dc power per conductor, $P_d = V_d \times I_d$

ac power per conductor, $P_a = V_a \times I_a \times \cos\phi$

The greater power transmission with dc over ac is given by the ratio of powers.

$$\frac{P_d}{P_a} = \frac{\sqrt{2}}{cos\ \varphi} = \begin{pmatrix} 1.414\ at\ p.f. = unity \\ 1.768\ at\ p.f. = 0.8 \end{pmatrix}$$

In practice, ac transmission is carried out using either single circuit or double circuit 3 phase transmission using 3 or 6 conductors. In such a case the above ratio for power must be multiplied by 2/3 or by 4/3.

In general, we are interested in transmitting a given quantity of power at a given insulation level, at a given efficiency of transmission. Thus for the same power transmitted P, same losses P_L and same peak voltage V, we can determine the reduction of conductor cross-section A_d over A_a.

Let R_d and R_a be the corresponding values of conductor resistance for dc and ac respectively, neglecting skin resistance.

For dc,

$$\text{Current} = \frac{P}{V_m}$$

$$\text{Power loss } P_L = \left(P/V_m\right)^2 R_d = \left(P/V_m\right)^2 \times \left(\rho l / A_d\right)$$

For ac

$$\text{Current} = \frac{P}{\left(V_m/\sqrt{2}\right)\cos\phi} = \frac{\sqrt{2}P}{V_m \cos\phi}$$

$$\text{Power loss, } P_L = \left(\frac{\sqrt{2}P}{V_m \cos\phi}\right)^2 R_a$$

$$= 2\left(P/V_m\right)^2 \times \left(\rho l / \left(A_a \cos^2\phi\right)\right)$$

Equating power loss for dc and ac

$$\left(P/V_m\right)^2 \times \left(\rho l / A_d\right) = 2\left(P/V_m\right)^2 \times \left(\rho l / \left(A_a \cos^2\phi\right)\right)$$

$$\frac{A_d}{A_a} = \frac{\cos^2\phi}{2}$$

$A_d = 0.5$ at unity power factor

$A_d = 0.32$ at 0.8 power factor

The result has been calculated at unity power factor and at 0.8 lag to illustrate the effect of power factor on the ratio. It is seen that only one-half the amount of copper is required for dc transmission than ac transmission with the same power transmission at unity power factor, and less than one-third is required at the power factor of 0.8 lag.

(b) Use of Ground Return Possible

In the case of HVDC transmission, ground return (especially submarine crossing) may be used, as in the case of a monopolar dc link. Also the single circuit bipolar dc link is more reliable, than the corresponding ac link, as in the event of a fault on one conductor; the other conductor can continue to operate at reduced power with ground return. For the same length of transmission, the impedance of the ground path is much less for dc than for the corresponding ac because dc spreads over a much larger width and depth. In fact, in the case of dc the ground path resistance is almost entirely dependent on the earth electrode resistance at the two ends of the line, rather than on the line length. However it must be borne in mind that ground return has the following disadvantages. The ground currents cause electrolytic corrosion of buried metals, interfere with the operation of signaling and ships' compasses, and can cause dangerous step and touch potentials.

(c) Smaller Tower Size

The dc insulation level for the same power transmission is likely to be lower than the corresponding ac level because of less potential stress for same working voltage. . Also the dc line will only need two conductors whereas three conductors (if not six to obtain the same reliability) are required for ac. Thus both electrical and mechanical considerations dictate a smaller tower. Right-of-Way of typical dc and ac transmission line structure for approximately 2000 MW [16].

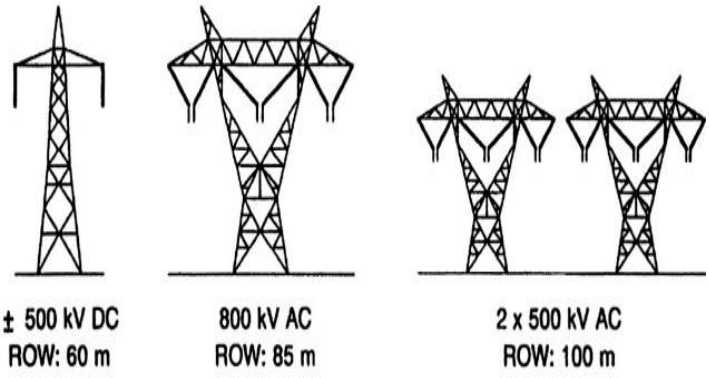

Figure 2.17 Right-of-Way of typical dc and ac transmission line

(d) No skin effect

Under ac conditions, the current is not uniformly distributed over the cross section of the conductor. The current density is higher in the outer region (skin effect) and result in under utilization of the conductor cross-section. Skin effect under conditions of smooth dc is completely absent and hence there is a uniform current in the conductor, and the conductor metal is better utilized.

(e) Less corona and radio interference

Since corona loss increases with frequency (in fact it is known to be proportional to f+25), for a given conductor diameter and applied voltage, there is much lower corona loss and hence more importantly less radio interference with dc Due to this bundle conductors become unnecessary and hence give a substantial saving in line costs. Tests have also shown that bundle conductors would anyway not offer a significant advantage for dc as the lower reactance effect so beneficial for ac is not applicable for dc.

(f) No Stability Problem

The dc link is an asynchronous link and hence any ac supplied through converters or dc generations do not have to be synchronized with the link. Hence the length of dc link is not governed by stability. In ac links the phase angle between sending end and receiving end should not exceed 30^o at full-load for transient stability (maximum theoretical steady state limit is 90^o).

Note: $\theta = \frac{\omega}{l_c}$ per km $= (2 \times 180 \times 50)/(3 \times 10^5) \approx 0.06^o$/km [45]

The phase angle change at the natural load of a line is thus 0.6^o per 10 km.

The maximum permissible length without compensation is around 30/0.06 = 500 km. with compensation, this length can be doubled to 1000 km.

(g) Asynchronous interconnection possible

With a.c. links, interconnections between power systems must be synchronous. Thus different frequency systems cannot be interconnected. Such systems can be easily interconnected through HVDC links. For different frequency interconnections both convertors can be confined to the same station.

In addition, different power authorities may need to maintain different tolerances on their supplies, even though nominally of the same frequency. This option is not available with ac, with dc there is no such problem.

(h) Lower short circuit fault levels

When an ac transmission system is extended, the fault level of the whole system goes up, sometimes necessitating the expensive replacement of circuit breakers with those of higher fault levels. This problem can be overcome with HVDC as it does not contribute current to the ac short circuit beyond its rated current. In fact it is possible to operate a dc link in "parallel" with an ac link to limit the fault level on an expansion. In the event of a fault on the dc line, after a momentary transient due to the discharge of the line capacitance, the current is limited by automatic grid control. Also the dc line does not draw excessive current from the ac system.

(i) Tie line power is easily controlled

In the case of an ac tie line, the power cannot be easily controlled between the two systems. With dc tie lines, the control is easily accomplished through grid control. In fact even the reversal of the power flow is just as easy.

Inherent problems associated with HVDC

(a) Expensive convertors

Expensive Convertor Stations are required at each end of a dc transmission link, whereas only transformer stations are required in an ac link.

(b) Reactive power requirement

Convertors require much reactive power, both in rectification as well as in inversion. At each convertor the reactive power consumed may be as much at 50% of the active power rating of the

dc link. The reactive power requirement is partly supplied by the filter capacitance, and partly by synchronous or static capacitors that need to be installed for the purpose.

(c) Generation of harmonics

Convertors generate a lot of harmonics both on the dc side and on the ac side. Filters are used on the ac side to reduce the amount of harmonics transferred to the ac system. On the dc system, smoothing reactors are used. These components add to the cost of the convertor.

(d) Difficulty of circuit breaking

Due to the absence of a natural current zero with dc, circuit breaking is difficult. This is not a major problem in single HVDC link systems, as circuit breaking can be accomplished by a very rapid absorbing of the energy back into the ac system. (The blocking action of thyristors is faster than the operation of mechanical circuit breakers).

(e) Difficulty of voltage transformation

Power is generally used at low voltage, but for reasons of efficiency must be transmitted at high voltage. The absence of the equivalent of dc transformers makes it necessary for voltage transformation to be carried out on the ac side of the system and prevents a purely dc system being used.

Economic Comparison

The HVDC system has a lower line cost per unit length as compared to an equally reliable ac system due to the lesser number of conductors and smaller tower size. However, the dc system needs two expensive convertor stations which may cost around two to three times the corresponding ac transformer stations. Thus HVDC transmission is not generally economical for short distances, unless other factors dictate otherwise. Economic considerations call for a certain minimum transmission distance (break-even distance) before HVDC can be considered competitive purely on cost.

Estimates for the break even distance of overhead lines are around 500 km with a wide variation about this value depending on the magnitude of power transfer and the range of costs of lines and equipment [45]. The breakeven distances are reducing with the progress made in the development of converting devices. Figure 2.18 shows that variation of costs of transmission with distance for ac and dc transmission [16]. AC tends to be more economical than dc for distances less than the “breakeven distance” but is more expensive for longer distances. The

breakeven distances can vary between 400 to 700 km in overhead lines depending on the per unit line costs.

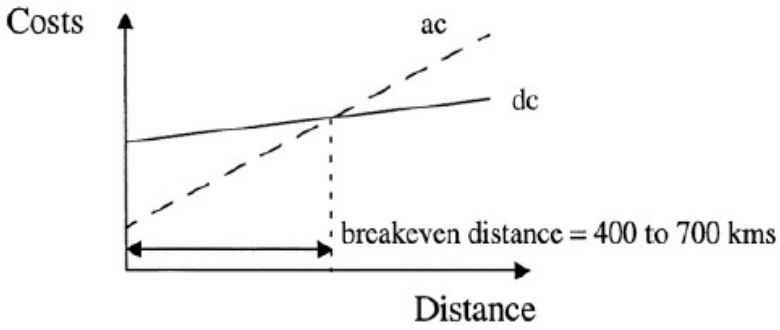

Figure 2.18 Comparative costs of dc links and ac links with distance

CHAPTER THREE

DESIGN AND MODELING OF MAIN COMPONENTS OF HVDC SYSTEM

This chapter deals with the modeling and design of main components of an HVDC transmission system. Modeling of each component has been discussed based on Cigré HVDC bench mark model, which includes transmission line conductor, converters, converter transformers, Ac filters and dc smoothing reactors. Generator and Infinite bus (External Grid) data has been collected from EEPCo. Accordingly each main component has been designed to meet the requirement of an HVDC transmission system to transfer 5250 MW power from the Generation to the Menagesha bus bar (National grid).

According to EEPCo Power Company the HVDC transmission system should fulfill an *N-1 contingency criterion* i.e. during one pole outage the remaining poles should carry the capacity of the whole transmission system. Bus voltages should be between 0.95 pu to 1.05 pu (or ±5% tolerance) [42].

3.1 Components of HVDC transmission system

The following Figure is the schematic diagram of the main components of an HVDC Transmission System [40, 44].

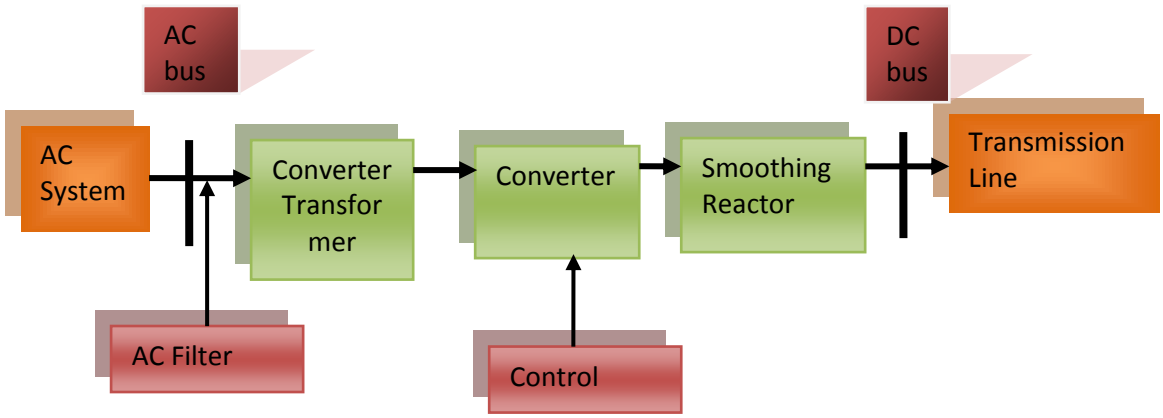

Fig. 3.1 HVDC system components

The most relevant components that comprise an HVDC system are the following:

The **Thyristor valves** make the conversion from AC to DC and thus are the main component of any HVDC converter. Each single valve consists of a certain amount of series connected thyristors with their auxiliary circuits.

The **Converter Transformers** transform the voltage level of the AC bus bar to the required entry voltage level of the converter.

The **Smoothing reactor**, which main functions are:

- Reduce the rate of rise of dc current following disturbances on either side of the converter. This in turn reduces the number of commutation failures following ac voltage reductions and limits the current peak seen by the rectifying station during dc line short circuits.
- To provide high impedance to the flow of the harmonic currents, reduce their magnitude and thus making the dc current more smooth

The **Harmonic Filters**, on the AC side of a HVDC converter station, which have two main duties:

- To absorb harmonic currents generated by the HVDC converter
- To supply reactive power

DC Transmission circuit, which include DC Transmission line and earth electrode.
The **Control** in this part, the parameters like current, voltage, and power of the Transmission line, in case of faults happening, will be controlled by placing:

- Constant current controllers in the Rectifier side
- Both current and gamma angle controllers on the Inverter side of an HVDC transmission system.

3.2 HVDC SYSTEM Modelling

3.2.1 CIGRÉ HVDC System Model

The **International Council on Large Electric Systems** or **CIGRE** is a world organization in the field of high voltage electricity. It was founded in Paris, France in 1921. The scope of its activities includes the technical and economical aspects of the electrical grid, as well as the environmental and regulatory aspects [5].

More specifically, CIGRE's objectives are

- Facilitate the technical exchanges among the actors of production and transmission of electrical energy ;
- Communicate the state of the art and the technical knowledge in these fields ;
- Inform the decision makers and regulators in the field of high voltage electricity by means of publication on its magazine *Electra* or through the organization of biannual conferences, named Sessions that take place on the even years in Paris, France.

Through the years, CIGRE has become a privileged meeting place for actors in the field of electrical energy: researchers, solution providers, utilities, regulators and normalization institutions, and generally all electrical engineers involved with electrical power.

Power Circuit Modeling [9]

1) Converter Model: The converters (rectifier and inverter) are modeled using six-pulse Graetz bridge block, which includes an internal firing control, and an internal firing angle (α) /extinction angle (γ) measurements.

2) Converter Transformer Model: Two transformers on the rectifier side are modeled by three-phase two winding transformer, one with grounded Wye – Wye connection and the other with grounded Wye – Delta connection. The model uses tap setting arrangements. The inverter side transformers use a similar model as the Rectifier side.

In this thesis work the transformer tap changers are not simulated. The tap position is rather at a fixed position determined by a multiplication factor applied to the primary nominal voltage of the converter transformers (0.90 on the rectifier side; 0.96 on the inverter side) [40]. This is because during fault occurrence controlling system parameters using alpha angle controller has been faster response than controlling using tap changing transformer [36].

3) DC Line Model: The dc line is modeled using Tower type with smoothing reactors inserted on both sides.

In this thesis work the converters are interconnected through a 574 km HVDC tower type line and 0.579 H smoothing reactors inserted on both sides.

4) Generation side: The generations on the rectifier side have been represented using three phase synchronous generators.

In this thesis work the Grand Renaissance HEPP has initial capacity 15 x 390 MVA [1]. The other parameters of the synchronous generator are shown in appendix A Table A.1.

5) External Grid: An infinite bus connected at the inverter ac side characterized by short circuit current and short circuit power. This external grid represents the remaining network of the grid system of which the transmission line is connected.

In this thesis work the external grid represents the national grid at Menagesha substation having bus bar voltage rating of 400 kV, 3 phase short circuit current Ik" max of 17.160 kA, and short circuit-power Sk" max of 11888.8 MVA and positive and Negative sequence impedances are $Z_1 = Z_2 = 0.1912\angle 97.33^o$ [1].

6) Filters and Reactive Support: Tuned filters and reactive support are provided at both the rectifier and the inverter ac sides. From the ac point of view, an HVDC converter acts as a source of harmonic currents. The order n of these characteristic harmonics is related to the pulse number p of the converter configuration: n = kp ± 1 for the ac current, k being any integer.

In this thesis work, p should be 12, so that injected harmonics on the ac side are 11, 13, 23, 25, etc. ac filters are used to prevent the odd harmonic currents from spreading out on the ac system. The filters are grouped in two subsystems. These filters also appear as large capacitors at fundamental frequency, thus providing reactive power compensation for the rectifier consumption. The converter reactive power demand is approximately 50% of the power transmitted at full load. The ac filters subsystem has high Q (32) tuned filters at the 11^{th} and 13^{th} harmonics and the low Q (0.3), or damped filter, used to eliminate the higher order harmonics, e.g., 17th and up. Extra reactive power is also provided by capacitor banks.

3.3 Selection of phase conductor of HVDC bipolar line

Phase conductor is one of the main components of the HVDC Transmission System. So this component should be designed well to fulfill the following assumptions.

- To provide satisfactory radio interference (RI), audible noise (AN) and corona loss performances;
- To transfer a maximum design power of 2625 MW at +/- 500 kV nominal voltages on bipolar line without neutral conductor;
- To transfer continuously the specified maximum continuous overload for the pole operation over ground return, tentatively adopted at 1750 MW
- To provide safety of the line, considering the mechanical loads from wind.

The optimal conductor selection process is complex and the choice of suitable conductor (and sub conductors) depends on the operating voltage, the power to be transmitted and the acceptable voltage drop and losses in the conductor.

3.3.1 Voltage drop considerations

For a single conductor configuration, maximum power to be transferred with 10% drop restriction voltage, resulted from [24]:

$$P_{\max} = \frac{V^2}{10 \times R_x \times L} \tag{3.1}$$

Where,

V = Sending end voltage, pole to ground, in our case 500 kV

R_x = dc resistance of the conductor in Ω / km

L = Distance in km

The rated value of the two bipolar lines under consideration is 5250 MW. So during one pole outage the healthy poles should carry 1750 MW (i.e. 5250/3 MW) to fulfill *N-1 contingency criteria* [42]. And the voltage selected is 500 kV based on the assumptions of same power capability to transfer with same transmission line voltage.

To transfer 1750 MW per one pole, with maximum 10% drop voltage the pole resistance must be less than:

$$R_x(\max) = \frac{V^2}{10 \times P_{\max} \times L} = \frac{500^2}{10 \times 1750 \times 574} = 0.024888\,\Omega / km$$

Or,

0.024888 x 4 = 0.099552Ω/km per conductor in case of 4 conductors per pole. Accordingly, conductors with electrical resistances lower than 0.099552 Ω/km are selected for further study as shown in Annex A.

3.3.2 Conductor Surface Voltage Gradient

High voltage gradients surrounding conductors (above about 18 kV/cm) will lead to a breakdown of the air in the vicinity of the conductor surface known as corona discharge. Generally, the breakdown strength of air is approximately 31 kV peak/cm or 22 kV rms/cm [46]. This is a useful guide for the selection of a conductor diameter or conductor bundle arrangement equivalent diameter. Corona discharge, radio interference and audible noise

generated cause problems with the reception of radio communication equipment and adversely affect the performance of power line carrier signals.

At higher voltage levels, and certainly at voltages of 400 kV and above, interferences due to the corona effect can be the dominant factor in determining the physical size of the conductor rather than the conductor thermal rating characteristic. Increasing the conductor diameter may be necessary in order to reduce the surface stress to acceptable levels. Obviously there is a limit with regard to the practical size, strength and handling capability for conductors. The bundling of conductors assists in the effective increase in overall conductor diameter and hence leads to lower stress levels.

The Radio Interference (RI), Audible Noise (AN) and corona loss performances depend on the conductor surface voltage gradients of the candidate conductors, taking into account different bundle arrangements. i.e. as the surface voltage gradient decreases RI, AN, and corona loss are also deceases.

The following transmission line geometry is considered for 500 kV bipolar transmission line as per [19]:

- 14 m (pole spacing)
- 11 m (conductor above ground level).

All selected conductors having electrical resistances lower than 0.099552 Ω/km should have surface voltage gradients less than 22 kV/cm [17, 46].

- Calculations of Voltage Gradients for HVDC transmission line conductor is given by [43]:

$$D = \frac{S}{\sin(\pi / n)}$$

$$deq = D\left(\frac{n \times d}{D}\right)^{1/n} \qquad (3.2\ a)$$

$$F = \left(1 + \left(\frac{2H}{P}\right)^2\right)^{1/n}$$

$$T = \frac{4H}{deq}$$

$$G_{av} = \frac{2V}{nd \ln(\frac{T}{F})}$$
$$G_{\max} = G_{av}\left(1 + \frac{d(n-1)}{D}\right) \quad (3.2\ b)$$

Conductor surface voltage gradients of a pole of 2, 3 and 4 Sub-conductors for the above selected conductors having a resistance less than 0.099552 Ω/km are calculated and shown in Annex A Table A.1. Conductors which have surface voltage gradient less than or equal to 22 kV/cm [17, 46] have been selected for further comparisons. As the number of conductor in a bundle increases the performance of the conductor concerning corona loss, RI, TVI decreases since the surface voltage gradient decreases as the number of conductors in a bundle increases. To achieve satisfactory corona effects, multiple conductor bundles instead of single conductors may have to be used [24].

It is common practice for EHV lines to use more than one conductor per phase, a practice called bundling. Bundling reduces the electric field strength at the conductor surfaces, which in turn reduces or eliminates corona and its results: undesirable power loss, communications interference, and audible noise. Bundling also reduces the series reactance of the line by increasing the Geometric Mean Radius (GMR) of the bundle [17].

Table 3.1 Conductor surface voltage gradients of a pole of 2, 3 and 4 Sub-conductors for a +/- 500 kV line.

Code name ACSR	Bundle Spacing ,S (m)	Conductor Dia. (mm)	Bundle Diam. (m)	Equiv. Bundle Dia.	F	T	Gmax (kV/cm) For n=2	Gmax (kV/cm) For n=3	Gmax (kV/cm) For n=4
Grackle	0.457	33.97	0.457	0.176206	2.20128	122.538	39	27	22
Pheasant	0.457	35.1	0.457	0.179113	2.20128	122.538	38	26	22
Martin	0.457	36.17	0.457	0.181822	2.20128	122.538	37	25	21
Plover	0.457	37.24	0.457	0.184492	2.20128	122.538	36	25	21
Falcon	0.457	39.26	0.457	0.18943	2.20128	122.538	34	24	20

The choice of conductors depends largely on corona and field-effect considerations. Those effects, however, are not expected to be a special problem for dc voltages up to ±1200 kV [15].

3.3.3 Maximum power to be transferred

The current carrying capacity (Ampacity) of a bare, overhead transmission line conductor is that current (amps) which may flow in it continuously while maintaining a steady maximum permissible temperature over its surface. The maximum permissible temperature is that which does not permanently and adversely affect the physical properties of the conductor material. The current carrying capacity of a conductor is based on the concept that under a state of thermal equilibrium, the total heat gained by the conductor due to energy loss within itself and by solar and sky radiation equals the total heat lost by the conductor by conduction to the metallic supporting it, by convection to the air surrounding it and by radiation to its surrounding objects [2].

For a bare stranded conductor, if the conductor temperature ($\underline{T_c}$) and the steady-state weather parameters (V_w, T_a, etc.) are known, the heat losses due to convection and radiation (q_c and q_r), the solar heat gain (q_s), and the conductor resistance $R(T_c)$ can be calculated by the formulas of equations 3.4, 3.5, 3.6, 3.7 respectively. The corresponding conductor current (I) that produced this conductor temperature under these weather conditions can be found from the steady-state heat balance. While this calculation can be done for any conductor temperature and any weather conditions, a maximum allowable conductor temperature (e.g., 75 °C to 150 °C) and "conservative" weather conditions (e.g., 0.6 m/s to 1.2 m/s wind speed, 30 °C to 45 °C summer ambient) are often used to calculate a steady-state thermal rating for the conductor.

3.3.3.1 Current-Temperature of bare overhead conductors [6, 7, 41]

Fundamental Heat balance equation is.

$$I = \sqrt{\frac{q_c + q_r - q_s}{R_{ac/T_c}}} \tag{3.3}$$

where,

I = thermal current flowing through the conductor

q_c = heat loss due to convection is given by:

$$q_c = \left[1.01 + 0.0372\left(\frac{D\rho_f V_w}{\mu_f}\right)^{0.52}\right] K_f \left(T_c - T_a\right)$$

(3.4)

q_r = heat loss due to radiation is given by:

$$q_r = 0.0178 D\varepsilon\left[\left(\frac{T_c + 273}{100}\right)^4 - \left(\frac{T_a + 273}{100}\right)^4\right] \quad (3.5)$$

q_s = Solar heat gain is given by

$$q_s = \alpha \times S \times D \quad (3.6)$$

R_{ac/T_c} = ac resistance of the conductor at conductor temperature

$$R_{ac/T_c} = R_{dc/T_c}\left(1 + 0.00519(m)^n K_1 + K_2\right) \quad (3.7)$$

$R_{dc/T_c} = \left(1 + a(T_c - 20)\right)\Omega/m$,

a = 0.004 for ACSR

a = 0.0036 for AAAC and AACSR

where,

$$m = 0.050133 f^{\frac{1}{2}}\left(R_{dc/T_c}\right)^{-\frac{1}{2}}$$

If m < 2.8

$$n = 3.9384 + 0.0896(\mathrm{m}) - 0.0513(\mathrm{m})^2$$

If 2.8 < m < 5

$$n = 4.5363 - 0.2949(m) + 0.0097(m)^2$$

And the constants K_1 and K_2 are given below

$$K_1 = \left(\cos\left(90\left(\frac{d}{D}\right)^p\right)\right)^{2.35}$$

$$p = 0.7 + 0.11(m) - 0.04(m)^2 + 0.0094(m)^3$$

K_2 = 0.15 for single aluminum layer ACSR

= 0.03 for three aluminum layer ACSR

= 0.003 for two or four aluminum layer ACSR

Table 3.2 Viscosity, density, and thermal conductivity of air [6]

Temperature T_{film}	Dynamic discosity μ_f	Air density ρ_f (kg/m^3)				Thermal conductivity of air k_f
°C	(Pa·s)	0 m	1000 m	2000 m	4000 m	W/(m·°C)
0	0.0000172	1.293	1.147	1.014	0.785	0.0242
5	0.0000174	1.270	1.126	0.995	0.771	0.0246
10	0.0000176	1.247	1.106	0.978	0.757	0.0250
15	0.0000179	1.226	1.087	0.961	0.744	0.0254
20	0.0000181	1.205	1.068	0.944	0.731	0.0257
25	0.0000184	1.184	1.051	0.928	0.719	0.0261
30	0.0000186	1.165	1.033	0.913	0.707	0.0265
35	0.0000188	1.146	1.016	0.898	0.696	0.0269
40	0.0000191	1.127	1.000	0.884	0.685	0.0272
45	0.0000193	1.110	0.984	0.870	0.674	0.0276
50	0.0000195	1.093	0.969	0.856	0.663	0.0280
55	0.0000198	1.076	0.954	0.843	0.653	0.0283
60	0.0000200	1.060	0.940	0.831	0.643	0.0287
65	0.0000202	1.044	0.926	0.818	0.634	0.0291
70	0.0000204	1.029	0.912	0.806	0.625	0.0295
75	0.0000207	1.014	0.899	0.795	0.616	0.0298
80	0.0000209	1.000	0.887	0.783	0.607	0.0302
85	0.0000211	0.986	0.874	0.773	0.598	0.0306
90	0.0000213	0.972	0.862	0.762	0.590	0.0309
95	0.0000215	0.959	0.850	0.752	0.582	0.0313
100	0.0000217	0.946	0.839	0.741	0.574	0.0317

The Viscosity, density, and thermal conductivity of air is manipulated from the Table 3.2 above at T_{film},

$$T_{film} = \left(\frac{T_c + T_a}{2} \right)$$

For our design purpose

$$T_{film} = \left(\frac{80 + 45}{2} \right) = 62.5\,℃,$$ at T_c=80℃ and T_a = 45℃ from Table 3.4

Table 3.3 Units and identification of letter symbols

Symbol	Descriptions	SI units
D	Conductor diameter	mm
I	Conductor current	A
q_s	Heat gain rate from sun	W/m
k_f	Thermal conductivity of air at temperature T_{film}	W/(m-°C)
R_{ac/T_c}	ac resistance of conductor at temperature	Ω/m

R_{dc/T_c}	dc resistance of conductor at temperature	Ω/m
T_a	Ambient air temperature	°C
T_c	Conductor temperature	°C
T_{film}	(Tc + Ta)/2	°C
V_w	Speed of air stream at conductor	m/s
α	Solar absorptivity (0.23 to 0.91)	------
ε	Emissivity (0.23 to 0.91)	-------
μ_f	Dynamic viscosity of air	Pa-s
q_c	Convected heat loss rate per unit length	W/m
q_r	Radiated heat loss rate per unit length	W/m
D	Conductor outer diameter	m
d	Conductor inner diameter	m
S	Direct Solar irradiation on conductor surface,	W/sq.m

The assumptions for checking the conductors with respect to their thermal behavior (steady state) are given in Table 3.4:

Table 3.4: Data's used for thermal power calculations [1]

parameters	Values
Highest ambient temperature (T_a)	45℃
Highest conductor temperature (T_c)	80℃
Solar absorption coefficient (α)	0.7
Emission factor (ε)	0.5
Wind speed (V_w)	0.6 m/sec

Table 3.5 Phase carrying capacity at 0.6 m/s wind velocity (see the thermal current carrying capacity of the conductors in Annex B)

Conductor type: ACSR	Conductor carrying Capacity (A)	Pole carrying capacity (MW) 4 conductors in bundle
Grackle	928	1855
Pheasant	964	1929

Martin	1001	2003
Plover	1036	2073
Falcon	1105	2210

For the bipolar line the current transmitted by each pole becomes (1312.5 MW/500 kV, i.e. 2.625 kA and the current of each sub conductors will be 656.25. During one pole outage, the current ratings of each of the remaining conductor reaches 875 A, so all the conductors listed in Table 3.5 can satisfy the *N-1 contingency criteria* since the calculated thermal power rating of the conductors is above 1750 MW.

3.3.4 Mechanical performance

Even though the conductors have the capacity to carry the power ratings specified, the conductors should also be further compared with respect to their mechanical performance, i.e. Sag. So sag has been calculated at different spans of the transmission line to see which conductor has better mechanical performance.

Sag and Tension in transmission line conductors [41]

The Sag and Tension of overhead line conductors is calculated based on the following rules and standards

Weight factor (δ): is linear mass of conductor per meter per unit cross sectional area of the conductor used to calculate the tension on the conductors.

$$\delta = \frac{W}{A} \tag{3.8}$$

Wind factors: includes both maximum wind pressure and wind load on the conductor

Wind pressure is given by

$$P_1 = KV^2 \tag{3.9}$$

Where,

P = wind pressure in lb. / sq. ft.

V = actual wind velocity in miles per hour

The value *K* is not strictly constant and depends on the shape and nature of the surface, barometric pressure and wind velocity.

The following approximate values are used:

For cylindrical surfaces k = 0.0025

For flat surfaces k = 0.0042

For 0.6 m/s wind speed or 1.8 miles/hour

$$P_1 = 0.0025 \times 1.8^2$$

$$P_1 = 4.5 \times 10^{-3}\ lb/ft^2$$

Or,

$$P_1 = 0.022\ kg/m^2$$

(a) Wind load 2/3 Max.

$$P_2 = \left(\frac{2}{3} \times P_1 \times \delta \times 1\right) kg/m \tag{3.10}$$

(b) (On conductor) Max.

$$P_3 = \left(P_1 \times \delta \times 1\right) kg/m \tag{3.11}$$

Loading factors: constants used to calculate the tension and sag of the conductor which are dependent on wind pressure and linear mass of conductor

Still wind

$$q_1 = 1 \tag{3.12a}$$

2/3 full wind

$$q_2 = \left(1 + \left(\frac{P_2}{W}\right)^2\right)^{\frac{1}{2}}$$

(3.12b)

Full wind

$$q_3 = \left(1 + \left(\frac{P_3}{W}\right)^2\right)^{\frac{1}{2}} \tag{3.12c}$$

Temperature factors: the temperature difference that affects the property of the conductor like module of elasticity and coefficient of linear expansion

$$E\alpha t = E\alpha(t_2 - t_1)$$

Tension Factors: used to calculate the stress on the conductors which depends strongly on the span length, weight factor and module of elasticity of the conductor.

$$\text{Still wind condition} = \frac{L^2\delta^2 E(q_1)^2}{24} \tag{3.13a}$$

2/3 full wind condition $= \dfrac{L^2\delta^2 E(q_2)^2}{24}$

(3.13b)

$$\text{Full wind condition} = \frac{L^2\delta^2 E(q_3)^2}{24} \quad (3.13c)$$

Sag factors: used to find out the sag at different spans and also depends on the weight factor and module of elasticity of the conductor.

$$\text{Still wind condition} = \frac{L^2\delta E q_1}{8} \quad (3.14a)$$

$$\text{2/3 full wind condition} = \frac{L^2\delta E q_2}{8} \quad (3.14b)$$

$$\text{Full wind condition} = \frac{L^2\delta E q_3}{8} \quad (3.14c)$$

Sags and Tensions

For most conductors still wind is the controlling factor. The tension limitation obtained at 32°C is the starting condition assumed.

At 32℃ still wind (Starting condition Assumed)

$$T_1 = \frac{U}{4} \quad (3.15)$$

$$f_1 = \frac{T_1}{A}$$

$$S_1 = \frac{L^2\delta q_1}{8 f_1} \quad (3.16)$$

Result,

$$T_{32}/q_1 = T_1$$

$$S_{32}/q_1 = S_1$$

Stress factor

$$K = f_1 - \frac{L^2\delta^2 E(q_1)^2}{24(f_1)^2}$$

At 45℃ still wind

$$(f_2)^2\left(f_2 - (K - E\alpha t_{45}\right) = \frac{L^2\delta^2 E(q_1)^2}{24}$$

$$T_2 = f_2 \times A \quad (3.17)$$

$$S_2 = \frac{L^2\delta q_1}{8 f_2} \quad (3.18)$$

Using the results from Annex C

Table 3.6 Conductor sags, calculated at 300 m, 400 m, and 500 m spans at 45℃

Conductor type: ACSR	300 m	400m	1000 m (for mountain areas)
Grackle	10.7402	15.87704	68.63554
Pheasant	9.028194	16.06667	70.02111
Martin	9.02965	16.07042	70.04821
Plover	9.029131	16.06923	70.03883
Falcon	10.77714	15.89934	68.4173

For mountain areas the sag calculated is more or less similar and all the conductors listed in Table 3.6 can be used for the proposed transmission line because no conductor has week steel core. But the ratio (Ultimate Tensile Strength to Tension) calculated in Table 3.7 is the controlling factor used to determine the mechanical performance of the conductors. This ratio should meet international standards (Indian Electricity Rules 1956, IS 802/1977 and IS 5613/1985) i.e. at every day temperature of 32 °C and maximum wind pressure, the Tension calculated should be less than or equal to 50% of the Ultimate Tensile Strength of the conductor [41].

Table 3.7 Ratio of Ultimate Tensile Strength to Tension of the conductors selected at 32℃

Conductor type: ACSR	300 m	f_2 (kgf/sq.cm)	Cross-sectional area (sq.cm)	Tension (kgf)	Ultimate Tensile Strength (kgf)	Ratio $\frac{\text{UTS}}{\text{Tension}} \geq 2$
Grackle	6.279469	601.049	6.799	4086.532	19006	4.650887
Pheasant	6.134158	614.443	7.268	4465.772	19777	4.428574
Martin	6.131813	614.733	7.721	4746.353	21001.33	4.424730
Plover	6.132521	614.631	8.187	5031.984	22271.39	4.425966
Falcon	6.020203	582.34	9.7548	5680.61	25445	4.479272

The tension calculate in Table 3.7 is below 50 % of the Ultimate Tensile Strength of the conductors. So the conductors have better mechanical performance Therefore all the conductors are selected for further assessment of their joule losses.

3.3.5 Economical performance

The conductors evaluated above are compared over a 35 years life span for their economic merits. The conductor which is cost effective will be selected for the dual bipolar transmission line.

Table 3.8 Assumption considered in conductor selection [1]

Description	Unit	Value
Economic Life of Transmission Lines	Years	35
Energy Cost	$/kWh	0.027
Capacity Cost or Energy generation cost	$/kW/yr	94.5
Discount rate	-	10%

Discount rate:

The interest rate used in discounted cash flow analysis to determine the present value of future cash flows. The discount rate takes into account the time value of money (the idea that money available now is worth more than the same amount of money available in the future because it could be earning interest).

Table 3.9 Joule losses of selected conductor comparisons

		4×Grackle (ACSR)	4×Pheasant (ACSR)	4×Martin (ACSR)	4×Plover (ACSR)	4×Falcon (ACSR)
D.C. resistance, Ohms/km	$R_{conductor}$	0.0472	0.0443	0.0417	0.0394	0.0354
D.C. resistance per pole, R=Rcond/4	R	0.0118	0.011075	0.010425	0.00985	0.00885
Current, to transfer 2625 MW, per bipolar line (or 1312.5MW per pole) in A		2625	2625	2625	2625	2625
50% of the current considered in calculations, in A	I_{max}	1312.5	1312.5	1312.5	1312.5	1312.5
Power loss, per pole: Power loss=I^2R in kW/km	P_L	20.32734	19.078417	17.95869	16.96816	15.24551
Annual demand charge cost: $C_d = P_L$*$94.5, in $/km	C_d	1727.8242	1621.6655	1526.488	1442.293	1295.868
Annual energy loss: $P_{el} = P_L$ * 2650 in kWh/km	P_{el}	53867.460	50557.8076	47590.53	44965.63	40400.6
Annual energy loss cost $C_{el} = P_{el}$ * 0.027in Dollar/km	C_{el}	1454.421	1365.0608	1284.944	1214.072	1090.816
Total annual loss cost, $C_d + C_{el}$ in $/km	C	3182.2456	2986.7263	2811.433	2656.366	2386.684

Annual Savings/km of Conductor, over ACSR Grackle, in $/km	S	-	-196	-370	-526	-796
Present value of saving, in $/km PV=S(1-(1+r)^-n)/r=S(1-(1+0.1)^-35)/0.1 PV circuit per pole in $/km		-	-1886	-3576	-5072	-7672
PV per bipolar line in $/km		-	-3772	-7152	-10144	-15344
PV circuit per 2 bipolar line in $/km			-7544	-14304	-20288	-30688

As per the conductors listed to the right in Table 3.9 their *cross sectional area* increases which increases their costs respectively but their *resistances* decreases and hence their joule loss cost decreases. It is better to consider these two characteristics of the conductors in order to come up with the net cost of the conductors. Table 3.9 is designed to calculate the joule losses employed in the conductors. Annual demand charge cost based on the capacity unit price cost (or, energy generation cost) and annual energy loss cost based on the energy unit price cost are evaluated to determine the total annual loss cost. To have more realistic results, the calculus was performed based by only of 50% of the rated power resulted the value of the K- constant of 2650 hours, which shall multiply the power losses [17]. The negative sign obtained for each conductor is the savings if each conductor is used in place of Grackle conductor (reference conductor selected for comparison) over the life time of the conductors.

Since the future value of an investment is worth more than its present value, one widely accepted approach of comparing options over their life-cycles is to bring all costs to a single point in time-the present. From the annual saving, the Present Value (PV) saving can be obtained using 10 % discount rate over a 35 years life time of the transmission line.

Table 3.10 Line minimum costs and Joule losses

Conductor type	Line cost USD/km [17]	Joule losses USD/km (saving)	Total USD/km
4xGrackle	309,294	0	309,294
4xPheasant	318,353	-3772	314,581
4xMartin	326,765	-7152	319,613
4xPlover	335,176	-10144	325,032
4xFalcon	348,118	-15344	332,774

From Table 3.10 it can be concluded that even though the unit price of the conductor's increases due to the increase in cross sectional area, the savings obtained over 35 years increases due to the decrease in resistance of the conductors which minimizes the cost of the conductors. Among the listed conductors Grackle conductor has minimum cost and this conductor is selected for the HVDC bipolar transmission line.

3.3.6 Selected conductor

ACSR Grackle, 4 Sub Conductor per pole, resulted as an economical solution for the dc line in case of:

- 2x1312.5 MW power transfers per bipolar
- 1x1750 MW power transfer in case one pole outage

3.4 LCC Converter model design

To fulfill *N-1 contingency criteria*, the converters should have a continuous and a short term overloading capability in the range of 10% to 30% [17].

3.4.1 The total reactive power consumed by the inverter

The total Generation power from the GERD is 5250 MW and each bipolar line has been designed to have a capacity of 2625 MW. Each converter consumes a reactive power that increases with increasing power. With normally acceptable rectifier ignition delay angle

(alpha) of 15 to 25 degrees and inverter extinction advance angle (gamma) of 15 to 25 degrees a converter consumes reactive power which is 50 % to 60 % of the real power transmitted [3]. Shunt capacitor banks is used to provide the reactive power needed by the converters. Part of the reactive power required is provided by the capacitor associated with the ac filters.

For the project under study, during faulty conditions the reactive power consumed by the converters is 1575 MVAR which is 60% of 2625 MW power (rated power of a single bipolar line) and this reactive power supply will be installed at Generation and Menagesha bus bars partly in the form of shunt capacitor banks and the remaining in the form of shunt ac filters.

3.4.2 Commutation Reactance of the Rectifier and Inverter

Commutation reactance is the reactance due to commutation overlap and it accounts for the voltage drop in the converters. In HVDC systems the commutation reactance is assumed to be the leakage reactance of the converter Transformer [44].

Rectifier commutating reactance

The rectifier, however, has a minimum α limit of about $5°$ to ensure adequate voltage across the valve before firing. In the case of thyristors, the positive voltage appearing across each thyristor before firing is used to charge the supply circuit providing the firing pulse energy to the thyristor. Therefore, firing cannot occur earlier than about $\alpha = 5°$. Consequently, the rectifier normally operates at a value of α within the range of $15° \; to \; 25°$ so as to leave some room for rectifier voltage to control dc power flow [36]. Since a too small value of the extinction angle γ will make the converter too vulnerable for commutation failures, it should never decrease below a certain minimum value $\gamma_{\min}$ ($\approx 17°$) [13]; values between $15° \; to \; 25°$ are typically used [15]. In normal operation, the overlap angle is less than $60°$; typically full-load values are in the range of $15° \; to \; 25°$ [36]. The alpha-min-in-inverter mode characteristic is typically about 100-110 degrees, and is required to limit any excursions (even transiently) of the inverter into the rectifier mode of operation. Furthermore, the value of 100^o-110^o ensures a minimum dc voltage at the inverter during a fast start-up of the dc link with $I_d = 0$.

Rectifier commutating reactance

The no load direct voltage, U_{do} can be obtained by [36]

$$U_d = \frac{U_{do}}{2}\left(\cos\alpha + \cos(\alpha + \mu)\right)$$

For $\alpha = 20°$ and $\mu = 15°$

$$250 = \frac{U_{do}}{2}\left(\cos(20) + \cos(35)\right)$$

$$U_d = U_{do}\cos\alpha - \Delta U_d$$

$$\Delta U_d = \frac{3Xc}{\pi} \times I_d$$

$$\Delta U_d = \frac{3Xc}{\pi} \times 2.625kA$$

$$X_C = 6.8351\ \Omega$$

Inverter commutating reactance

$$U_d = U_{do}\frac{\cos(\gamma) + \cos(\gamma + \mu)}{2}$$

For $\gamma = 17°$ and $\mu = 15°$ (to have a small commutating voltage drop)

$$250 = U_{do}\frac{\cos(17)+\cos(32)}{2}$$

$$U_d = U_{do}\cos\gamma - \Delta U_d$$

$$\Delta U_d = 14.999kV$$

$$\Delta U_d = \frac{3Xc}{\pi}\times I_d$$

$$X_C = 5.9837\ \Omega$$

Each bipolar line has a capacity of 2625 MW so that each pole is rated to 1312.5 MW. Each pole is composed of 12 Pulse converters on each side of the transmission line. The 12-pulse converters are composed of two 6-pulse converters connected in series having each a capacity of 656.25 MW. Pole to ground voltage rating of the 12-pulse converter is 500 kV so that the 6-pulse converters are rated to 250 kV and 2.625 kA (i.e. 656.25/250).The values listed in Table 3.7 are for 6 pulse converter. The HVDC system intended to carry 5250 MW power employs 16 such kind of converters for the two bipolar lines.

Merits of Higher pulse number (in this case 12-pulse)

- Higher average dc voltage per a cycle of ac wave.
- Lesser distortion of dc voltage and current wave forms. Reduced harmonics.
- Better utilization of converter transformers and valves.
- Reduced requirement of ac Filter Banks.

The modern HVDC converters are of 12 pulse connections shown in Figure 3.2 is achieved by two series connected 6-pulse converters [39].

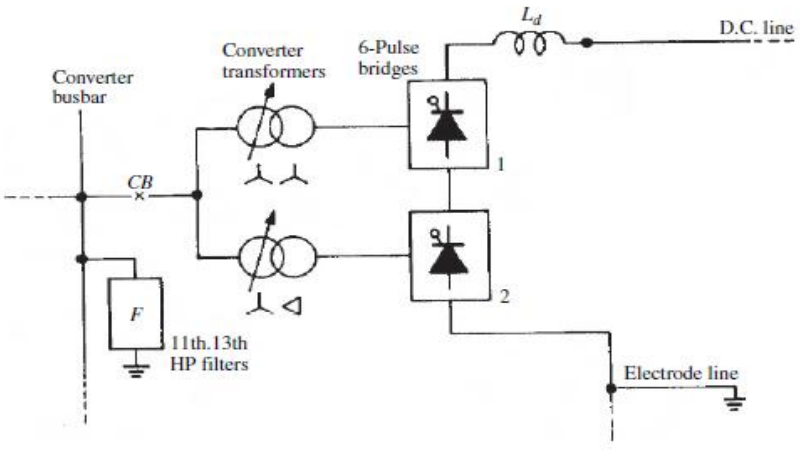

Figure 3.2 12 pulse Line Commutated Converters

Table 3.11 Summary of six pulse bridges component values.

Parameters	Rated values
Alpha, α	20^o
Extinction angle, γ	17^o
Commutation angle, μ	15^o
Commutation reactance, X_L (Rectifier)	6.8351 Ω
Commutation reactance, X_L (Inverter)	5.9837 Ω
Rated voltage (kV)	250 kV
Rated current (kA)	2.625 kA
Rated power (MW or MVA)	656.25 MW
Reactive power (MVAR)	1575 $MVAR$
Short term Overloading capability	10 to 30%

3.5 Converter transformer design

The converter transformers are mostly of conventional design. The standard 12-pulse converter configuration can be obtained with any of the following arrangements [15, 17]:

- Six single phase two-winding transformers;
- Three single phase three-winding transformers;
- Two three-phase two-winding transformers.

Selection of the converter transformer bank is primarily dependent on the maximum weight that can be transported to the site and the spare part policy. If the selected route has a limitation of 200 tones, only single-phase two-winding transformers are suitable which have a transport weight of about 170 tones for a 500 MW pole [17]

According to M. O. Faruque, Yuyan Zhang, and Venkata Dinavah [9], option three is selected to fulfill the requirement of the HVDC model developed in DigSILENT software. For the positive pole two transformers on the rectifier side are modeled by three-phase two winding transformer, one with grounded Wye – Wye connection and the other with grounded Wye – Delta connection and similarly same for the inverter side. For the negative pole of the bipolar line similar configurations of the transformers and the number of transformers needed are same as of the positive pole.

According to Figure 3.3, The RMS value of the transformer secondary current (total and not just the fundamental frequency component) I_{IRMS} is given by

$$I_{TRMS}^2 = \frac{1}{T}\int_0^T i^2(t)dt \quad , \quad I_{TRMS}^2 = \frac{1}{\pi}\int_{\frac{-\pi}{2}}^{\frac{\pi}{2}} i^2(t)dt$$

$$I_{TRMS}^2 = \frac{1}{\pi}\int_{-\pi/3}^{\pi/3} i_d^2 dt = \frac{2}{3}i_d^2 \quad , \quad I_{TRMS} = \sqrt{\frac{2}{3}}i_d$$

The alternating line current wave consists of rectangular pulses of amplitude i_d and width $2\pi/3$ rad as shown in Figure 3.3. The RMS value of the line-to-neutral transformer secondary voltage is given by

$$E_{LN} = \frac{\pi}{3\sqrt{6}}V_{do}$$

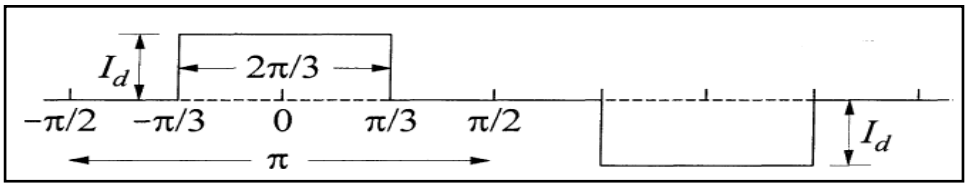

Figure 3.3 line current wave form

Transformer **volt-ampere rating** is given by 3-phase rating [36]

$$= 3E_{LN}I_{TRMS}$$
$$= 3\left(\frac{\pi}{3\sqrt{6}}\right)V_{do}\sqrt{\frac{2}{3}}I_d$$
$$= \frac{\pi}{3}V_{do}I_d$$

where,

V_{do} = ideal no-load direct voltage

I_d = rated direct current

Since 16 6-pulse converters are needed for the conversion process at the rectifier and inverter sides of the two bipolar transmission lines, A total of 16 converter transformers are needed for the two bipolar lines each have four converter transformers at the Generation side and four converter transformers at the Menagesha side.

3.5.1 Rectifier side ratings of converter transformer

The MVA rating of the rectifier (6-pulse converter) side converter transformer is given by [36].

$$MVA_{rating} = \frac{\pi}{3} \times U_{do} \times I_d$$

I_d is 2.625 kA. $U_{do} = 284.2775\ kV$ (Previously calculated)

$$MVA_{rating} = 781\ MVA$$

The primary side voltage is known. And the secondary voltage is given by

$$U_{do} = \frac{3\sqrt{2}}{\pi} E_{LL}$$

E_{LL}(Secondary) = 210.5 kV

The primary line to line voltage is 20 kV at the generation bus bar. So the transformer is rated at 20/210.5 kV (i.e. step-up transformer).And the transformer turns ratio T becomes 210.5/20, which is 11

3.5.2 Inverter side ratings of converter transformer

The MVA rating of the rectifier (six Pulse converters) side converter transformer for I_d = 2.625 kA and $U_{do} = 277\ kV$ becomes:

$$MVA_{rating} = 761\ MVA$$

The secondary side voltage is known. And the primary voltage is given by

$$U_{do} = \frac{3\sqrt{2}}{\pi} E_{LL}$$

E_{LL}(Primary) = 197 kV

The secondary line to line voltage is 400 kV. at the Menagesha side of the transmission line. So the transformer should be rated at 197/400 kV (i.e. step-up transformer).And the transformer turns ratio T become 400/205 which is 2.

3.6 AC side harmonic filters design

Equations (2.32) and (2.35) indicate that the use of two bridges (either in parallel or series on the dc side), one with a star–star and the other with delta–star or star–delta transformer (i.e. with a 30° phase shift between them), will inject only harmonic currents of orders n = 12k±1 into the ac system. For the sake of interpretation the Harmonic spectrum of the double bridge 12-pulse configuration again are illustrated in Figure 3.4

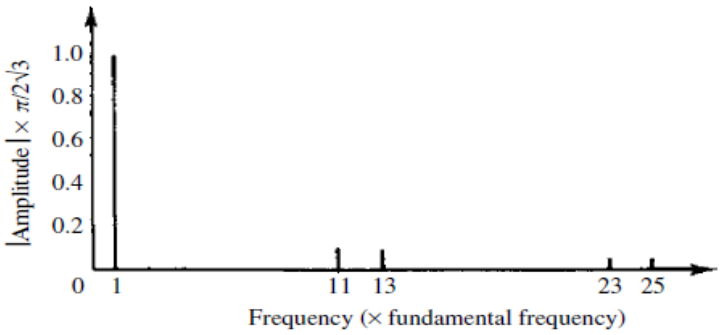

Figure 3.4 Frequency-domain representation of 12-pulse operation

A typical filter system for 12 pulse converter terminal is shown in Figure 3.5. The filter impedance is minimum at 11^{th} and 13^{th} harmonics resulting from the two series resonance tuned branches. The high pass filter maintains low impedance for higher harmonic frequency. This filter is used to eliminate, at the same time, a range of harmonic frequencies rather than implementing a single tuned filter for each high order harmonics.

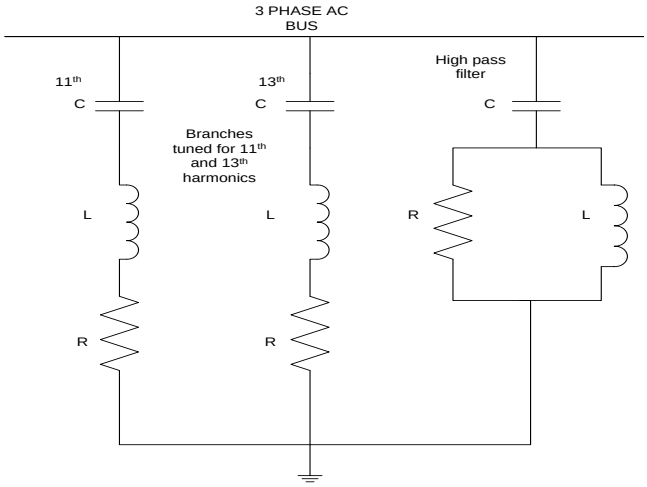

Figure 3.5 Typical filter system configurations

3.6.1 Design of Tuned Filters

A single tuned filter is a series *RLC* circuit tuned to the frequency of one harmonic (generally a lower characteristic harmonic). Its impedance is given by

$$Z_1 = R + j\left(\omega L - \frac{1}{\omega C}\right) \tag{3.19}$$

Which at the resonant frequency (f_n) reduces to *R*. There are two basic design parameters to be considered prior to the selection of *R*, *L* and *C*. These are

(a). The quality factor (Q) , and

(b). The relative frequency deviation (δ)

Quality factor (Q):

The quality of a filter (Q) determines the sharpness of tuning and in this respect filters may be either of a high or a low Q type. The former is sharply tuned to one of the lower harmonic frequencies (e.g. the fifth) and a typical value is between 30 and 60 [38]. The low Q filter, typically in the region of 0.5–5 [38], has low impedance over a wide range of frequency. When used to eliminate the higher-order harmonics (e.g. 17^{th} up wards) it is also referred to as a high-pass filter.

The relative frequency deviation (δ):

The extent of filter detuning from the nominal tuned frequency is represented by a factor δ. This factor includes various effects:

(i) variations in the fundamental (supply) frequency;

(ii) variations in the filter capacitance and inductance caused by ageing and temperature; and

(iii) Initial off-tuning caused by manufacturing tolerances and finite size of tuning steps.

For a capacitor temperature coefficient 0.05% per degree Celsius, the inductor temperature coefficient 0.01% per degree Celsius and ambient temperature 40℃ causes the same detuning as a change of system frequency of 1% [1, 38]. Therefore δ is often expressed as

$$\delta = \frac{\Delta f}{f_n} + \frac{1}{2}\left(\frac{\Delta L}{L_n} + \frac{\Delta C}{C_n}\right) \tag{3.20}$$

$$\delta = \frac{1}{100}\left(1 + 0.5(0.05 \times 40 + 0.01 \times 40)\right)$$

$$\delta = 0.022$$

Let the ac system impedance be of any magnitude but its phase angle restricted to $\phi < 75^{\circ}$ at any frequency. The optimum Q (giving the lowest harmonic voltage) is then obtained from equation stated below, i.e. $\phi = \pm 70°$ electrical degree for $11 \leq n \leq 15$ according to CIGRÉ WG 14.30 [37].

$$Q = \frac{\cot\left(\phi/2\right)}{2\delta} = \frac{\cos(\phi) + 1}{2\delta \sin(\phi)}$$

So,

$$Q = \frac{\cos 70 + 1}{2 \times 0.022 \times \sin 70}$$
$$Q = 32$$

The reactance of inductor or capacitor in ohms at the tuned frequency is

$$X_o = \omega_n L = \frac{1}{\omega_n C} = \sqrt{\frac{L}{C}}, \qquad C = \frac{1}{\omega_n X_o} = \frac{1}{\omega_n RQ}$$
$$Q = \frac{X_o}{R} \qquad L = \frac{X_o}{\omega_n} = \frac{RQ}{\omega_n}$$

Where,

$$\omega_n = \frac{1}{\sqrt{LC}}$$

3.6.2 Design of Damped Filters

A damped filter provides low impedance for a wide spectrum of harmonics without the need for subdivision of parallel branches, which increases switching and maintenance problems. The behavior of damped filters has been described with the help of two parameters [38]

$$f_o = \frac{1}{2\pi CR} \tag{3.21}$$

$$m = \frac{L}{R^2 C} \tag{3.22}$$

Where,

$f_0 = 17\ (i.e. 17th\ order\ harmonic)\ times\ fundamental\ frequency\ (50\ Hz)$

$$f_0 = 17 \times 50\ Hz$$

Typical values of *m* are between 0.5 and 2 [38].

The total filter capacitance is now given by [37]

$$C = \frac{Q^f}{2\pi f V^2}\left(1 - \frac{1}{n^2}\right) \tag{3.23}$$

Where,

f = is the fundamenta frequency in Hz

V = is the bus voltage in kV where the filters are going to connect.

n = Harmonic order

A typical converter will consume reactive power between 50-60% of its MW rating [16].The demanded reactive power of an HVDC converter becomes 1575 MVAR (60% of 2625 MW)

According to [36] about 30% would be in filter form divided among the 11th, 13th and high pass filters

So,

$$Q^f = 0.3 \times 1575\ MVAR$$

$$Q^f = 472.5\ MVAR$$

And the remaining $1102.5\ MVAR$ will be installed as Shunt Capacitor on the same bus bar at the Generation 20 kV and Menagesha 400 kV bus bar.

3.6.3 Harmonic filters at the generation 20 kV bus bar

Harmonic filters are used to keep the harmonic contribution of large nonlinear plant components such as HVDC converters under control, normally by the connection of passive filters. The components of a single tuned filter are evaluated below.

$$C_n = \frac{Q_{11}{}^f}{2\pi f V^2}\left(1-\frac{1}{n^2}\right)$$

$$C_{11} = \frac{157.5}{2\pi \times 50 \times 20^2}\left(1-\frac{1}{11^2}\right) = 1.2429\times 10^{-3}\,F$$

$$C_{11} = 1.2429mF$$

$$L_{11} = \frac{1}{(2\pi fn)^2 C_{11}}$$

$$L_{11} = \frac{1}{(2\pi \times 50\times 11)^2 \times 1.2429\times 10^{-3}} = 6.7367\times 10^{-5}\,H$$

$$R_{11} = \frac{2\pi fnL_{11}}{Q}$$

$$R_{11} = \frac{2\pi \times 50\times 11\times 6.7367\times 10^{-5}}{32} = 7.2751\times 10^{-3}\,\Omega$$

The same procedure for the 13th harmonic filter

$$C_{13} = 1245.929\ \mu\text{F}$$

$$L_{13} = 0.04811941\ H$$

$$R_{13} = 0.00614135\ \Omega$$

The damped arm components are found from equations (3.21) and (3.22). By choosing m = 1 and fo = 17 × 50 = 850 Hz. Since C has been fixed above (i.e.$1.2429mF$), the resulting values of inductor and resistor are 0.02806965 mH and 0.1557802 Ω, respectively.

3.6.4 Harmonic filters at the 400 kV Menagesha bus bar.

$Q_{11}{}^f$ is the reactive power supplied by each of the capacitors of the harmonic filters that are connected to the bus bars.

$$C_n = \frac{Q_{11}{}^f}{2\pi f V^2}\left(1-\frac{1}{n^2}\right)$$

$$C_{11} = \frac{157.5}{2\pi \times 50 \times 400^2}\left(1-\frac{1}{11^2}\right) = 3.1074\times 10^{-6} F$$

$$C_{11} = 3.1074\mu F$$

$$L_{11} = \frac{1}{(2\pi f n)^2 C_{11}}$$

$$L_{11} = \frac{1}{(2\pi \times 50 \times 11)^2 \times 3.1074\times 10^{-3}} = 0.02694H$$

$$R_{11} = \frac{2\pi f n L_{11}}{Q}$$

$$R_{11} = \frac{2\pi \times 50 \times 11 \times 0.02694}{32}$$

$$R_{11} = 2.9100\Omega$$

The same procedure for the 13th harmonic filter

$$C_{13} = 3.114822\ \mu F$$

$$L_{13} = 19.24776\ H$$

$$R_{13} = 2.456538\ \Omega$$

The damped arm components are found from equations (3.21) and (3.22) by choosing m = 1 and fo = 17 × 50 = 850 Hz. Since C has been fixed above (i.e.$3.1074\ \mu F$), the resulting values of inductor (L) and resistor (R) are 11.2824 mH and 60.2565 Ω, respectively.

3.7 Smoothing Reactor Design.

The transmission capability of an HVDC link is defined by its rated dc system voltage and the continuous dc current. It is a general practice to require about 20% over current capability above rated current for limited duration (1–2 h) [6]. The smoothing reactor must be designed to meet these loading requirements.

One criteria used on the choice of the optimal size of a dc smoothing reactor based on the acceptable performance of the reactor, is the so-called S_i-factor as per [27]

$$S_i = \frac{U_d}{L \times I_{dn}} \tag{3.24}$$

The value of Si varies between $0.23 ms^{-1}\ to\ 0.95\ ms^{-1}$[27]. So, the size of the smoothing reactor, Ld. For U_d = 500 kV, I_{dn} = 2.625 kA, and L_T = 31.8 mH is

For Si = $0.95\ ms^{-1}$

$$0.95 = \frac{500kV}{(3.5 \times LT + Ld)(2.625 + 0.2 \times 2.625kA)}$$

$$Ld = 56mH$$

For Si = $0.23ms^{-1}$

$$0.23 = \frac{500kV}{(3.5 \times LT + Ld)(2.625 + 20\%(2.625kA)}$$

$$Ld = 579mH$$

Accordingly a standard inductance value of 579 mH is selected. But for dynamic state simulation the inductor value should be higher than this rated value (as high as 1 H). Since the higher the reactor inductance, the smaller the remaining harmonic currents presents on the dc transmission line [36].

3.8 HVDC Controllers Designs

3.8.1 Basics principles of HVDC controllers

HVDC link is a transmission system consisting ac/dc converter station (Rectifier station) at the sending end, transmission line, and dc/ac converter station (Inverter station). Sometimes it is used to connect asynchronous ties (i.e. different frequency labels, 50/60 Hz). The single line diagrams in Figure 3.6 (a) shows a HVDC link and an equivalent circuit is shown in Figure 3.6 (b) [13].

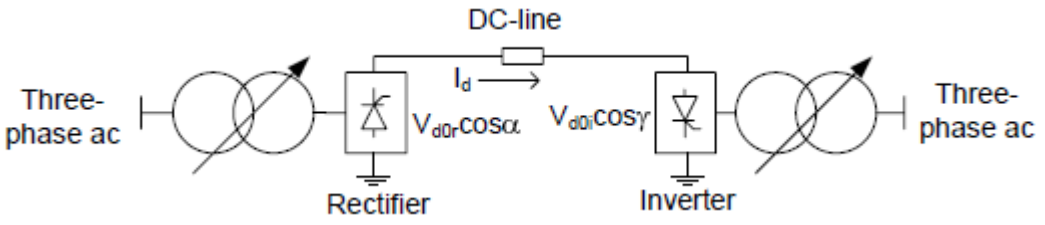

(a)

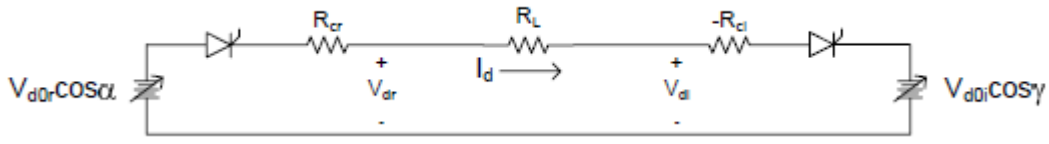

(b)

Figure 3.6 Single diagram of HVDC system: (a) Schematic diagram of a HVDC link. (b) Equivalent circuit.

The direct current, I_d, flowing from rectifier to the inverter is [13]:

$$I_d = \frac{V_{dor}\cos\alpha - V_{doi}\cos\gamma}{R_L + R_{cr} - R_{ci}} \tag{3.25}$$

The dc voltage at the rectifier dc terminals can be expressed as:

$$V_{dr} = V_{dor}\cos\alpha - R_{cr} I_d \tag{3.26}$$

V_{dor} and V_{doi} are the no-load direct voltage in the rectifier and the inverter respectively, R_{cr} and R_{ci} are the equivalent commutation resistance (due to commutation overlap it accounts for the voltage drop in the converters) and R_L is the line resistance.

By controlling the voltages $V_{dor}\,cos\alpha$ and $V_{doi}\,cos\gamma$ the dc current or the active power can be controlled. This is done either by controlling the rectifier valve ignition angle α or extinction angle γ of an inverter, or by controlling V_{dor} and V_{doi} by the transformer tap changer. Control of valve ignition angle is used for rapid action [13].

3.8.2 Operation requirements

In practice the line and converter resistance are relatively small, hence a small difference between V_{dor} and V_{doi} causes a large change in I_d. This implies that if α and γ are kept constant and small changes in the ac voltage magnitude are made at either end, the direct current can vary over a wide range. Such variations are unacceptable for a satisfactory performance of the power system.

The power factor should be as high as possible. This is important for several reasons, e.g. to avoid excessive consumption of reactive power, to reduce the amplitude of the harmonics and to minimize the stresses on the valves and the transformers. The power factor of the converter can approximately be expressed as [13].

$$\cos\phi = 0.5\left[\cos\alpha + \cos(\alpha+\mu)\right] \qquad \text{for rectifier operation}$$
$$\cos\phi = 0.5\left[\cos\gamma + \cos(\gamma+\mu)\right] \qquad \text{for inverter operation}$$

To achieve high power factor the angle α for a rectifier and γ for inverter must be kept low.

In order to secure a certain positive voltage across the valve at firing the firing control in the rectifier operation is arranged so that the angle will not be decreased below a certain minimum value$\alpha_{\min}$ (≈ 5°). Since a too small value of the extinction angle γ will make the converter too vulnerable for commutation failures, it should never decrease below a certain minimum value$\gamma_{\min}$ (≈ 17°).

3.8.3 Control characteristics

The control characteristics are best explained by using the steady-state voltage-current characteristics. These characteristics represent the relationship between I_d through and V_d

across the converters, which are suitable for explaining how the converter stations work together for controlling the flow of power on the dc line.

The $V_d - I_d$ characteristics of a rectifier are, described by Equation (3.27):

$$V_d = 1.35V_{LL}\cos\alpha - \left(\frac{3\omega L_s}{\pi}\right)I_d \tag{3.27}$$

Where, V_{LL} is the rms value of line-to-line voltages and L_S is the ac-side inductance. We see from the expression that there are three variables, V_{LL}, α and I_d, which define the level of the direct voltage. The maximum V_d is obtained if $\alpha = \alpha_{min}$ at its minimum value, and the rectifier will operate at constant ignition angle (CIA), the $V_d - I_d$ characteristics starts at a value obtained by using Equation (3.28).

$$V_d = 1.35V_{LL}\cos\alpha_{\min} \tag{3.28}$$

And CIA being represented by a line of negative slope (segment FA in Figure 3.7) for increasing I_d.

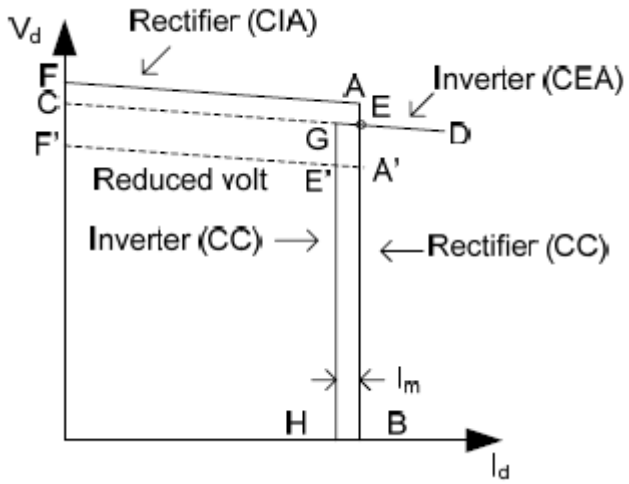

Figure 3.7 Steady-state characteristics for converter control.

The segment AB in Figure 3.7 represents the normal constant current (CC) control mode. Operation with constant current and variable α results in vertical line in the $V_d - I_d$ diagram. This is the normal mode of rectifier operation in which the rectifier controls the direct current by varying α to meet the voltage on the dc side. Consequently, the complete rectifier characteristics at normal voltage are defined by FAB and E ~~is~~ at the point of operation.

At reduced voltage the CIA characteristic would follow F'A' and the inverter CEA characteristic (CD) would not intersect F'A'B, this would cause the current and the power to be reduced to zero, and the system would run down. In order to avoid the above problem, the

inverter is also provided with a current controller, which is set at a value lower than the current setting for the rectifier. The resulting inverter CC characteristic is given by the section GH.

The difference between rectifier and inverter current order is called the current margin and is denoted by I_m in Figure 3.7 and it is normally around 0.1 p.u. so as to ensure that the two constant current characteristics do not cross each other due to errors in measurement or other causes [13].

If the ac voltage in the inverter network is slightly reduced i.e. V_{di} is reduced, the rectifier must increase it's α in order to keep the direct current at the requested level and the new point of operation will be A'. If the ac voltage reduction occurs in the rectifier network i.e. V_{dr} is reduced, the inverter current control system will react to the decreased direct current and increase γ. Thus the inverter takes over the current control and restores stable operation with direct current equal to the current reference in the inverter, and the new point of operation will be E'.

3.8.4 Stability Model of Converters

The stability model shown in Figure 3.8 is used to study the dynamic performance (like fault recovery) of the converters during faults happening on the HVDC system [44]. The internal circuit of the converters needs "alpha" and "frequency" as input variables and generates on the output side currents, voltages, power and extinction gamma angle order etc. due to result variables where they can hold the results of every outputs of the converters.

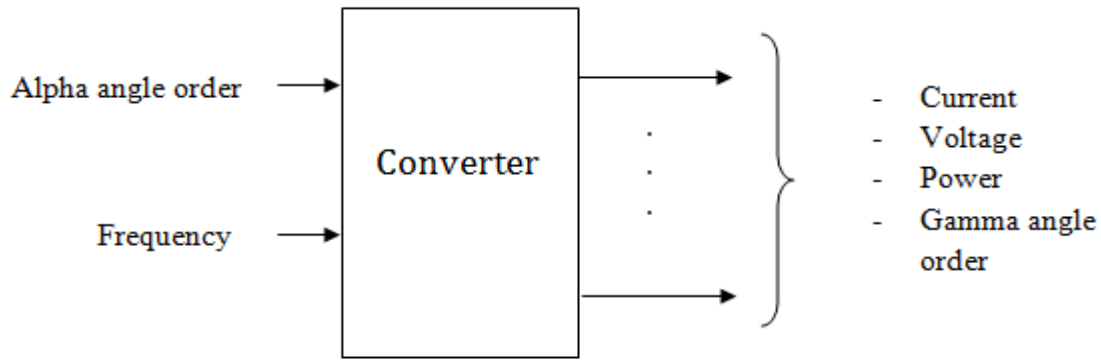

Figure 3.8 Stability model of Converter

3.8.5 Cigré Control System Model [9]

In this section the control models that have been used for the rectifiers and inverters has been discussed. In the rectifier side current controllers are used and in the inverter side both current controller and extinction angle controller are used.

1) Rectifier Control model: The rectifier control system uses constant current control technique. From the output of the converters dc current is taken and is compared with a reference current to produce the error signal. The error signal is then passed through a PI controller, which produces the necessary firing angle order. The firing circuit inside the converter uses this information to generate the equidistant pulses for the valves [9].

2) Inverter Control model: The Extinction Angle Control or γ control and current control have been implemented on the inverter side. The measured current is then subtracted from the reference limit to produce an error signal that is sent to the PI controller to produce the required angle order. The γ control uses another PI controller to produce alpha angle order for the inverter. The two angle orders are compared, and minimum of the two is used to calculate the firing instant [9].

3.8.6 HVDC control scheme

According to [4, 9, 14], Figure 3.9 is developed. This Figure shows a basic control scheme for an HVDC converter. The scheme includes current controller for the Rectifier operation and both current and extinction angle (or gamma) controller for inverter operation. The phase locked loop (PLL), built in model, component detects the phase voltages and generate one of the input parameters of the converters for their dynamic operation i.e. “frequency”. The individual components are described in the following subsections.

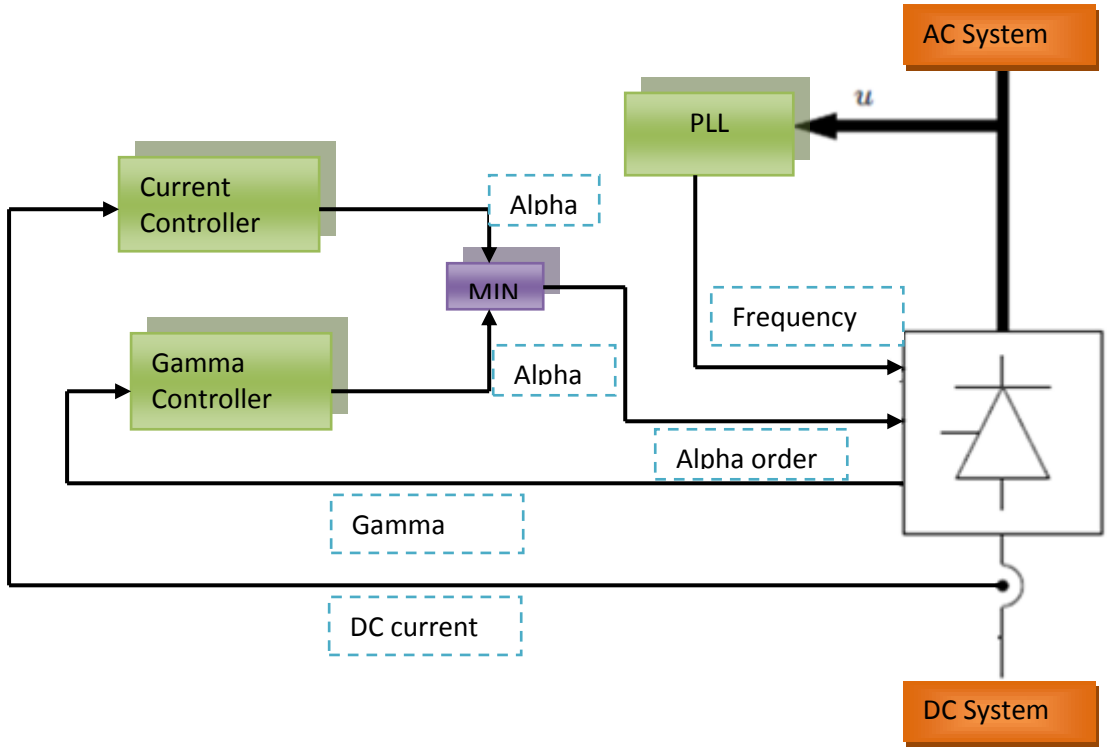

Figure 3.9 Basic HVDC control scheme

3.8.6.1 Current controller

Constant Current Controller [44] shown in Figure 3.10 is included on both the rectifier and the inverter; the functions are principally equal in the two stations. There may be some differences in parameter settings inside the block. The actual direct current is measured and its difference to the reference signal is calculated. The current error is fed to a PI controller (limited within alpha-min = 5 degrees to alpha-max = 90 degrees.), which outputs the firing angle order. The limits may in general be provided by other modules but are set to fixed values here [13].

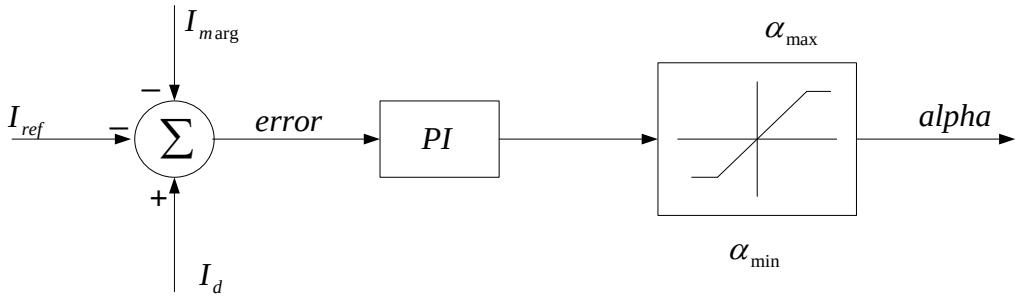

Figure 3.10 Current controller

3.8.6.2 Gamma controller

When operating an HVDC converter as an inverter, care must be taken that the commutation ends well before the voltage across the outgoing valve becomes positive again. This is achieved by the gamma controller.

In Figure 3.11 [16] it is shown that once a measurement of the gamma angles from the six valves of the convertor are obtained, the minimum value is selected. This value is then compared to the desired value of gamma and an error signal is generated and fed to a PI controller. This gamma error signal is used in a similar manner to the current controller at the rectifier to generate the firing pulses for the converter [16].

The difference between the commutation margin γ, i.e. the delay between the extinction of a valve and the valve voltage becoming positive, and a fixed set-point is used in a PI controller for the firing angle order. If the actual margin is larger than necessary, the PI controller saturates at the maximum limit α_{max} . Otherwise, the firing angle is reduced until γ equals the set value [14]. In DigSILENT simulation, the relation α+μ+γ = π can be used to calculate the margin from the known firing and overlap angles.

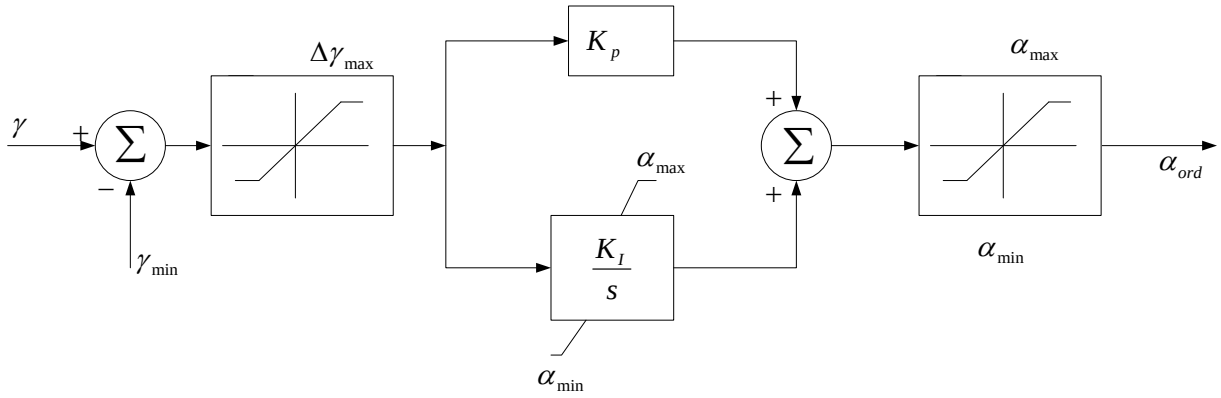

Figure 3.11 Gamma controller

The proportional and integral gains of the PI controllers need to be optimized to provide satisfactory dynamic and steady state properties to the control system. The gains are selected as part of an iterative trial-and-error process with the tests that will be discussed later and optimization of these gains is a non-trivial exercise [16].

3.8.6.3 Phase locked loop

This element is able to measure the frequency and phase of a voltage in the system. The measurement location will be a bus bar. The PLL will return the phase and the frequency of the measured voltage. However, the input voltage is defined by a composite model i.e. node

voltage measurement or directly by a node-reference in the input-dialogue box of the PLL [14].

Table 3.12 is the overall summary of the components of the HVDC transmission system. This transmission line elongates 574 km and is modeled using 579 mH Smoothing Reactor inserted at both ends of the transmission lines. The transmission lines are made up of four poles having four sub conductors in each.

Table 3.12 Summary of HVDC Transmission System

Station	Converter		Shunt	Converter Transformer	
	12-pulse bridge	Rating MW	MVAR	MVA	Voltage ratio Y-Y,Y-Δ
Generation side	2×(±500 kV dc)	2×2625	2×1575	8×781	20/210
Menagesha side	2×(±500 kV dc)	2×2625	2×1575	8×761	205/400
Station	Controllers				
	Current Controller	Gamma Angle Controller	α min, α max angles	γ min, Angle	
Generation side (Rectifier)	*	-	$5°, 90°$	-	
Menagesha side (Inverter)	*	*	$110°, 150°$	$17°$	

CHAPTER FOUR
TECHNICAL AND ECONOMICAL COMPARISONS OF HVDC WITH HVAC

Bulk power could be transferred using HVDC or HVAC transmission system from a remote generating station to the load center. Before implementation of those transmission systems, technical performance and cost comparison between HVAC and HVDC system needs to be carried out before implementation.

From the technical comparison point of view, each transmission system has been evaluated based on comparative parameters, like transmission line efficiency, and corona loss, to come up with an optimal transmission system.

In order to compare the cost, all main system components must be taken into consideration. For the dc alternative, investment cost of converter terminals, ac input/output equipment, filters, and the interconnecting transmission line must be accounted [8]. For the ac alternative, investment cost of transformers, the overhead line, light load compensation, and reactive power compensation must be accounted [8]. Beside to the investment cost, running cost of each transmission lines has been calculated in terms of energy cost. Finally, life cycle cost of each of the transmission lines for 35 years is evaluated. The assumptions used for comparison HVAC with HVDC are [21].

- *Two dual circuit HVAC line, and*
- *Two bipolar overhead HVDC lines with the same voltage and power ratings.*

4.1 Technical Aspect

4.1.1 Transmission system efficiency

While designing a transmission line care must be taken on the loss of power within a transmission system to maintain the efficiency of the transmission system within desirable limit. This section covers comparison of HVDC and HVAC transmission systems in terms of the power loss of each transmission system components. The major transmission system components for HVDC are: converters station at each end of the transmission line and the transmission line itself. For HVAC major transmission system components are: Step-Up transformers at the generation side, Transmission line, and Step-Down transformers at the Menagesha side.
The transmission line designed by EEPCo planning office employs two double circuit 500 kV transmission line. Each of 15 Generation units are connected to 15 (350 MVA) transformers which are used to step up the

voltage from 20 kV to 500 kV. At the receiving end (at Menagesha), there are 7× (750 MVA, 500/400 kV) transformers that are used to step down the voltage level of the transmission line to the main grid voltage level i.e. 400 kV.

On the other hand the proposed HVDC transmission line employs two ±500 kV bipolar transmission line. Each bipolar line has four rectifiers at the sending end and 4 inverters at the receiving end that are used for the conversion of voltage from ac to dc and then back to ac respectively. Each converter has converter transformers used to step up the voltage levels as per the design requirements.

Depending on the overall transmission system components, the performance of the transmission system with respect to power losses has been evaluated to determine which transmission system is best performing.

Since the generator data's and the main grid data at the Menagesha substation is same for both the HVAC and HVDC transmission systems, these are not involved in the performance comparison parameters such as generation efficiency.

HVAC transmission system

Table 4.1 PSS/E HVAC system simulation output data.

Parameters	Generation Station	Sending end	Receiving end	Menagesha Station
Power, MW	5250	5181.6	4994.4	4967.9
Voltage, kV	20	500	480	400

The generation power is 5250 MW. The power coming out from the step up transformers is 5181.6 MW. The power losses in these transformers become 68.4 MW. So each transformer has 4.56 MW power losses. So, the efficiency of these 20/500 kV transformers becomes $\eta_{su} = 0.9869$.

From the PSSE simulation study of the HVAC transmission line developed by EEPCo, the power at the sending end of the transmission line is 5181.6 MW and the power at the receiving end of the transmission line is 4994.4 MW. So, the power loss in the transmission line is 187.2 MW. The efficiency of the 500 kV transmission line becomes $\eta_{TL} = 0.9638$.

The power received at the end of the transmission line (500 kV side Menagesha) and the power received at Menagesha 400 kV side is 4994.4 MW and 4967.9 MW respectively. So, the power loss in the step down transformers becomes 26.5 MW. So, the efficiency of the 500/400 kV transformers becomes $\eta_{SD} = 0.9946$.

The transmission system efficiency of the HVAC without corona loss is given by:

$$\eta_{Total} = \eta_{SU} \times \eta_{TL} \times \eta_{SD}$$

$$\eta_{Total} = 0.9460$$

In percentage, the efficiency of HVAC transmission line designed by EEPCo becomes 94.60 %. It has to be mentioned) and the total power loss becomes 282 MW or 5.4 % of the total generation power.

The voltage regulation of the HVAC is

$$\frac{500-480}{480}\times 100\% = 4.2\%$$

HVDC transmission system

Table 4.2 DigSILENT HVDC system simulation output data.

Parameters	Generation Station	Sending end	Receiving end	Menagesha Station
Power, MW	5249	5242	5055	5050
Voltage, kV	19.45	499	481	397

The full load losses for 500 kV bipolar HVDC line should be below 6.44% of the transmitted power [7]. The generation power is 5249 MW and the power at the sending of the transmission line is 5242 MW. So, the power loss in the rectifiers become 7 MW (0.133% loss, below the standard value, 0.6% [35]) and the efficiency of the rectifiers becomes η_{RC} = 0.9987. The power at the receiving end of the transmission line is 5055 MW and thus the efficiency of the transmission line becomes η_{TL}= 0.9644 and the power loss within the transmission line is 187 MW. The power received at the Menagesha station 400 kV side is 5050 MW. So, the power loss in the inverters become 5 MW (0.1 % loss) and the efficiency of the inverters becomes η_{IC} = 0.999.

So the efficiency of the bipolar HVDC transmission system becomes:

$$\eta_{Total} = \eta_{RC} \times \eta_{TL} \times \eta_{IC}$$
$$\eta_{Total} = 0.9622$$

The total loss of the two bipolar HVDC transmission systems becomes 199 MW.

The voltage regulation of the HVDC is

$$\frac{499-481}{481}\times 100\% = 3.74\%$$

Table 4.3 Transmission system comparisons without corona power loss

Comparison parameters	HVAC Transmission system	HVDC Transmission system
Transmission line efficiency	94.60 %	96.22 %
Voltage Regulation	4.2 %	3.72%
Loss	282 MW	199 MW

Without inclusion the corona loss, the HVDC transmission system is a bit more regulated than an HVAC transmission system. From the efficiency calculation the power loss of an HVDC transmission system is lesser than that of an HVAC transmission system.

4.1.2 Corona loss calculations

The real power loss due to corona, called corona loss, depends on meteorological conditions, particularly rain, and on conductor surface irregularities

AC corona losses are important to the design of the bundle conductor. With only a few kW/km of loss in fair weather, the level may increase 10-100 times during conditions of rain and may reach several hundred kW/km. DC corona losses are, however, of less concern to the design of the conductor bundles, since the increase during rain or hoarfrost is much smaller than with ac, only about 2-3 times [22].

The power loss due to corona for HVDC can be expressed [30]

$$P_{loss} = [2V(k+1)K_c \times n \times r \times 2^{0.25(g-g_o)}] \times 10^{-3} kW/circuit-km \quad (4.1)$$

where,

V = is the pole to ground voltage in kV

n = is the number of subconductors

r = is the radius of each subconductor in cm

g = maximum conductor surface gradient at operating voltage (in kV/cm)

g_o = 22 δ kV/cm where δ = relative air density

K_c = conductor surface coefficient which varies from less than 0.15 for smooth, clean conductor to more than 0.35 for conductor with imperfections

$k = (2/\pi)\tan^{-1}(2H/S)$

H = mean height of conductor

S = pole spacing

The relative air density δ is given by [30]

$$\delta = \frac{2.92P}{273+T} \quad (4.2)$$

The maximum gradient g is given by [30]

$$g = \frac{[1+(n-1)(r/R]V}{nr.\ln\frac{2H}{\left(nrR^{n-1}\right)^{1/n}[(2H/S)^2+1]^{1/2}}} \quad (4.3)$$

Where, R = radius of the circle passing through the centers of all sub-conductors in a bundle, in cm.

The corona loss evaluation of HVDC is started by having the following data.

Table 4.4 Conductor configuration and Rated values for HVDC transmission System [6, 19]

Items	Unit	Values
Rated Voltage (V)	kV	500
Radius of each sub conductor (r)	cm	1.699
Distance between Component conductor centers (S)	cm	45.7
Pole Spacing (a)	cm	1100
Min height of conductor above ground (h)	cm	1400
Number of component conductors in bundle (n)	-	4
Barometric pressure	kpa	73.749
Temperature	℃	40

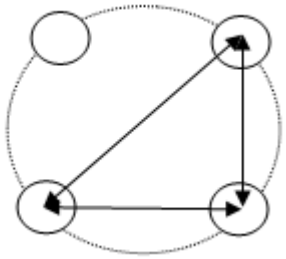

Figure 4.1 Configuration of a phase conductor having 4 sub conductors

$$(2R)^2 = 45.7^2 + 45.7^2$$

$$R = 32.31cm$$

$$g = \frac{[1+(4-1)(1.699/32.31)]\times 500}{4\times 1.699\times \ln\frac{2\times 1400}{\left(4\times 1.699\times (32.31)^{4-1}\right)^{1/4}[(2\times 14/11)^2+1]^{1/2}}}$$

$$g = 22\,kV/cm$$

And

$$\delta = 0.688$$
$$g_o = 22 \times \delta \, {kV}/{cm}$$
$$g_o = 15.1362 \, {kV}/{cm}$$
$$k = (2/\pi)\tan^{-1}(2H/S)$$
$$k = (2/\pi)\tan^{-1}(2 \times 14/11)$$
$$k = 0.762$$

Corona loss per pole per km is

$$P_{loss} = [2V(k+1)K_c nr \times 2^{0.25(g-g_o)}] \times 10^{-3} kW/pole-km$$
$$P_{loss} = [2 \times 500 \times (0.762+1) \times 0.15 \times 4 \times 1.699 \times 2^{0.25(22-15.1362)}] \times 10^{-3} kW/pole-km$$
$$P_{loss} = 5.9 kW/pole-km$$

For a total length of the line per phase

$$P = (5.9 kW/(pole-km)) \times 574 km$$
$$P = 3.386 MW$$

For a total length of the transmission line, the total corona loss of the two bipolar lines (i.e. 4 poles)

$$P = (3.386 MW/pole) \times 4$$
$$P = 13.544 MW$$
$$or,$$
$$P = 0.26\%$$

The power loss due to corona for HVAC

Calculations of Voltage Gradients for HVAC based on [26]

$$E = \left(\frac{V}{\sqrt{3}}\right) \frac{\beta}{\left(r \ln\left(\left(\frac{a}{R_e}\right)\left(\frac{2h}{\sqrt{4h^2+a^2}}\right)\right)\right)} \tag{4.4}$$

Where,

$$\beta = \frac{\left(1+(n-1)\frac{r}{R}\right)}{n}$$

$$R_e = Rn\sqrt{\frac{nr}{R}}$$

$$R = \frac{S}{2\sin\frac{\pi}{n}}$$

Table 4.5 Conductor configuration and rated values for HVAC transmission System [6]

Items	Unit	Values
Rated Voltage (V)	kV	500
Radius of Conductor (r)	cm	1.755
Distance between Component conductor centers (S)	cm	45
Phase Spacing (a)	cm	1150
Height of conductor above ground (h)	cm	1200
Number of component conductors in bundle (n)	-	4

First find out side radius of the bundle which is given by

$$R = 31.82cm$$

Factor for Multiple Conductors

$$\beta = 0.29$$

Equivalent Radius of bundle conductor

$$R_e = 59.783cm$$

The Conductor Surface Voltage Gradient become

$$E = 18.54\,{}^{kV}\!/_{cm}$$

The disruptive critical corona voltage of four bundle conductors can be obtained by [25]

$$V_{cr}^{b} = Em_o\delta \times \frac{4}{1+\frac{4.242r}{S}} \times r \times \ln\frac{GMD}{d_{SC}^{b}} \qquad (4.5)$$

Known values

$$\delta = 0.688$$

$$E = 18.54\,{}^{kV}\!/_{cm}$$

$$m_o = 0.85$$

$$D_{SC}^{b} = 0.218m$$

$$GMD = \sqrt[3]{a_{12}a_{23}a_{31}}$$

$$GMD = \sqrt[3]{11.5 \times 11.5 \times 23}$$

$$GMD = 14.489m$$

Where,

a_{12}, a_{23}, and a_{31} are the respective phase to phase distances

The disruptive critical corona voltage of four bundle conductors can be obtained by

$$V_{cr}^{b} = 18.54 \times 0.85 \times 0.688 \times \frac{4}{1 + \frac{4.242 \times 1.755}{45}} \times 1.755 \times \ln \frac{14.489}{0.218}$$

$$V_{cr}^{b} = 274.074kV$$

The corona loss for high voltage ac transmission line is given by [39]

$$P = \frac{241}{\delta}(f + 25)\left(\frac{R}{a}\right)^{1/2}\left(V_{phase} - V_{cr}^{b}\right)^{2} \times 10^{-5} kW/(phase - km) \quad (4.6)$$

Known values

$$V_{phase} = 500/\sqrt{3} = 288.675kV$$

$$V_{cr}^{b} = 274.074kV$$

$$D_{SC}^{b} = 0.218m = 21.8cm$$

$$f = 50Hz$$

$$S = 45cm$$

$$P = \frac{241}{0.688}(50 + 25)\left(\frac{31.82}{1150}\right)^{1/2}\left(288.675 - 274.074\right)^{2} \times 10^{-5} kW/(phase - km)$$

$$P = 9.32kW/(phase - km)$$

For 3-phase line

$$P = 27.96kW/km$$

For a total length of the line per phase

$$P = (27.96kW/km) \times 574km$$

$$P = 16.05MW$$

For two double circuit three phase (i.e. four 3-phases) transmission line. The total corona loss of the HVAC transmission line is.

$$P = (16.05 \times 4)MW$$

$$P_{Total} = 64.2MW$$

$or,$

$$P_{Total} = 1.223\%$$

In normal fair weather condition, the corona loss per phase per km for both HVAC and HVDC is 6 kW/km [22]. The HVAC transmission line has 9.32 kW/km corona loss that is beyond the standard value. But for HVDC, the corona loss per km is 5.9 kW/km which is around the standard value. Under abnormal condition, corona loss (kW/km) for HVDC increases only about 2-3 times. But HVAC With only a few kW/km of loss in fair weather, the level may increase 10-100 times during conditions of rain or frost and may reach several hundred kW/km [22].

The total corona loss of the HVAC transmission line is 64.2 MW and for the HVDC transmission line, the total corona loss is 13.544 MW. So that the corona effects such as radio interference, television interference and audible noise become more sever in HVAC line than HVDC line and thus HVAC transmission line has an impact to the Environment.

Table 4.6 Transmission system comparisons with corona power loss

Comparison parameters	HVAC Transmission system	HVDC Transmission system
Transmission line efficiency	93.40 %	96 %
Loss	346 MW	213 MW

The overall efficiency of the HVAC transmission system becomes 93.4 %, and the loss is 6.66 %. For HVDC the overall efficiency of the transmission system becomes 96 %, and the loss is 4 %. Losses at full load allowed for 500 kV two bipolar HVDC is 6.44 % and for two double circuits 500 kV HVAC transmission systems are 6.93 % [7].

So, from the efficiency calculations 133 MW power can be saved if two 500 kV bipolar HVDC transmission system is implemented for the proposed transmission line.

4.2 Economical aspect

In the previous section HVDC and HVAC transmission systems was compared based on the transmission line efficiency and corona loss comparison and seen that HVDC has better performance with respect to efficiency. In addition to this evaluation made above, the two systems have been evaluated in terms of the investment cost and energy cost as follows.

4.2.1 HVAC Investment cost

The detail investment cost is found in Annex D. The following Table 4.7 is only the summarized investment cost for the HVAC transmission system [6].

Table 4.7 Total investment cost of HVAC transmission line

Items	Total Price (USD)
Total Substation Cost	442,690,000
Transmission line Cost	688,800,000
Total Cost	1,131,490,000
Engineering and Administration (5% of the Total cost)	56,574,500.00
Total Project Cost	1,188,064,500.00
Physical Contingency (5% of the Total Project cost)	59,403,225.00
Price Contingency (10% of the Total Project cost)	118,806,450.00
Grand Total Project Cost	1,366,274,175.00

4.2.2 HVDC Investment Cost

The cost of a transmission line comprises of the capital investment required for the actual infrastructure (i.e. Right of Way (RoW), towers, conductors, insulators and terminal equipment) and costs incurred for operational requirements (i.e. losses) [16]. And the capital investment cost of converter stations includes cost of converter transformer, ac filters, valves, control and etc as it is shown in Figure 4.2 [21].

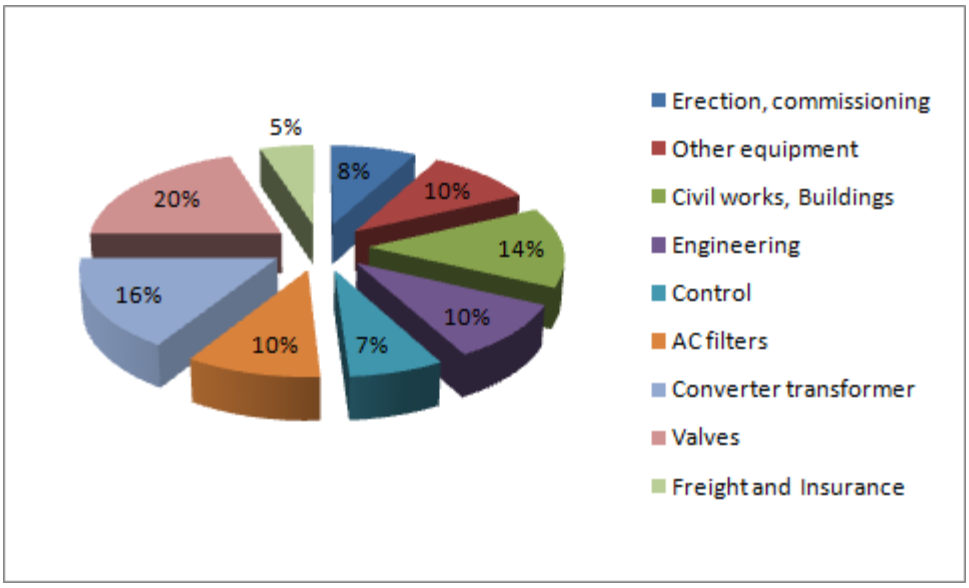

Figure 4.2 Cost structure for converter stations

The price per km for the bipolar OH line is 309,294 USD/km and for the converter station the average unit cost assumed is 64.7 kUSD/MW [23]. Two bipolar lines have been assumed with a capacity of each is 2625 MW. The average investment cost of HVDC overhead transmission system is done based Environmental and Social Impact Assessment (ESIA) & Resettlement Action Plan (RAP) cost for an HVDC Transmission system (4.0%), Physical Contingencies (5.0%), Price Contingencies (4.0%) and Engineering (4.5%) [17].

Physical Contingencies vs. Price Contingencies

It is common to encounter the term contingencies in project cost estimation and is an important concept in economic analysis of projects. Contingencies come in two categories:

- Physical contingencies - represent the estimated costs of the additional real resources expected to be required and therefore are always included in the economic analysis.
- Price contingencies - can arise either from expected changes in relative prices of project inputs or from expected general inflation and changes in the value of the monetary unit in which costs are measured. Only in the first case are they included in the economic analysis.

Table 4.8 Average investment cost of HVDC bipolar transmission system.

Cost item	2×(±500 kV, 2625 MW) Bipolar Transmission line Cost Estimation	
Line length	km	574
Line Costs	USD /km	618,588.00
total Line Costs	USD	355,069,512.00
ESIA & RAP of Line	%	4
Subtotal EIA & RAP Costs	USD	14,202,780.48
Power of one Converter unit	MVA	656.25
unit cost	kUSD /MVA	64.7
Converter cost	k USD	42,459.38
Total converter cost	k USD	679,350.00
Subtotal cost	USD	1,048,622,292.48
Physical Contingencies (5%)	USD	52,431,114.62
Price Contingencies (5%)	USD	52,431,114.62
Engineering (4.5%)	USD	47,188,003.162
Total cost	USD	1,200,672,524.890

From the Investment cost comparison, it is seen that, the two double circuit HVAC transmission system costs about 1.37 Billion USD and the two bipolar HVDC transmission system costs about 1.20 Billion USD. It is obvious to see that 0.17 Billion USD investment cost can be saved if two bipolar HVDC transmission system is implemented instead of two double circuit HVAC transmission line as proposed by EEPCo.

According to ABB (is a leader in supplying HVDC transmission system equipments all over the world) Power Technologies posted in 2012 [22], the trend of power electronic components, for use in the main circuit of an HVDC transmission, being developed means that the relative cost of HVDC transmissions is reduced as the components become cheaper as a result of continuing innovative technological developments. Thus a large converter station costs about 50 kUSD/MW which is cheaper in current dollars compared with the situation 20 years ago.

Table 4.9: Average investment cost of HVDC bipolar transmission system

Cost item	2×(±500 kV,2625 MW) bipolar Transmission line Cost Estimation	
Line length	km	574
Line Costs	USD /km	618,588.00
total Line Costs	USD	355,069,512.00
ESIA & RAP of Line	%	4
Subtotal EIA & RAP Costs	USD	14,202,780.48
Power of one Converter unit	MVA	656.25
unit cost	kUSD /MVA	50
converter cost	k USD	32,812.50
Total converter cost	k USD	525,000.00
Subtotal cost	USD	894,272,292.48
Physical Contingencies (5%)	USD	44,713,614.62
Price Contingencies (5%)	USD	44,713,614.62
Engineering (4.5%)	USD	40,242,253.162
Total cost	USD	1,023,941,774.890

According to Table 4.9 the savings of using an HVDC transmission system has been increased to 0.35 Billion USD compared to HVAC transmission system due to continuing innovative technological developments.

4.2.3 Power Loss Cost Calculations

All transmission lines have losses in that a small portion of the energy flowing through the conductors leaves a line as heat. The cost of losses dependes on the resistance of the conductors, current levels and dollar value of power and energy [18].

Life cycle costing

Money has a time value because of the existence of interest. The concept of compounding money due to an interest payment is well known. If an investment is made the principal will compound each year as interest is paid again and again on the principal plus the interest earned. The result is that the future value of an investment is worth more than its present value.

One widely accepted approach of comparing options over their life-cycles is to bring all costs to a single point in time-the present. This can be done by applying present value (PV) factors to all costs to provide an overall PV cost.

Calculation of the PV for the transmission line loss

1. Account the cost data

Losses: Electrical losses occur 24 hours a day, every day. As stated before, electrical losses are primarily dependent on the square of the current flowing through the conductor. The cost of losses also increase with time and the cost data used in the study is detailed below in Table 4.10.

Table 4.10 data used for PV cost analysis [6-10]

Description	**Unit**	**Value**
Economic Life of transmission line	Years	35
Energy cost	$/kWh	0.027
Capacity cost or Energy generation cost	$/kWh	0.02724*
Load factor	-	0.57
Loss factor	-	0.38*
Discount rate	-	10%

Load factor (electrical): is the average power divided by the peak power over a period of time. In the electricity industry, load factor is a measure of the output of a power plant compared to the maximum output it could produce.

Loss factor: is the ratio of average/peak losses during a designated time period.

The discount rate: The interest rate used in discounted cash flow analysis to determine the present value of future cash flows. The discount rate takes into account the time value of money (the idea that money available now is worth more than the same amount of money available in the future because it could be earning interest)

* The capacty cost in $\$/(\text{Kw}-\text{year})$ is converted to $\$/\text{Kwh}$ as per [10].

$$C_c(\$/(\text{Kw}-\text{year})) = C_c(\$/\text{Kwh}) \times 0.396 \times 8760 \text{ hours}$$

Since C_c= 94.5 $/kW/Year [6]

$$C_C = \frac{94.5}{(0.396 \times 8760)} = 0.02724 \, \$/kWh$$

*Loss factor for the Extra High Voltage (EHV) lines is assumed to be 0.38 [10].

2. Calculation of the annual cost

Losses

The annual cost of losses is given by [18].

$$LC = \frac{RI^2 8760}{1000 L_D^2}\left(L_o E_c + C_c\right) \tag{4.7}$$

3. Calculate the Life Cycle Cost

The formula used for finding the present value (PV) of an annually recurring loss cost (LC) is the following [31]:

$$PV = LC \times \left(\frac{(1+d)^N - 1}{d(1+d)^N}\right)$$

or,

$$PV = LC \times \left(\frac{1-(1+d)^{-N}}{d}\right) \tag{4.8}$$

So the life cycle cost analysis is done based on Table 4.8. The conductor selected for HVDC transmission line is Grackle having a resistance of 0.0472 Ω/km and the conductor used for HVAC is Pheasant having a resistance of 0.043 Ω/km. Since the transmission line conductor is bundled with 4 sub conductors, the equivalent resistance for HVDC become 0.0118 Ω/km and for HVAC become 0.01075 Ω/km. The annual loss cost of each of the transmission lines is shown below in Table 4.11

Table 4.11 Annual loss cost of HVDC and HVAC transmission line conductors.

	R (ohm/km)	I (A)	L_D	L_o	E_c	C_c	LC (USD/km/year)	PV (USD/km)
Grackle	0.0118	1312.5	0.57	0.38	0.027	0.02724	82,210.31	792,849.30
Pheasant	0.01075	842	0.57	0.38	0.027	0.02724	92,469.72	891,792.71

From the loss cost analysis the unit loss cost over a 35 years period for HVDC is 792,849.30 USD/km and for HVAC is 891,792.71 USD /km. Over a 35 years period, the loss cost for HVDC is around 0.455 Billion USD and for HVAC 0.512 Billion USD. Therefore, 0.057 Billion USD can be saved over the life cycle of the transmission lines. Even through the ohm/km of an HVDC line is

greater than the HVAC line, the savings is due to the number of conductors in HVAC line (i.e. 12) is greater than that of HVDC line which is 4.

To see the economic advantages of each of the transmission lines over the distance specified i.e. 574 km, the total cost i.e. the investment cost and the loss cost of each transmission lines is considered as it is shown in Figure 4.3. This figure is developed using M-file code written in Mathlab.

Table 4.12 Data's used for the M-file code

	Total Station cost (USD)	Transmission line unit price per km	Loss cost unit price per km
For HVDC	679,350,000	618,588	82,210.31
For HVAC	442,690,000	1,200,000	92,469.72

M-file code

```
km = 0:100:600;
HVDC = (679350000+(618588).*km+82210.31.*km)/10^9;
HVAC = (442690000+1200000.*km+92469.72.*km)/10^9;
plot (km,HVDC,km,HVAC)
grid on
```

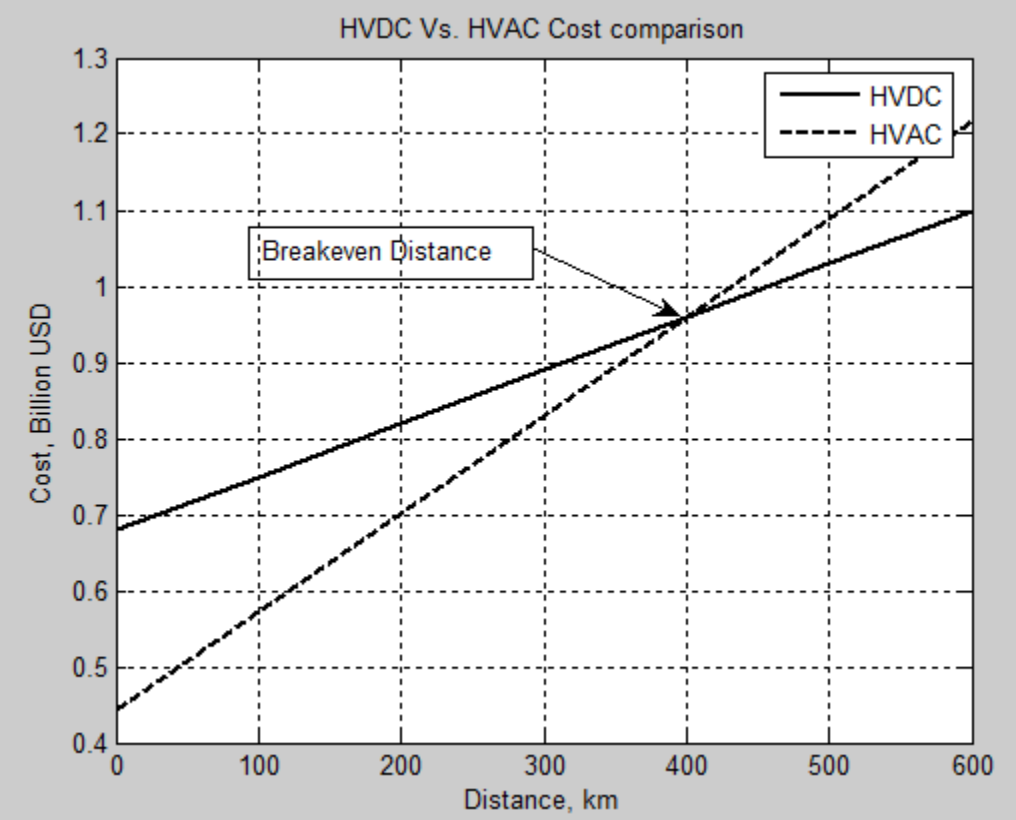

Figure 4.3 Comparison of HVDC and HVAC transmission lines

Figure 4.3 shows the variation of costs of transmission systems with distance for ac and dc transmission. AC tends to be more economical than dc for distances less than the "breakeven distance" but it is expensive for distances greater than the "breakeven distance". The break even distance obtained is around 400 km which is less than 574 km. It can be conclude that HVDC is more economical, interms the investment cost and loss cost, than HVAC for the transmission lengh specified. The substation costs for HVDC system is expensive than the HVAC system, but the loss cost of the HVAC transmission line is more expensive than the HVDC transmission line this is due to the number of conductors used for HVAC line which is greater than that of HVDC line.

CHAPTER FIVE

SIMULATION OF THE HVDC SYSTEM

In this chapter the performance of a bipolar HVDC transmission line is evaluated by initiating disturbances at different location of the transmission line. Before the discussion of the dynamic performance of the HVDC transmission system, the steady state and performance of ac filters for the harmonic load are simulated

5.1 The Bipolar HVDC System model

The HVDC bipolar model shown in Figure 5.1 is developed using DigSILENT software. Two models have been used for the simulation. The first is the Cigré HVDC Benchmark model developed in DigSILENT software [19] and the second is an HVDC bipolar transmission system developed in Mathlab/Simulink [40]. In this thesis work, these two models have been used to develop the bipolar HVDC transmission system for the Grand Renaissance Hydro Electric Power Plant (GRHEPP). This ± 500 kV bipolar line carries half of the generation power i.e. 2625 MW. Each pole has a bundle of 4 sub conductors and carries 1312.5 MW power. Two such kind of bipolar line is needed for the project under study.

The main components used to build the bipolar HVDC transmission system are listed below [19, 40]:

- Rectifier/Inverter converters
- Converter transformers
- Smoothing reactors
- Dc transmission lines
- Ac filters
- Generators, and
- External grid (infinite bus)

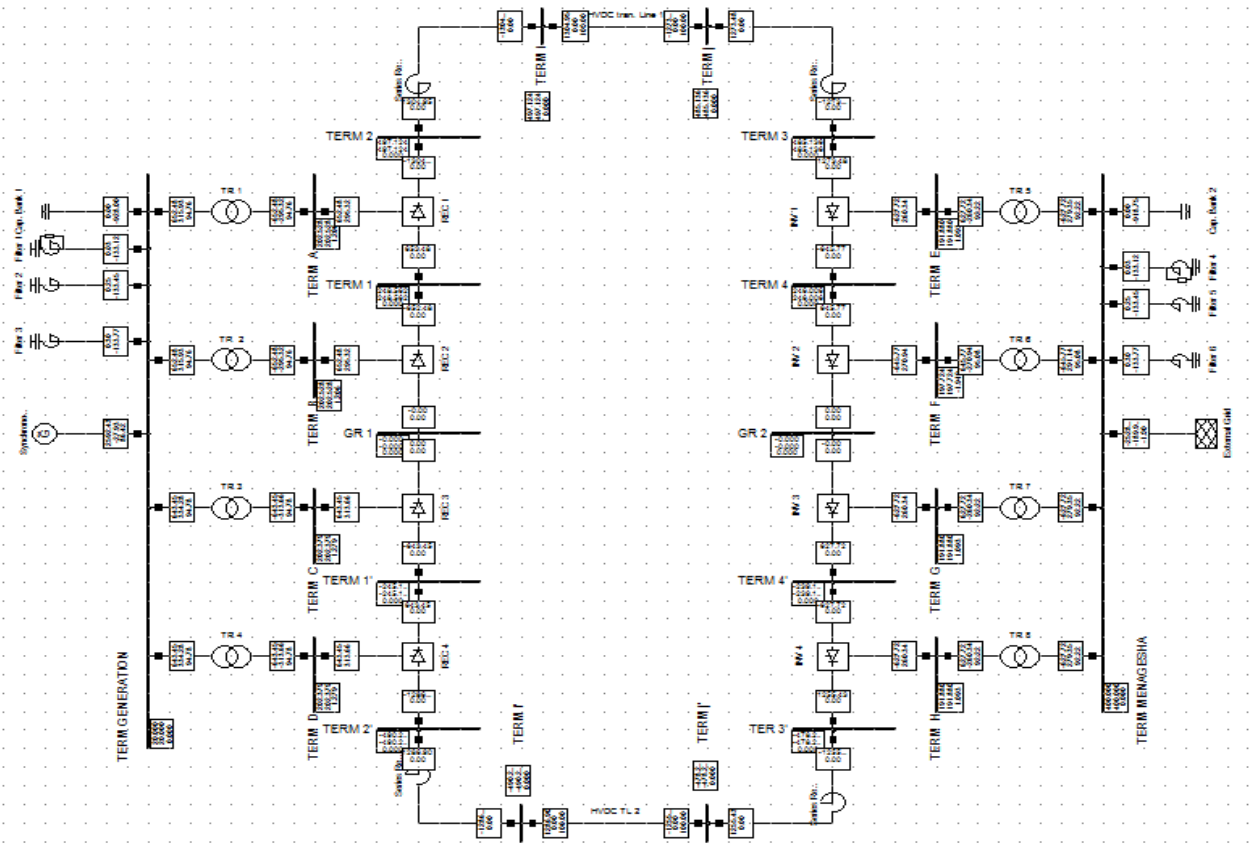

Figure 5.1 HVDC bipolar transmission line developed in DigSILENT

5.2 Steady State load flow of the System

A Steady State simulation does not consider the effects of time. It assumes that the plant or system has reached steady operating conditions. Steady State simulation of an HVDC transmission system model is done on DigSILENT software tool without creating disturbances or faults on the system. The purpose of the steady state simulation is to evaluate the time response of the system output that has reached steady operating conditions. In this load flow simulation Pole voltage, Pole current and Pole power has been simulated at the sending and receiving end of the transmission system. As it is seen on the wave shape outputs, these quantities come to their steady state values.

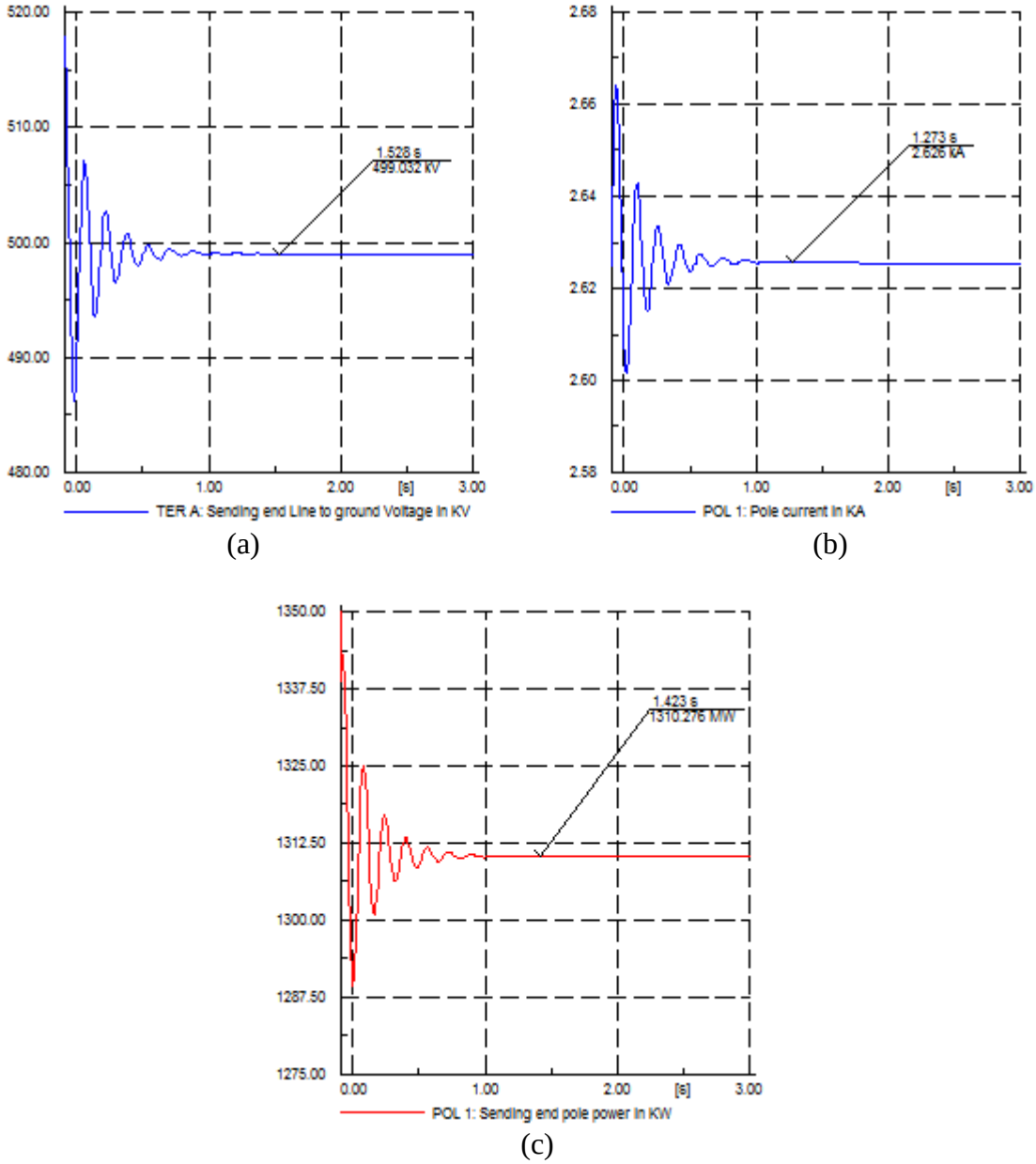

Figure 5.2 Steady state Simulation at the rectifier side. a) Sending end pole voltage. b) Pole current. c) Sending end Power of a single pole.

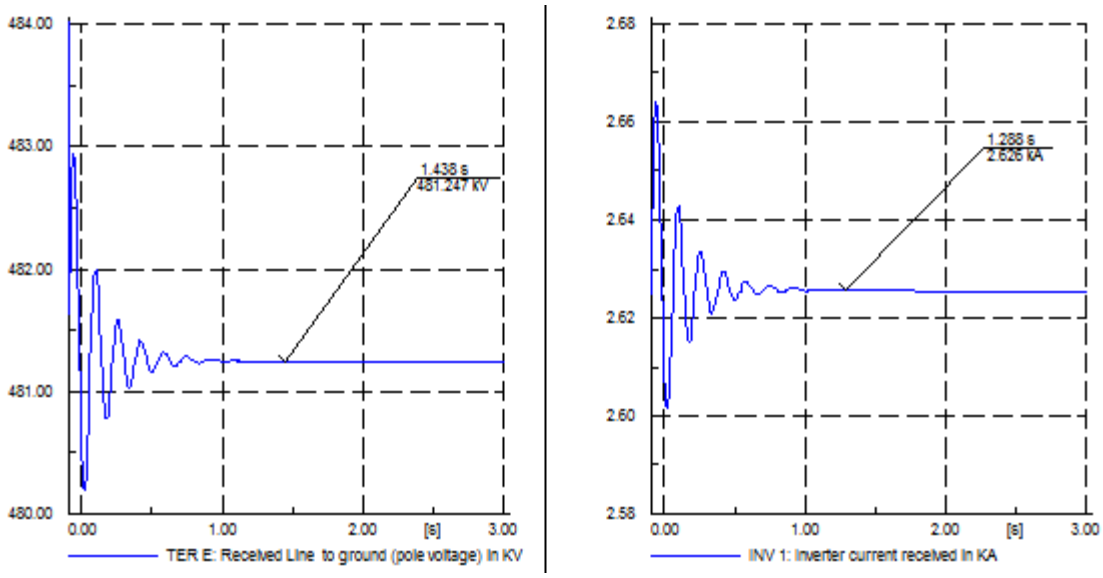

(a) (b)

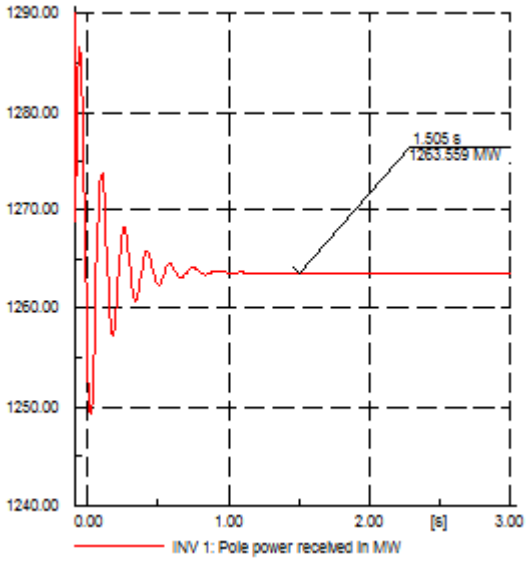

(c)

Figure 5.3 Steady State Simulation at the Inverter side. a) Receiving end pole voltage. b) Pole current. c) Receiving end Power of a single pole.

In Figure 5.2 (a) the dc voltage at the sending end of the transmission line is 499.0 kV or 1 p.u. and also in Figure 5.3 (a) the dc voltage at the receiving end of the transmission line is 481.2 kV or 0.96 p.u. these pole voltages falls within the range set by EEPCo. i.e. 0.95 to 1.05 p.u or (±5%, bus voltage variation). The voltage of the remaining bus bars and connecting terminals of the bipolar transmission system are also falls in the range stated before. And the current flowing through each pole is 2.626 kA which is nearly equal to the rating value of a single pole line i.e. 2.625 kA. The

power loss within one pole of the transmission line is 46.7 MW. For the two bipolar transmission line the power loss become 186.8 MW.

5.3 Harmonic load flow of the System

Harmonic load flow of the HVDC system is made to evaluate the performance of the shunt harmonic filters connected to each of 20 kV Generation bus bar and 400 kV Menagesha bus bar. These harmonic filters are used to eliminate harmonic orders such as 11^{th}, 13^{th}, 23^{th} and 25^{th} which are the dominant harmonics present for each of the 12 pulse converters (for bipolar line two 12 pulse converters are needed) The remaining harmonics are eliminated due to the phase shift transformers connected for each 12 pulse converters. The performance of the harmonic filters is evaluated based on the following specifications.

Current distortion specifications are defined as per [37] as follows:

Specified limits on HD are in the range of 0.5% to 1.5% (most typically 1%)

Specified limits on THD are in the range of 1% to 4%.

5.3.1 Rectifier Harmonics

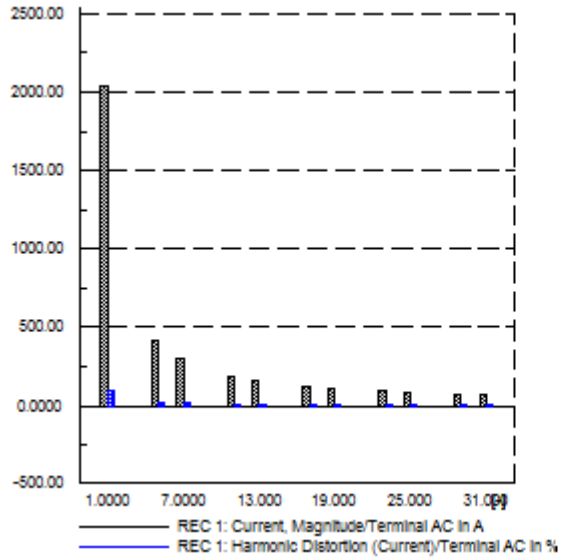

(a)

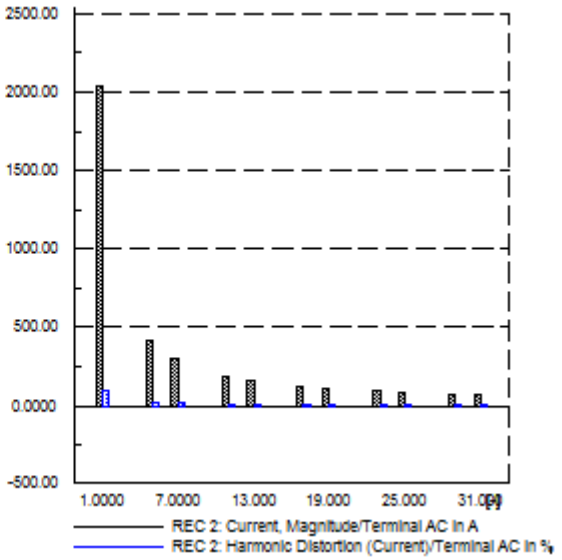

(b)

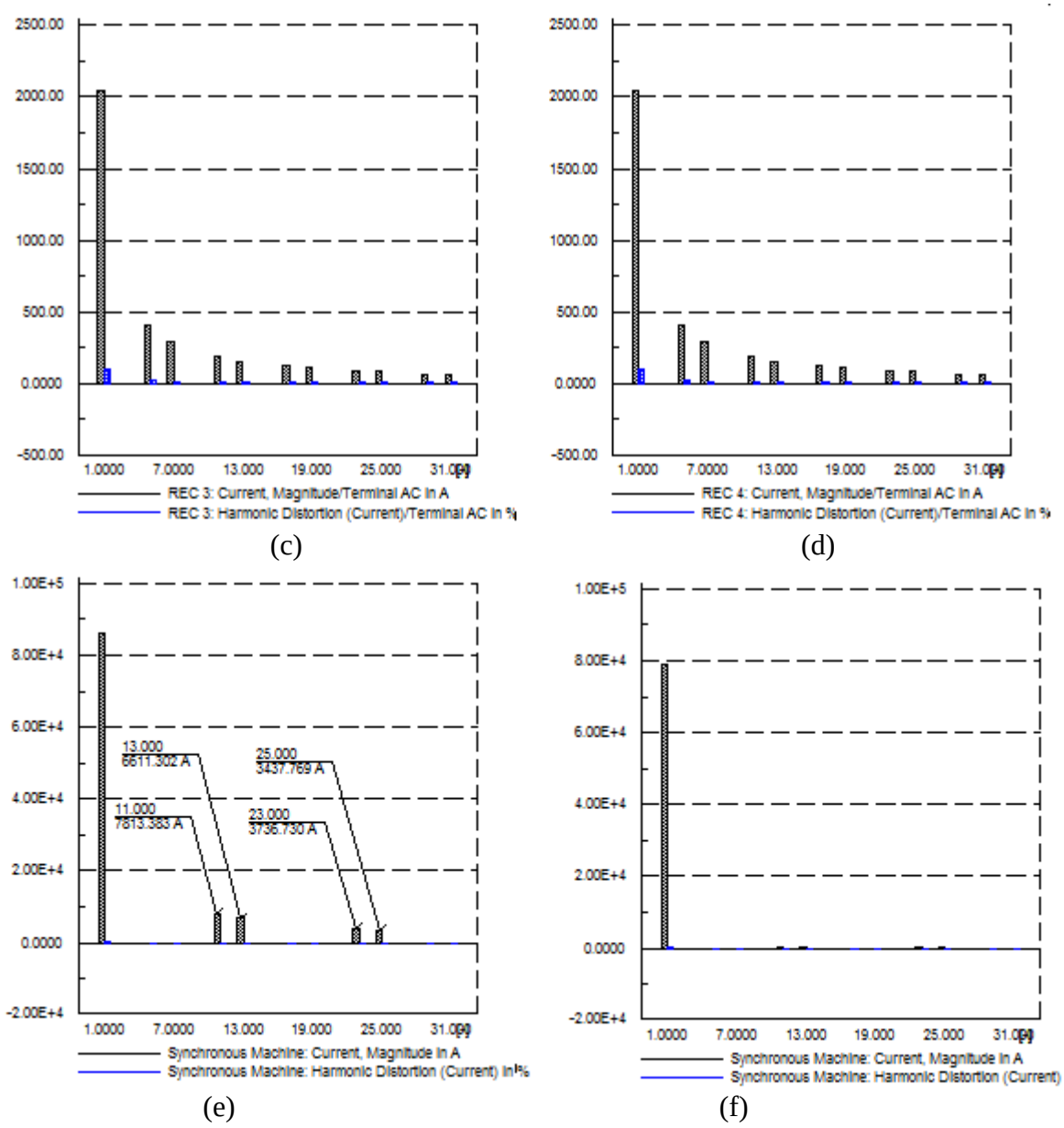

Figure 5.4 Harmonics on the Rectifier ac side. (a-d) are the harmonics present in each arm of the rectifiers present in the ac side e) Harmonics at the generation bus bar before filtering f) Harmonics at the generation bus bar after filtering

In Figure 5.4 (a-d) all the characteristic harmonics are presented for each ac side arm of the rectifiers. At the 20 kV generation bus bar the 5^{th} , 7^{th}, 17^{th} , 19^{th}, 29^{th} , and 31^{th} harmonics are eliminated due to the phase shift transformers but for 12 pulse converters still 11^{th} , 13^{th} , 23^{th}, and 25^{th} harmonics will remain the dominant harmonic as it is seen in Figure 5.4 (e) and needs harmonic filters to get eliminated.

From the harmonic simulation the THD at the Generation bus bar, where the harmonic filters are placed, before filtering is 40.03 %. This is beyond the standard values i.e. 1 % up to 4 %. After filtering the THD becomes 0.91 %.

5.3.2 Inverter Harmonics

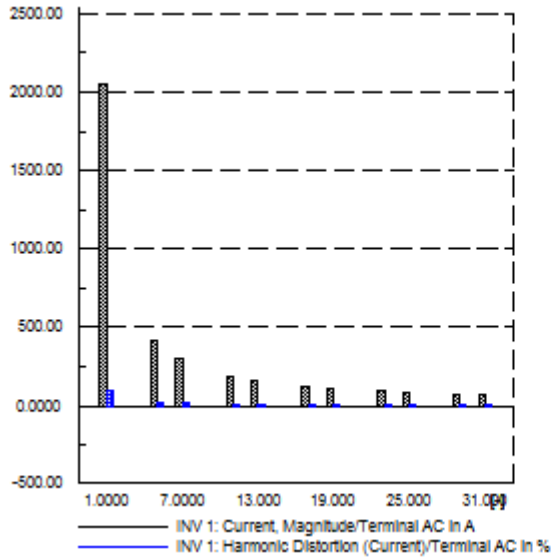

(a)

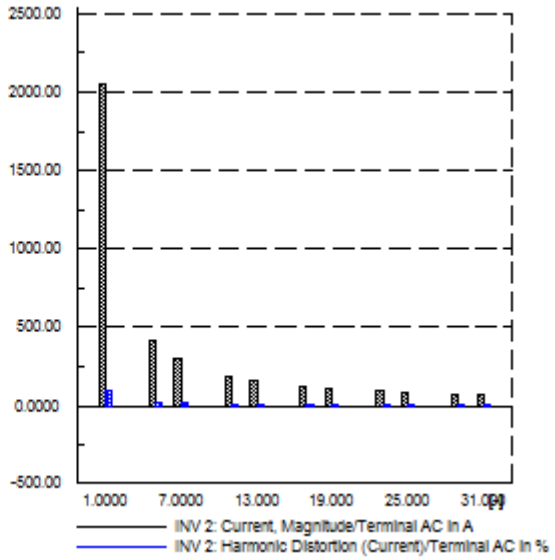

(b)

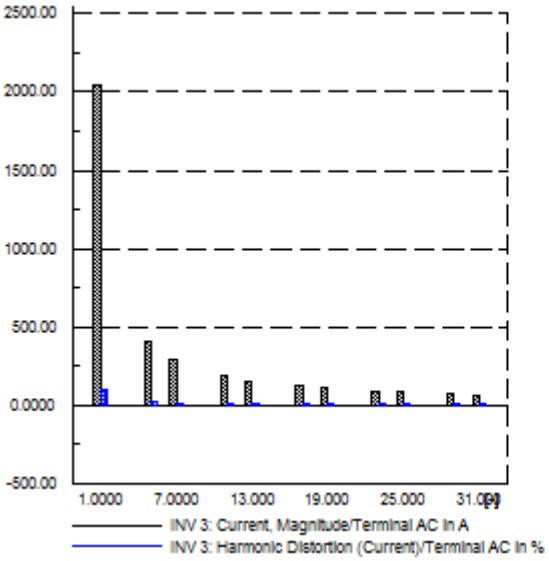

(c)

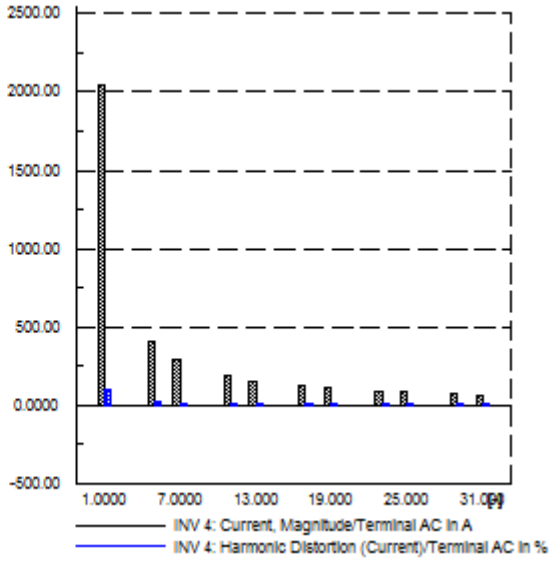

(d)

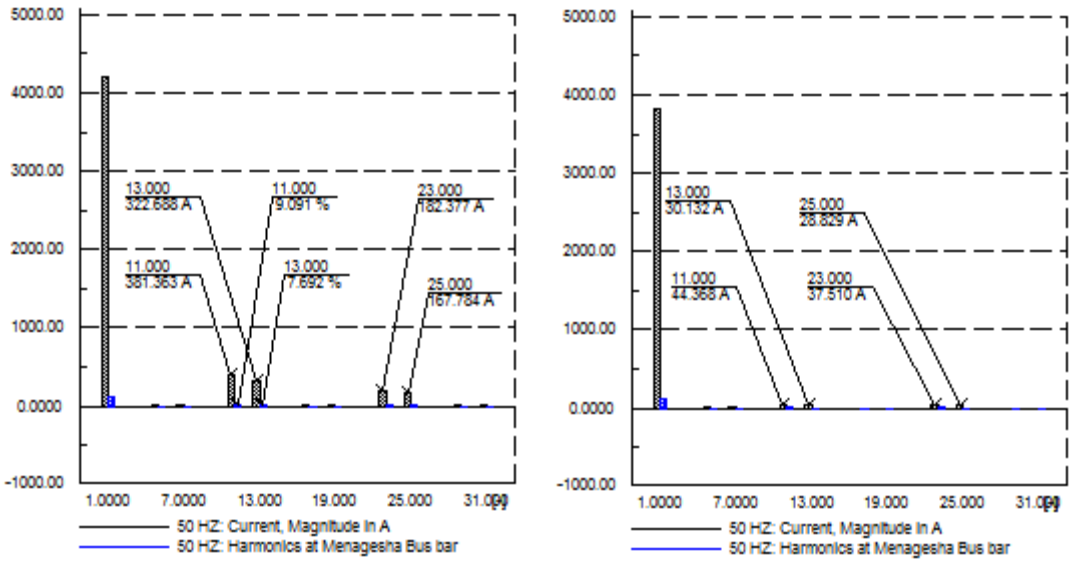

(e) (f)

Figure 5.5 Harmonics on the Inverter ac side. (a-d) are the harmonics present in each arm of the Inverters present in the ac side e) Harmonics at the Menagesha bus bar before filtering f) Harmonics at the Menagesha bus bar after filtering

In Figure 5.5 (a-d) all the characteristic harmonics are presented for each ac side arm of the rectifiers. At the 400 kV Menagesha bus bar the 5^{th} , 7^{th}, 17^{th} , 19^{th}, 29^{th} , and 31^{th} harmonics are eliminated due to the phase shift transformers but for 12 pulse converters still 11^{th} , 13^{th} , 23^{th}, and 25^{th} harmonics will remain the dominant harmonic as it is seen in Figure 5.5 (e) and needs harmonic filters to get eliminated.

From the harmonic simulation the THD at the Menagesha 400 kV bus bar, where the harmonic filters are placed, is 6.43 % before filtering which is out of the standard range i.e.1 % to 4 %. After filtering the THD becomes 0.94 %. The maximum HDs present at the Menagesha 400 kV bus bar are for the 11^{th} and 13^{th} harmonics. For each harmonics before filtering the HD is 9.091 % and 7.692 % respectively and this is out of the range i.e. 0.5 % to 1.5 %. But after the insertion of harmonic filters the HD becomes around to 0.

So, the harmonic shunt filters have an effective harmonic elimination performance in dealing with current harmonics generated at the Rectifier and Inverters that are injected to the ac side of the converters.

5.4 Dynamic Simulation of the System

A Dynamic simulation does consider the effects of time. It assumes that the plant or system is in a state of change. The specific objective of the dynamic simulation studies is to evaluate the stability and performance of the system after disturbances happening on the system. And dynamic simulation has also used for proper choice of circuit breakers and protective relaying. The magnitude of currents that would flow under short-circuit conditions shall be determined by fault analysis. The majority of the system faults are not three-phase faults /symmetrical faults/ but faults involving one line-to-ground or occasionally two lines-to-ground/unsymmetrical fault/. Even though it is infrequent, the symmetrical three phase fault analysis has to be carried out, as it generally leads to most severe fault currents from which the system shall be protected. It is this value, which is usually referred to determine the breaking capacity of circuit breakers. These breakers are placed in front of each of the phase shift transformers of the Rectifiers and after the phase shift transformers of the Inverters.

According to [6], three-phase short circuit faults are the standards used to test the dynamic performance of the transmission lines. In this thesis work, a three-phase short circuit fault is used as the standard fault type applicable to 20 kV Generation bus bar and 400 kV Menagesha bus bar. Transient Stability of the system is checked by applying the fault type on the system in the following sequence as per [6].

- For one second run system without disturbance
- Apply disturbance at T = 1sec
- Clear fault within 100 ms
- Needs 4 cycles to reach steady state operation after the fault is cleared.

A **grid code** is a technical specification which defines the parameters of a facility connected to a public electric network has to meet to ensure safe, secure and economic proper functioning of the electric system. The facility can be electricity generating plant, a consumer, or another network. The grid code is specified by an authority responsible for the system integrity and network operation.

In Ethiopia there is no grid code. So, it is difficult to compare weather the quantities that are under study may fulfill the regulations of the power company. However, for the project under study a reference is taken from Ethio-Kenya HVDC transmission line feasibility study, the voltage dips

during three phase short circuits faults may fall to zero. Accordingly all the parameters of the controllers are adjusted to come up with an optimal dynamic performance of the system.

5.4.1 Rectifier side ac system faults

For three-phase faults happening on the 20 kV Generation bas bar, the rectifier commutation voltage drops slightly. This results in a reduction of rectifier and inverter voltages and hence the direct (pole) current. The current controller of the rectifier decreases α to restore current by increasing voltage. The inverter control system will react to the decreased direct current and increase γ. Thus the rectifier and inverter controllers restore stable operation.

Rectifier simulation output

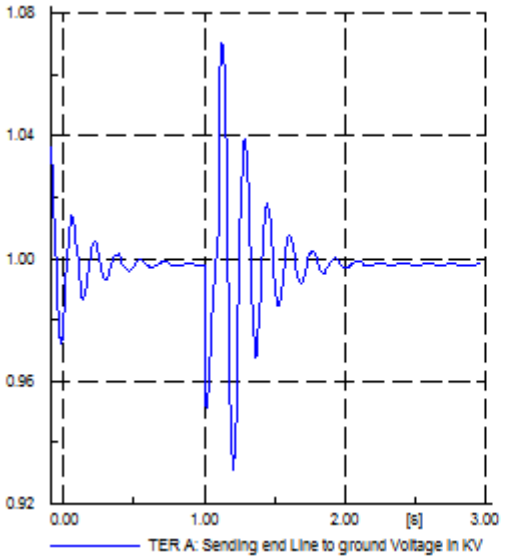

(a)

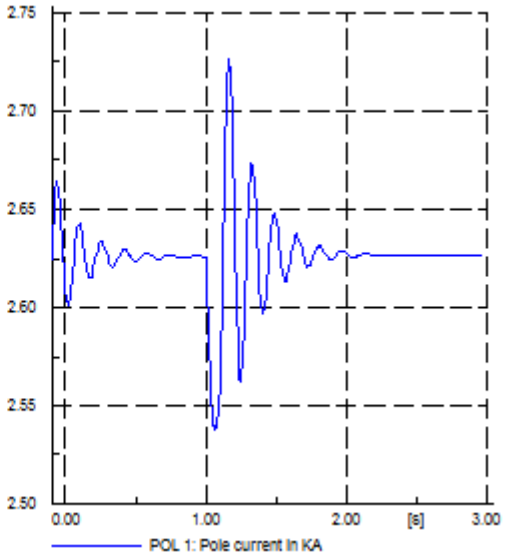

(b)

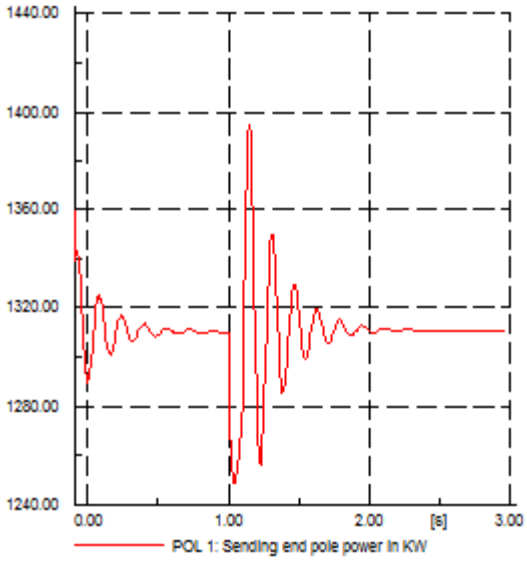

(c)

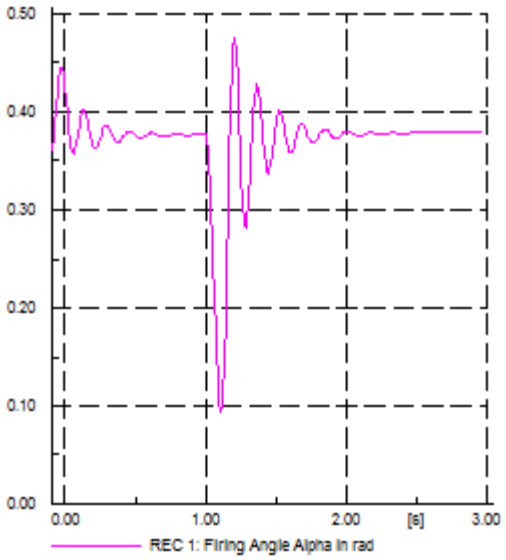

(d)

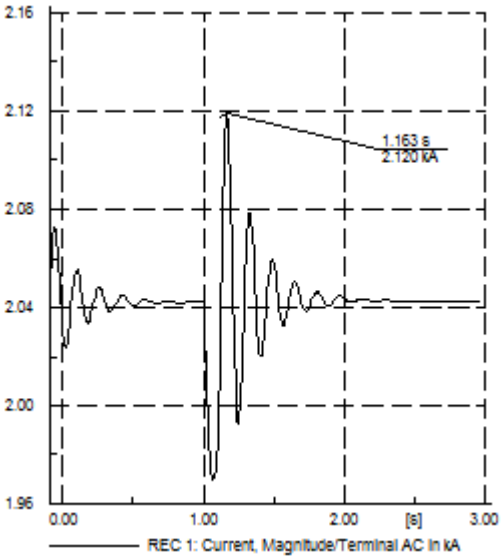

(e)

Figure 5.6 Dynamic state simulations on the Rectifier side due to faults on the Rectifier ac side. a) Line to ground pole voltage at the sending end. b) Pole current. c) Sending end real power d) Firing angle (alpha) e) Current in each phase shift transformers.

Inverter side simulation outputs

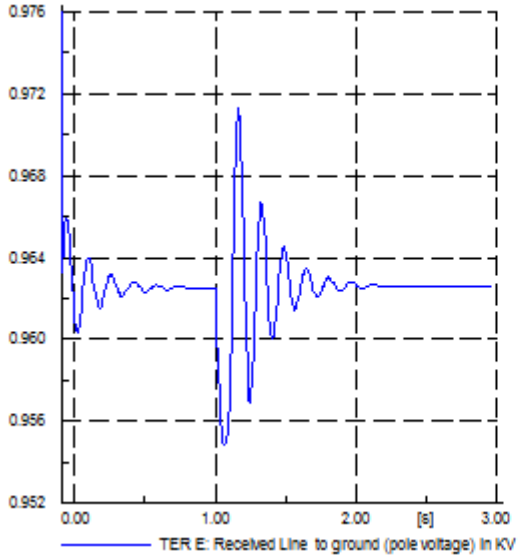

(a)

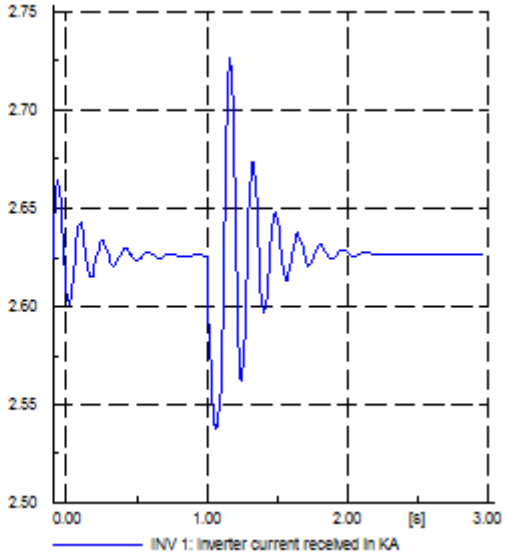

(b)

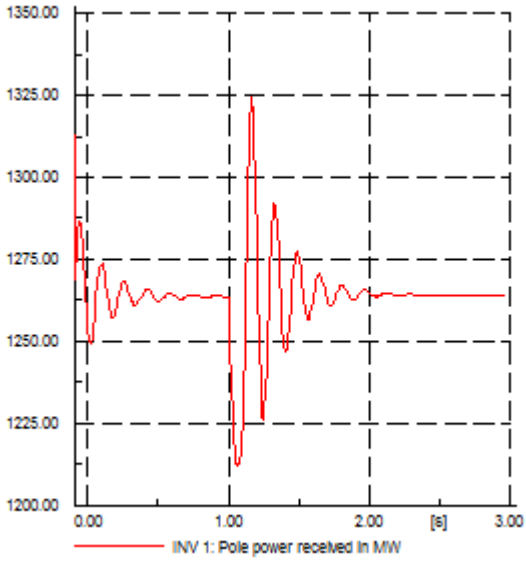

(c)

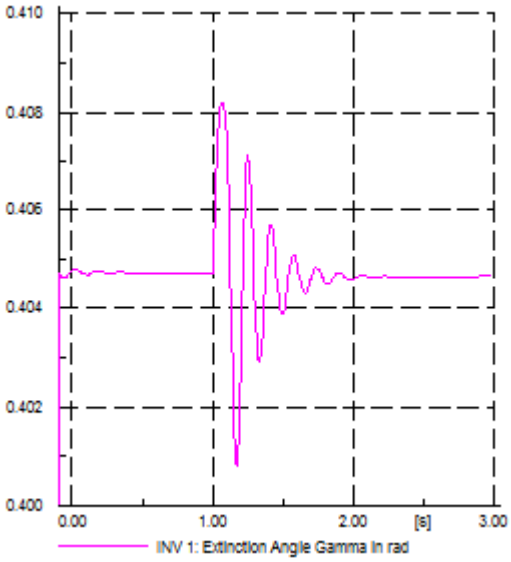

(d)

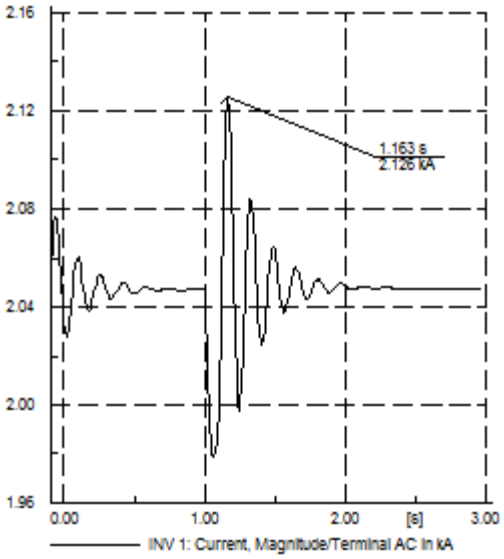

(e)

Figure 5.7 Dynamic state simulations on the Inverter side due to faults on the Rectifier ac side. a) Line to ground pole voltage at the receiving end. b) Pole current. c) Receiving end real power d) Extinction angle gamma. e) Current in each phase shift transformers

From Figure 5.6-5.7 (a) during fault happening on the 20 kV bus bar, the voltage dips at the sending end and receiving end of the transmission lines are 0.953 p.u. and 0.955 p.u. respectively. Under normal conditions the rectifiers control angle alpha ranges from $15° \; to \; 25°$ [3] but under abnormal or faulty conditions the control angle alpha shouldn't be below 5° [13]. From Figure 5.6 (d) alpha angle is 0.095 p.u. or 5.44° that is enough to operate the rectifier and recover back the system to its original steady state. Under abnormal conditions the Inverter control angle gamma should be above 17° [13]. From Figure 5.7 (d) the smallest value of gamma is 0.4007 p.u. or 23°. So, gamma angle satisfies the criteria. From Figure 5.6-5.7 (e) during the occurrence of the fault at the 20 kV Generation bus bar the current shoots up to 2.120 kA and 2.126 kA at each of the Rectifier and Inverter ac sides. So, the circuit breakers chosen should stand this overshoot current.

5.4.2 Inverter side ac system faults

For remote three-phase faults happening at the Menagesha 400 kV bus bar this results in small voltage dips at the inverter and hence increase in direct current occurs. Both the rectifier and the inverter controls respond to the changes. The rectifier increases it's α in order to keep the direct

current at the requested level. And the inverter control system will react to the increased direct current and decreases γ.

Rectifier side Simulation outputs

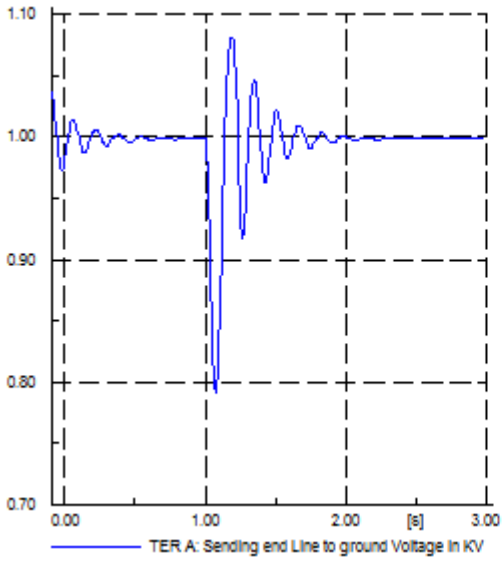

(a)

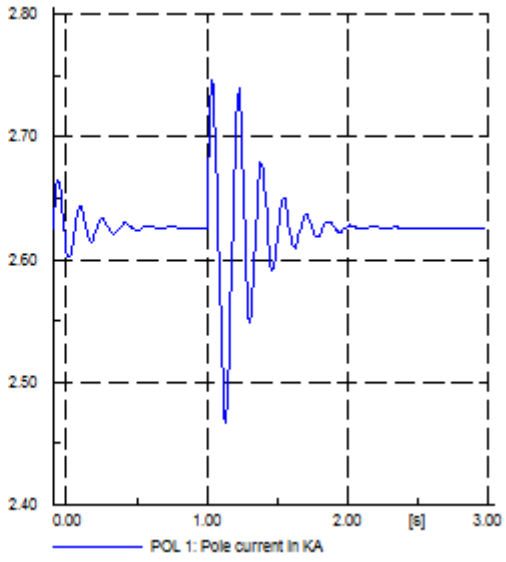

(b)

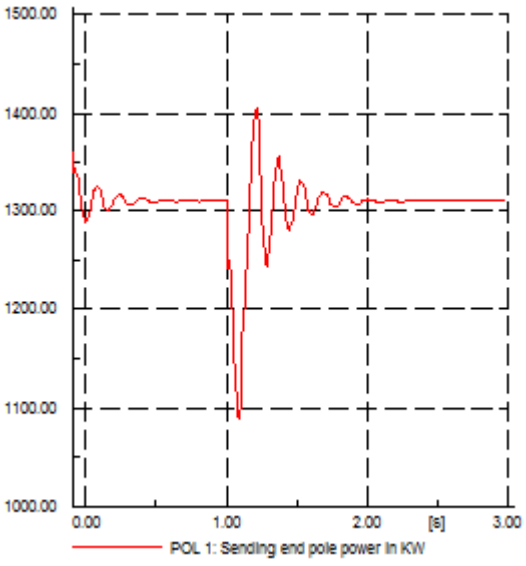

(c)

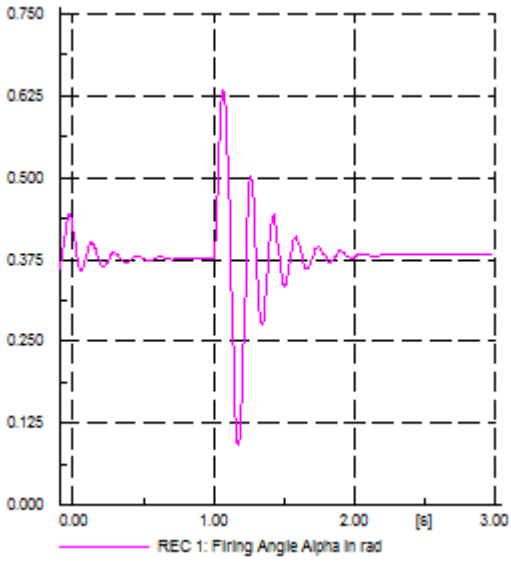

(d)

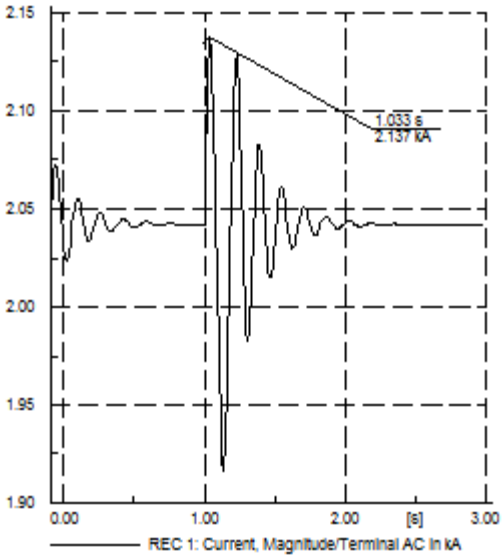

(e)

Figure 5.8 Dynamic state simulations on the Rectifier side due to faults on the Inverter ac side. a) Line to ground pole voltage at the Sending end. b) Pole current. c) Sending end real power of a single pole. d) Firing angle (alpha) e) Current in each phase shift transformers

Inverter side simulation outputs

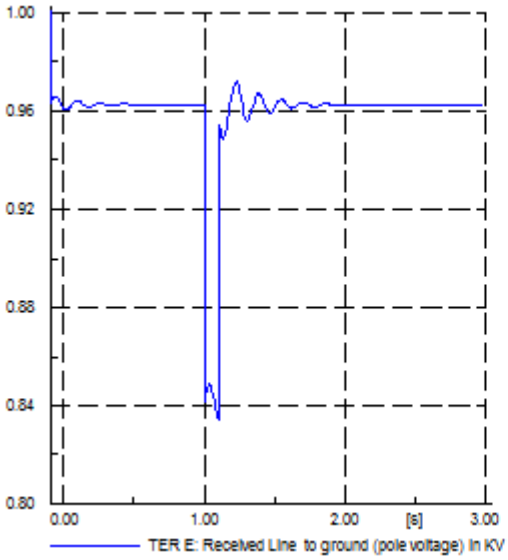

(a)

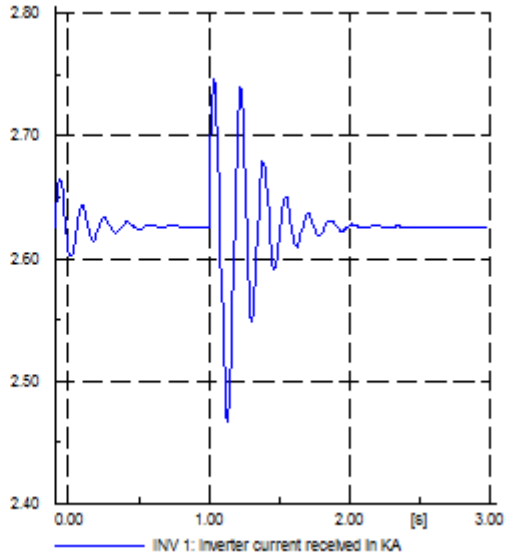

(b)

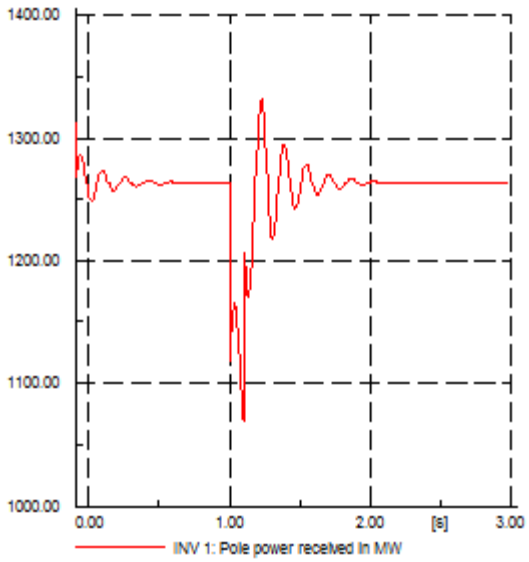

(c)

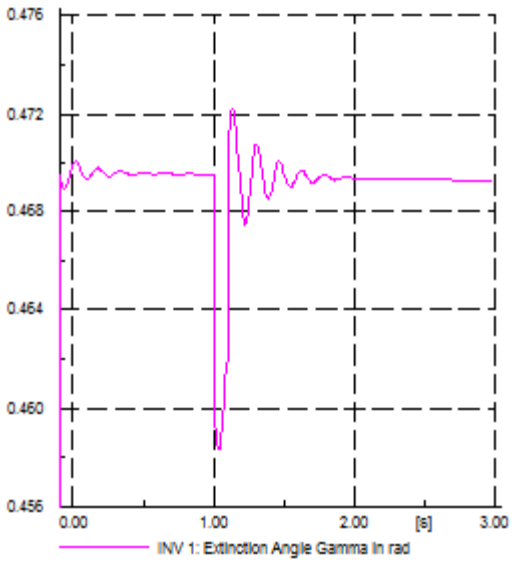

(d)

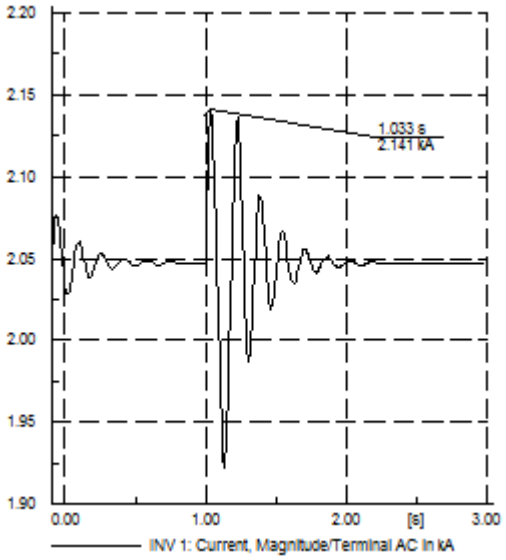

(e)

Figure 5.9 Dynamic state simulations on the Inverter side due to faults on the Inverter ac side a) Line to ground pole voltage at the receiving end. b) Pole current. c) Receiving end power of a single pole. d) Extinction angle gamma e) Current in each phase shift transformers

From Figure 5.8-5.9 (a) during fault happening on the 400 kV bus bar, the voltage dips at the Rectifier and Inverter are 0.835 p.u and 0.791 p.u. respectively. From Figure 5.9 (d) the smallest value of gamma is 0.458 p.u. or 26°. Under abnormal conditions the Inverter control angle gamma should be above 17° [13]. So, gamma angle satisfies the criteria. From Figure 5.8-5.9 (e) during the

occurrence of the fault at the 400 kV Menagesha bus bar the current shoots up to 2.137 kA and 2.141 kA at each of the Rectifier and Inverter ac sides. So, the circuit breakers chosen should stand this overshoot current.

2.137 kA and 2.141 kA are the maximum fault currents happening on each ac side of the Rectifiers and Inverters. So, the overall current rating of the circuit breakers at the Rectifier ac side and Inverter ac side should stand 2.137 kA and 2.141 kA respectively.

Finally the system cleared from the occurrence of three phase short circuit faults after four cycles which fulfills EEPCo criteria.

CHAPTER SIX

CONCLUSIONS, RECOMMENDATIONS AND SUGGETIONS FOR FUTURE WORK

Through the work done on this thesis the following conclusions are drawn.

6.1 Conclusions

Modeling of an HVDC transmission system is made based on Cigre HVDC bench mark model. Based on the bench mark model each components of an HVDC transmission system are designed. The designed HVDC bipolar transmission line fulfills the *N-1 Contingency criteria*.

An HVDC line has less power loss than an HVAC. The overall transmission system efficiency of the HVDC line is found to be for this particular case is 96 % and for HVAC line is 93.38 %. It has been seen in the evaluation that 133 MW power can be saved if two ±500 kV bipolar HVDC is employed for the Grand Renaissance Hydro Electric Power Project. For a total length of the transmission line, the total corona loss of the two bipolar lines is 13.544 MW and for an HVAC line the total power loss due to corona is 64.20 MW indicating that the HVDC is advantageous compared with the HVAC with respect to corona loss.

Due to the innovative technology progress the investment cost of an HVDC transmission system is lower than an HVAC transmission system and hence for an HVDC transmission system the investment cost is 17.4 Billion Birr and for HVAC it is 23.2 Billion Birr. Therefore, the savings become 5.95 Billion. The break even distance obtained for the case investigated is around 400 km which is less than the distance between Grand Renaissance Hydro Electric Power Plant to the EEPCo Main Grid at Menagesha substation which is 574 km, which indicates clearly that the HVDC is more economical compared to HVAC for the transmission distance length.

During steady state simulations the bus bar voltages falls within the limit set by EEPCo i.e. from 0.95 to 1.05 p.u. (or, ±5 %). From harmonic simulations the characteristic harmonics (5^{th}, 7^{th}, 17^{th}, 19^{th}, 29^{th} and 31^{th}) are cancelled out due to the phase shift transformers. The remaining harmonics (11^{th}, 13^{th}, 23^{th}, and 25^{th}) are eliminated using harmonic filters. THD at the Generation 20 kV and Menagesha 400 kV bus bars before connecting the shunt filters are 40.03 % and 6.43 %. After the insertion of the harmonic filters THD become 0.91 % and 0.94 % respectively and falls within the standard range i.e. 1 % to 4 %. And the HD of the each of the harmonic orders, after filtering, is

nearly to zero. In transient state simulations, during the occurrence of the fault the minimum voltage dips at the Rectifier and Inverter are 0.835 p.u and 0.791 p.u. respectively. Current rating of the circuit breakers at the Rectifier and Inverter ac sides should stand 2.137 kA and 2.141 kA respectively. After the occurrence of the fault at the Generation and Menagesha bus bars, the system comes to its steady state operation after 4 cycles. This fulfills the standard set by EEPCo.

6.2 Recommendations

Based on the result of this thesis work, it is strongly recommended that EEPCo has to implement an HVDC transmission system for the proposed transmission line length for the Grand Renaissance Hydro Electric Power Plant.

The power company, EEPCo has to develop Grid code which helps researchers to evaluate their designs to meet EEPCo's standard criteria's.

6.3 Suggestions for Future Works

In year 2017 (when the grand renaissance dam starts to generate power) most of transmission lines and transformers in the system are highly loaded, it is obvious that loss of any transmission line result in overloading, voltage dip and even partial or total blackouts during contingency. Thus contingency analysis is performed to ascertain the risks that contingencies pose to an electrical power system like transmission lines, transformers and etc. ***PowerFactory***'s (DigSILENT) contingency analysis module offers two distinct contingency analysis (non-probabilistic) methods: these contingency analyses should be done to the bipolar HVDC transmission system to determine power transfer margins or for detecting the risks inherent in changed loading conditions.

Single Time Phase Contingency Analysis:

The non-probabilistic (deterministic) assessment of failure effects under given contingencies, within a single time period.

Multiple Time Phase Contingency Analysis:

The non-probabilistic (deterministic) assessment of failure effects under given contingencies, performed over different time periods, each of which defines a time elapsed after the contingency occurred. It allows the definition of user defined post-fault actions.

REFERENCES

[1] EEPCo, "Grand Renaissance HEPP EEPCo EHV Power Transmission Project Feasibility Study", 2011.

[2] Kala Meah, and Sadrul Ula, "Comparative Evaluation of HVDC and HVAC Transmission Systems", IEEE, 2007

[3] M. P. Bahrman, P.E., "HVDC Transmission Overview", Downloaded from IEEE Xplore on November 20, 2008

[4] K. Pawani, Sachidanand Ojha , Rama Mishra " Recent Advances in High-Voltage Direct-Current Power Transmission System", International Journal of Advanced Technology & Engineering Research (IJATER), ISSN NO: 2250-3536 VOLUME 2, ISSUE 2, MARCH 2012.

[5] http://en.wikipedia.org/wiki/IEEE

[6] IEEE Power & Energy Society, "IEEE Standard General Requirements and Test Code for Dry-Type and Oil-Immersed Smoothing Reactors for DC Power Transmission", 14 February 2009.

[7] Bahrman M P, Johnson B K, "The ABCs of HVDC Transmission", IEEE power & energy magazine March/April 2007.

[8] IEEE Power Engineering Society, "IEEE Standard for Calculating the Current-Temperature of Bare Overhead Conductors", 30 January 2007.

[9] M. O. Faruque, Yuyan Zhang, and Venkata Dinavah, "Detailed Modeling of CIGRÉ HVDC Benchmark System Using PSCAD/EMTDC and PSB/SIMULINK", IEEE Transaction on Power Delivery, vol. 21, N0. 1, JANUARY 2006.

[10] D.G. Roice, R.J. Gursky, and Z. E. Trad, "Cost of Electrical Power Losses for use in Economic Evaluations", IEEE Transactions on Power Systems, Vol. 4, No. 2, May 1989

[11] Michael Bahrman, "HVDC Transmission an Economic Complement to ac Transmission", ABB, February 2-3, 2009.

[12] Michael Bahrman, "HVDC and FACTS Economical complements to ac transmission", ABB Grid Systems, DOE Concepts of Future Electric Transmission, March 4, 2009.

[13] Jonas Karlsson, "Simplified control model for HVDC Classic", Master of Science Thesis, Royal Institute of Technology, Stockholm, 2006.

[14] Wolfgang Hammer, "Dynamic Modeling of Line and Capacitor Commutated Converters for HVDC Power Transmission", Ph.D. dissertation, Swiss Federal Institute of Technology, Zurich, 2003

[15] J. Arrillaga, Y.H. Liu, N.R. Watson, "Flexible Power Transmission The HVDC Options", University of Canterbury, New Zealand ,2007.

[16] Vijay K. Sood, "HVDC and FACTS Controllers Applications of Static Converters in Power System", Kluwer Academic Publishers, Boston, 2004

[17] FICHTNER, "Ethiopia-Kenya Power Systems Interconnection Project", Basic Design Report, Volume 2, February 2009

[18] ACRES International Corporation, "Life-Cycle Cost Studies for Overhead and Underground Electric Transmission Lines", New York, July 1996.

[19] J. Duncan Glover, Mulukutlas S. Sarma, Thomas J. Overbye, "Power System Analysis and design", Fifth edition, Global Engineering, 2010.

[20] Energize, "Analysis and planning of a 1400 km HVDC link", PB Power, August 2005

[21] Roberto Rudervall, J.P. Charpentier, Raghuveer Sharma, "High Voltage Direct Current (HVDC) Transmission Systems Technology Review", ABB Power Systems, Presented at Energy Week 2000, Washington, D.C, USA, March 7-8, 2000

[22] Lars Weimers, "Bulk power transmission at extra high voltages, a comparison between transmission lines for HVDC at voltages above 600 kV DC and 800 kV AC.", ABB Power Technologies AB, 2012.

[23] A. L'Abbate, G. Fulli, "Modeling and Application of VSC-HVDC in the European Transmission System", International Journal of Innovations in Energy Systems and Power Vol. 5 no. 1, April 2010

[24] A. Singh, A.C. Britten, R. Stephen, D. Muftic, "Optimised Conductor and Conductor Bundle Solutions for Long Distance HVDC Transmission", Inaugural IEEE PES 2005 Conference and Exposition in Africa Durban, South Africa, 11-15 July 2005

[25] http://www.pdu.edu.eg. (Book Material corona discharge.pdf) Downloaded June 06 2012

[26] IEE Power Series 17, "High Voltage Engineering and Testing", ANNEXURE – B Calculation of Conductor Surface Voltage Gradient, Appendix 3.4.

[27] D.J.Melvold, W.F.Long, "Back-to-Back HVDC System performance with different Smoothing Reactors", IEEE Transaction on Power Delivery, Vol. No. 1, January 1989

[28] CET international, "Current HVDC project in China", December, 2010.

[29] ATCO Electric, "Eastern Alberta HVDC Transmission Project", May 2010

[30] K.R.Padiyar, "HVDC power transmission systems Technology and system interactions", New Age International (P) Ltd. 2005.

[31] Amy S. Rushing, "Energy Price Indices and Discount Factors for Life-Cycle Cost Analysis", Annual Supplement to NIST Handbook 135 and NBS Special Publication 709 September 2011.

[32] Sieglinde K.Fuller Stephen R.Petersen, "Life-Cycle Costing Manual for the Federal Energy Management Program", NIST Handbook 135, 1995.

[33] Michael Bahrman, P.E., "HVDC Transmission", IEEE PSCE Atlanta, November 1, 2006

[34] Nader Samaan, Member, IEEE, Robert Zavadil, Member, IEEE, J. Charles Smith, Senior Member,IEEE, and Jose Conto, Member, IEEE, "Modeling of Wind Power Plants for Short Circuit Analysis in the Transmission Network", IEEE, 2008.

[35] D.M. Larruskain, I. Zamora, A.J. Mazón, O. Abarrategui, J. Monasterio, "Transmission and Distribution Networks: AC versus DC", Spain, 2002.

[36] P. KUNDUR, "Power System Stability and Control", MCGRAWHILL, 1994.

[37] Dipti Khare, "Reactive Power Compensation and Harmonic Filters for HVDC Classic", ABB Group, March, 2009.

[38] J.Arrillaga, N.R.Watson, "Power System Harmonics", John Wiley & Sons, Ltd, 2nd Edition, 2003.

[39] S.Rao, "EHVAC, HVDC Transmission and Distribution Engineering", Khanna Publisher, , 3rd Edition, Delhi, 2008

[40] Hydro-Québec and The MathWorks, "SimPowerSystems User's Guide", 2011.

[41] B. K. Ghoda, "DICABS Conductors technical Catalogue", Diamond Cables Limited.

[42] Ethiopian Electric Power Corporation (EEPCo)

[43] HATCH, "DC1010-Voltage and Conductor Optimization", The Lower Churchill Project, April 2008.

[44] "DIgSILENT PowerFactory/Reference document/ Technical reference", Germany, 2007. [Available at: http://www.digsilent.de]

[45] J R Lucas, "High Voltage Engineering", 2001

[46] C. R. Bayliss and B. J. Hardy, "Transmission and Distribution Electrical Engineering", Newnes, 3rd edition, 2007

APPENDICES

Appendix A: Generation data and EEPCo Main Grid (Menagesha Bus bar) data

Table A.1 Generation Data [1]

System parameter	unit	value
Synchronous Reactance		
X_d	pu	2
X_q	pu	2
Transient Reactance		
$X_{d'}$	pu	0.3
Sub- Transient Reactance		
$X_{d''}$	pu	0.2
$X_{q''}$	pu	0.2
Zero sequence data		
X_0	pu	0.1162
R_0	pu	0.00145
Negative sequence data		
X_2	pu	0.1932
R_2	pu	0.02039
Inertia		
Inertia time constant(rated to Pgn) H	sec	10
Mechanical Damping	pu	0
Stator resistance/Leakage reactance		
r_{str}	pu	0
x_l	pu	0.1
x_{rl}	pu	0
Rotor type		
Salient pole	---	---
Transient time constants		

System parameter	unit	value
$T_{d'}$	sec	1
Sub- Transient time constants		
$T_{d''}$	sec	0.035
$T_{q''}$	sec	0.035
Steady state short circuit current		
I_{kd}	pu	1.2
Nominal frequency		
Frequency	Hz	50
Machine type		
IEC909/IEC60909 (Salient pole series 1	----	----
Generation Bus bar	kV	20

Table A.2 EEPCO Main Grid data [1]

System parameter	unit	value
Main grid	kV	400
Short circuit current (Ik'') in year 2017 GC	kA	$17.1604\angle -97.33^{o}$
Short Circuit MVA power (Sk'') in year 2017 GC	MVA	11889.07
Z_1=Z_2	ohm	$11.655\angle 97.33$ *

* The equivalent positive and negative sequence impedances are calculated using the following formula:

$$Z_1 = Z_2 = \frac{400\angle 0^{o}}{\sqrt{3}\times 17.1604\angle -97.33} = 11.655\angle 97.33\Omega$$

The base impedance is

$$Z_{base} = \frac{V_{baseLL}^2}{MVA_{base}} = \frac{400^2}{2625} = 60.95238\Omega$$

So, positive and negative sequence impedances in pu is $Z_1 = Z_2 = 0.1912\angle 97.33^{o}$

Appendix B: DIgSILENT implementation of the controllers

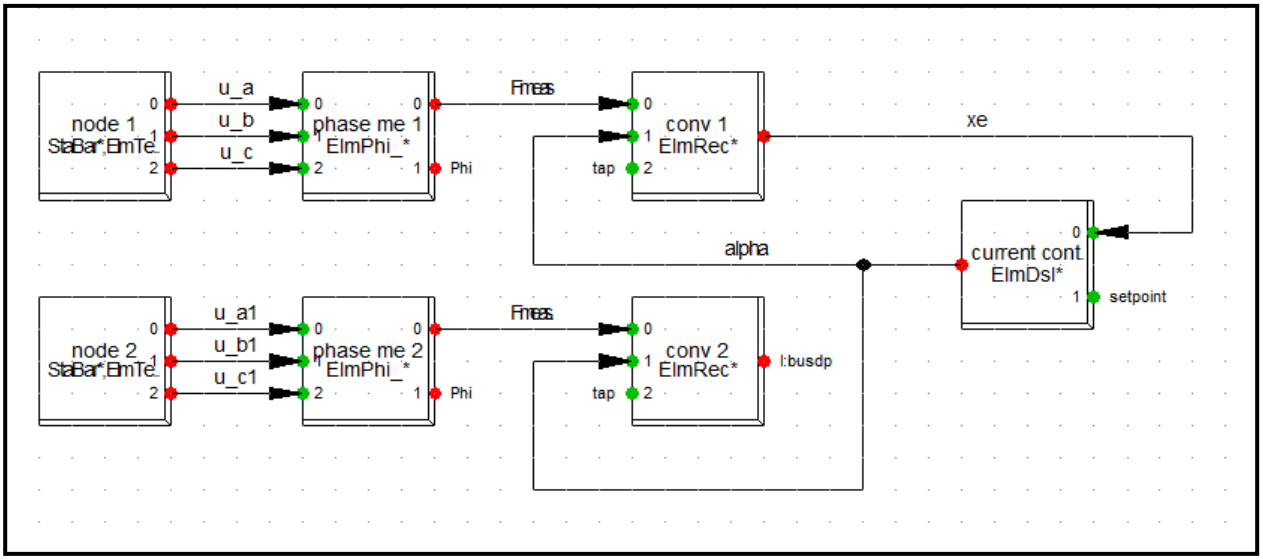

Figure B.1 Current controller implementation at the rectifier side

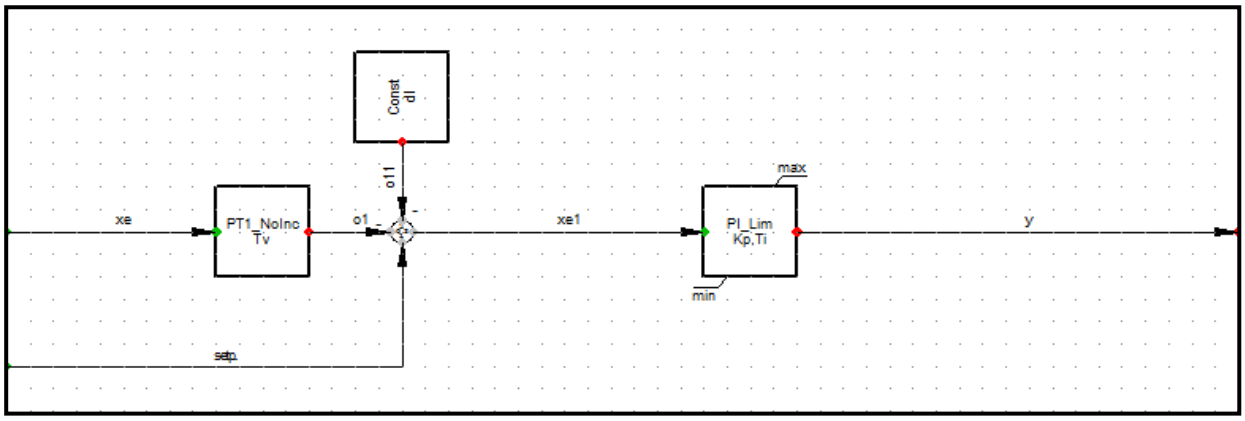

Figure B.2 Current controller [4]

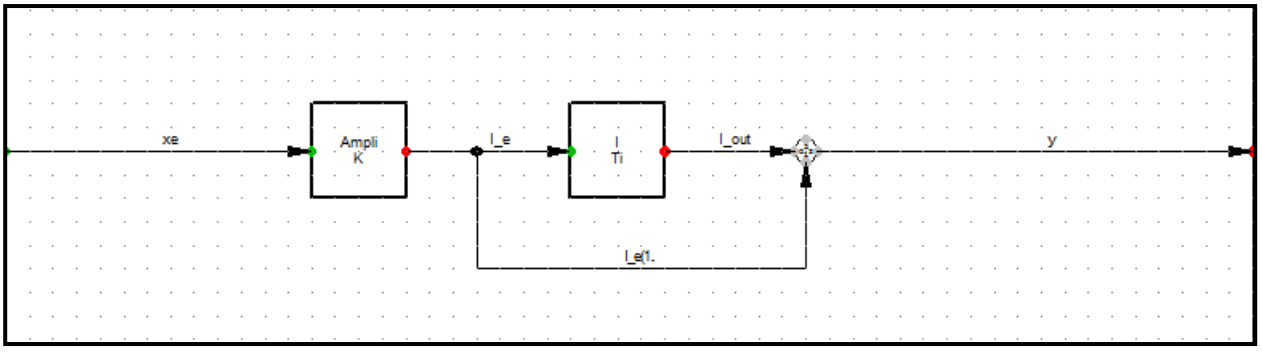

Figure B.3 PI controller [4]

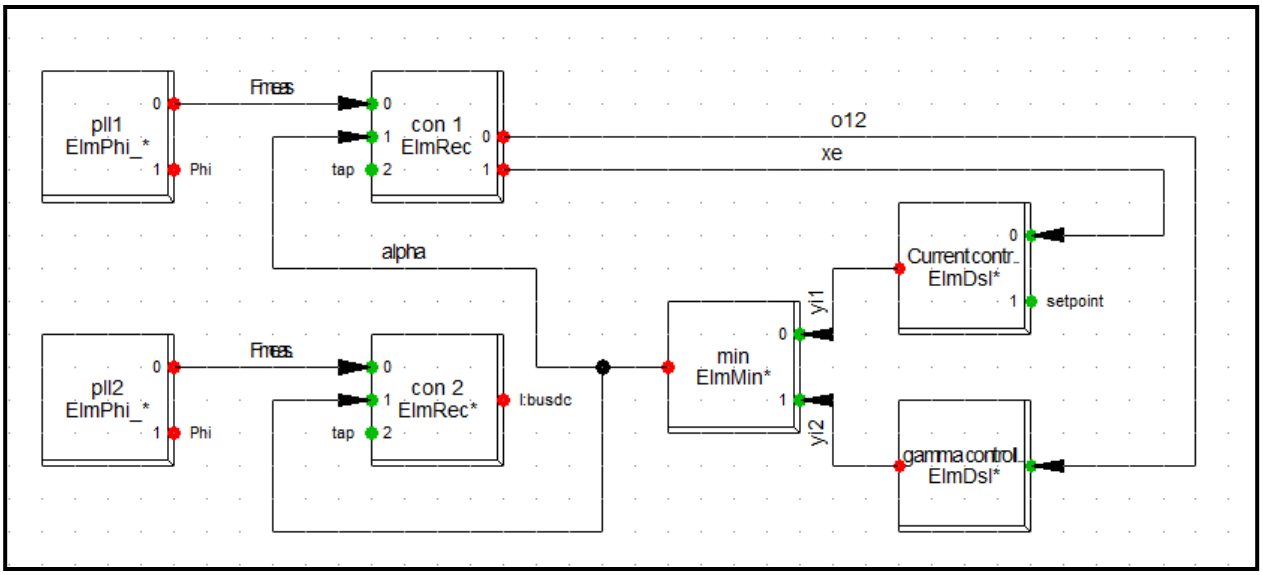

Figure B.4 Current and Gamma controller implementation on the Inverter side

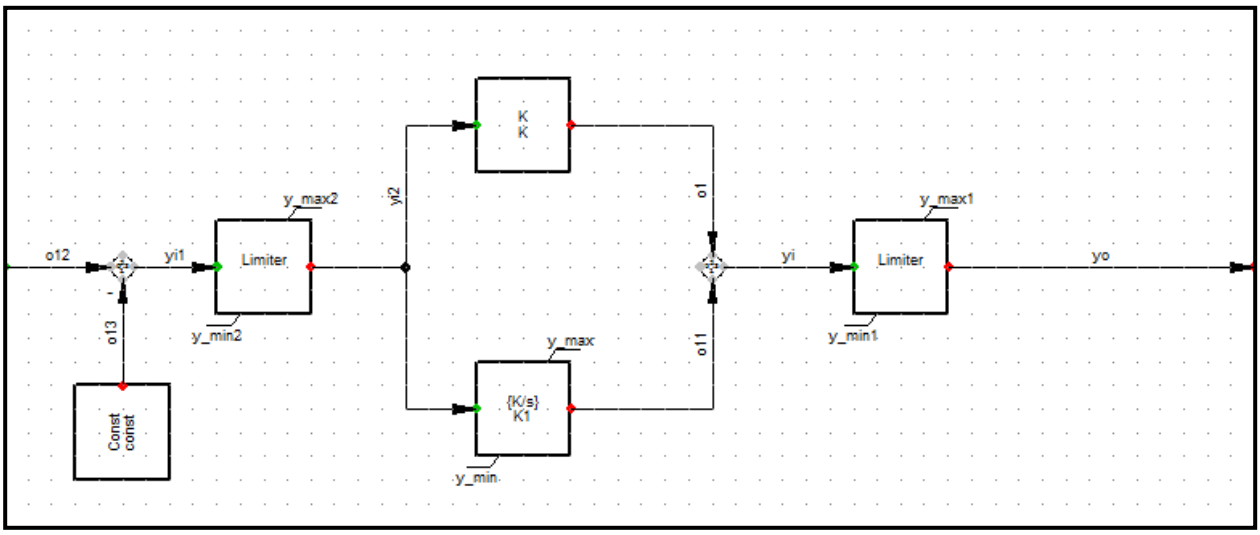

Figure B.5 Gamma controller

Appendix C: Controllers parameters

Table C.1 Rectifier Current Controller

Parameters	Values
Tv	0.1
Kp	6
Ti	1.1
dl	0

min	0.087266 rad (5°)
max	1.57 rad (90°)

Table C.2 Inverter Current Controller

Parameters	Values
Tv	0.1
Kp	6
Ti	1.1
dl	0.1
min	1.91986 rad (110°)
max	2.61666 rad (150°)

Table C.3 Inverter Gamma angle Controller

Parameters	Values
K1	36
K	0.3
const	0.2967 rad (17°)
y_min	1.92 rad (110°)
y_min2	0.2967 rad (17°)
y_min1	1.92 rad (110°)
y_max	2.61 rad (150°)
y_max2	0.52333 rad (30°)
y_max1	2.61 rad (150°)

ANNEXES

Annex A: Surface voltage gradient of selected conductors and Surface voltage gradient for conductor bundles having 2, 3, and 4 subconductors. Following conductors with electrical resistances less than 0.099552 Ω/km are selected for Surface voltage gradient calculations

Conductor code name	№ of cond., n	Bundle Spacing ,S (m)	Conductor Dia. (mm)	Bundle Diam.(m)	Equiv. Bundle Dia.	F	T	Gav (kV/cm)	Gmax (kV/cm)
Eagle	2	0.457	24.22	0.457	0.148785349	2.201289	122.5383	51.36139	54
Peacock	2	0.457	24.19	0.457	0.148693174	2.201289	122.5383	51.42509	54
Squab	2	0.457	24.51	0.457	0.149673445	2.201289	122.5383	50.75369	53
Wood Duck	2	0.457	25.27	0.457	0.151976248	2.201289	122.5383	49.22726	52
Teal	2	0.457	25.24	0.457	0.15188601	2.201289	122.5383	49.28577	52
Kingbird	2	0.457	23.9	0.457	0.147799188	2.201289	122.5383	52.04907	55
Rock	2	0.457	24.84	0.457	0.150677669	2.201289	122.5383	50.07942	53
Grosbeak	2	0.457	25.15	0.457	0.151614973	2.201289	122.5383	49.46214	52
Scoter	2	0.457	25.9	0.457	0.153859026	2.201289	122.5383	48.02984	51
Egret	2	0.457	25.9	0.457	0.153859026	2.201289	122.5383	48.02984	51
Flamingo	2	0.457	25.38	0.457	0.152306664	2.201289	122.5383	49.0139	52
Gannet	2	0.457	25.76	0.457	0.153442628	2.201289	122.5383	48.29087	51
Crow	2	0.457	26.28	0.457	0.154983612	2.201289	122.5383	47.33534	50
Stilt	2	0.457	26.32	0.457	0.155101515	2.201289	122.5383	47.26341	50
Starling	2	0.457	26.68	0.457	0.156158637	2.201289	122.5383	46.62567	49
Redwing	2	0.457	27.43	0.457	0.158338309	2.201289	122.5383	45.35081	48
Tern	2	0.457	27.03	0.457	0.157179579	2.201289	122.5383	46.02193	49
Condor	2	0.457	27.72	0.457	0.159173113	2.201289	122.5383	44.87636	48
Cuckoo	2	0.457	27.72	0.457	0.159173113	2.201289	122.5383	44.87636	48
Drake	2	0.457	28.11	0.457	0.160288927	2.201289	122.5383	44.25375	47
Mallard	2	0.457	28.96	0.457	0.162694315	2.201289	122.5383	42.95486	46
Crane	2	0.457	29.07	0.457	0.163003006	2.201289	122.5383	42.79232	46
Ruddy	2	0.457	28.74	0.457	0.162075168	2.201289	122.5383	43.28368	46
Canary	2	0.457	29.52	0.457	0.164259794	2.201289	122.5383	42.14	45
Rail	2	0.457	29.61	0.457	0.16451	2.201289	122.5383	42.01192	45
Cardinal	2	0.457	30.42	0.457	0.166744955	2.201289	122.5383	40.89326	44
Ortlan	2	0.457	30.81	0.457	0.167810429	2.201289	122.5383	40.37562	43
Curlew	2	0.457	31.68	0.457	0.170163216	2.201289	122.5383	39.26682	42
Bluejay	2	0.457	31.98	0.457	0.170967014	2.201289	122.5383	38.89846	42
Finch	2	0.457	32.85	0.457	0.173276946	2.201289	122.5383	37.86827	41
Grackle	2	0.457	33.97	0.457	0.176206073	2.201289	122.5383	36.61975	39
Pheasant	2	0.457	35.1	0.457	0.179112814	2.201289	122.5383	35.44082	38
Martin	2	0.457	36.17	0.457	0.181822386	2.201289	122.5383	34.39239	37
Plover	2	0.457	37.24	0.457	0.184492168	2.201289	122.5383	33.40421	36
Falcon	2	0.457	39.26	0.457	0.189429776	2.201289	122.5383	31.6855	34
ASTER 228	2	0.457	19.6	0.457	0.133844686	2.6	105.0328	68.96958	72
ASTER 288	2	0.457	22.05	0.457	0.141963728	2.6	105.0328	61.3063	64

ASTER 570	2	0.457	28.42	0.457	0.161170345	2.6	105.0328	47.56523	51

Surface voltage gradient for conductor bundles having 2, 3, and 4 subconductors

Conductor Code name	G_{max} For n = 2	G_{max} For n = 3	G_{max} For n = 4
Eagle	54	36	30
Peacock	54	36	30
Squab	53	36	30
Wood Duck	52	35	29
Teal	52	35	29
Kingbird	55	37	30
Rock	53	35	29
Grosbeak	52	35	29
Scoter	51	34	28
Egret	51	34	28
Flamingo	52	35	29
Gannet	51	34	28
Crow	50	34	28
Stilt	50	34	28
Starling	49	33	27
Redwing	48	32	27
Tern	49	33	27
Condor	48	32	27
Cuckoo	48	32	27
Drake	47	32	26
Mallard	46	31	26
Crane	46	31	25
Ruddy	46	31	26
Canary	45	30	25
Rail	45	30	25
Cardinal	44	30	24
Ortlan	43	29	24
Curlew	42	28	24
Bluejay	42	28	23
Finch	41	28	23
Grackle	39	27	**22**
Pheasant	38	26	**22**
Martin	37	25	**21**
Plover	36	25	**21**
Falcon	34	24	**20**
ASTER 228	72	47	36
ASTER 288	64	42	33
ASTER 570	51	34	26

N.B those conductors whose surface voltage gradient less than **22 KV/cm** are selected for further analysis.

Annex B Thermal power Carrying capacity

Conductor Code name	Diameter (mm)	Ws	q_{c1}	q_r	$R_{dc(@20)}$/ (1000ft)	Rdc (ohm/m)	$R_{dc\ @\ 80}$
Grackle	33.97	18.03807	52.76278684	17.92677	0.0144	4.72464E-05	5.8586E-05
Pheasant	35.1	18.6381	53.65075539	18.5231	0.0135	4.42935E-05	5.4924E-05
Martin	36.17	19.20627	54.47901111	19.08776	0.0127	4.16687E-05	5.1669E-05
Plover	37.24	19.77444	55.29558692	19.65242	0.012	0.000039372	4.8821E-05
Falcon	39.26	20.84706	56.80703788	20.71843	0.0108	3.54348E-05	4.3939E-05

Continued …

d	d/D (inner Dia./Outer Dia.)	m	if mr< 2.8, n	if m> 2.8 < 5.0, n	p	K_1	$R_{ac@\ 80}$	I	power
11.3284	0.333482	1.464581	3.959588066	4.125201452	0.804834339	0.586133	6.12E-05	927.5091	1855.018
11.7094	0.333601	1.512613	3.956555817	4.112423984	0.807399554	0.587846	5.75E-05	964.9912	1929.982
12.065	0.333564	1.559527	3.953365639	4.099987114	0.809916847	0.589773	5.42E-05	1001.505	2003.009
12.4206	0.333528	1.604368	3.950105309	4.088139524	0.812339234	0.59162	5.13E-05	1036.851	2073.702
13.081	0.333189	1.691153	3.9432094	4.065321006	0.817091816	0.595669	4.64E-05	1105.137	2210.273

Annex C: Sag calculation of the selected ACSR conductors, for Span length of 300 m at 32℃

	Diameter D in m	Weight (Kg/m)	Cross. Area, (sq.cm)	Ultimate Tensile Strength (kgf)	Module of Elasticity, N/(sq.mm)	Coefficient of Linear Expansion,1/ ℃	S/AL	Module of Elasticity, kgf/Sq.cm	Nominal Span, m
Grackle	0.03398	2.281	6.799	19006	62700	0.0000193	19/54	639540	300
Pheasant	0.0351	2.435	7.268	19777	62700	0.0000193	19 &54	639540	300
Martin	0.03617	2.587	7.721	21001.33	62700	0.0000193	19 & 54	639540	300
Plover	0.03724	2.743	8.187	22271.39	62700	0.0000193	19 & 54	639540	300
Falcon	0.03926	3.03986	9.7548	25445	62700	0.0000193	19 &54	639540	300

Continued …..

Weight factor	Wind load(P2)	Wind load(P3)	Still wind loading factor, q2	Still wind loading factor, q3	t32	Temprature Factors, t=0 °C	Tempratur e Factors, t=45 °C	Tempratu re Factors, t= 80 °C	Tension factors @ still wind q1=1	Tension Factors @ 2/3 full wind

0.335490513	0.000498373	0.000748	1.00000002	1.000000054	0	-394.9799	160.460586	592.469856	269935167.4	269935180.3
0.33503027	0.0005148	0.000772	1.00000002	1.000000005	0	-394.9799	160.460586	592.469856	269195052.7	269195064.8
0.335060225	0.000530493	0.000796	1.00000002	1.000000047	0	-394.9799	160.460586	592.469856	269243193.3	269243204.7
0.335043361	0.000546187	0.000819	1.00000002	1.000000045	0	-394.9799	160.460586	592.469856	269216091.4	269216102.1
0.311627096	0.000575813	0.000864	1.00000002	1.000000004	0	-394.9799	160.460586	592.469856	232899956.1	232899964.4

Continued …

Tension Factors @ full wind	Sag Factors @ still wind	Sag Factors @ 2/3 full wind	Sag Factors @ full wind	Tension (T1) in kg	f1	Sag (S1) in m	Stress factor, K	Tension per unit area,f2 (kg/sq.cm)	Tension (T2) in kg	Sag (S2) in m
269935196.4	3774.268275	3774.268365	3774.268	4751.5	698.8528	5.400662949	146.1545299	601.049	4086.532	6.279469
269195079.8	3769.090534	3769.090618	3769.091	4944.25	680.2766	5.540526875	98.5805687	614.443	4465.772	6.134158
269243218.8	3769.427535	3769.427615	3769.428	5250.333	680.0068	5.543220358	97.7451023	614.733	4746.353	6.131813
269216115.5	3769.237816	3769.237891	3769.238	5567.848	680.084	5.542312357	98.01301511	614.631	5031.984	6.132521
232899974.9	3505.804835	3505.804897	3505.805	6361.25	652.1149	5.376054235	104.4419987	582.34	5680.61	6.020203

Annex D Cost Estimate of Grid connection of GRHEPP **[1]**

No.	*Description*	*Unit*	*Qty.*	*Unit Cost(USD)*	*Total Cost(USD)*
1	500 kV line bay, double bus	each	4	1,800,000	7,200,000
2	500 kV transformer bay, double bus	"	1	1,700,000	1,700,000
3	500kV 4X135 Mvar line connected shunt reactor	MVA	540	24,000	12,960,000
		Total			21,860,000

No.	*Description*	*Unit*	*Qty.*	*Unit Cost(USD)*	*Total Cost(USD)*
1	500 kV line bay, double bus	each	8	1,800,000	14,400,000
2	500 kV Buscoupler bay	"	1	1,700,000	1,700,000
3	500kV shunt reactor bay	"	1	1,700,000	1,700,000
7	500kV, serious capacitor bay, double bus	"	16	1,800,000	28,800,000
4	500kV 1X45 Mvar line connected reactor	MVA	45	24,000	1,080,000
6	500kV Series Capacitor	"	4000	48,000	192,000,000
5	500kV 8X135 Mvar line connected reactor	"	1080	24,000	25,920,000
8	Substation Basics	lot	1	1,600,000	1,600,000
9	General civil work	lot	1	500,000	500,000
		Total			267,700,000

No.	*Description*	*Unit*	*Qty.*	*Unit Cost(USD)*	*Total Cost(USD)*
1	500 kV incoming line bay, double bus	each	4	1,800,000	7,200,000
2	500 kV transformer bay, double bus	"	7	1,700,000	11,900,000
3	500 kV Bus coupler bay	"	1	1,700,000	1,700,000
4	500/400kV 750 MVA transformer	"	7	15,000,000	105,000,000
5	400 kV transformer bay, double bus	"	7	1,100,000	7,700,000
6	400 kV line bay, double bus	"	4	1,200,000	4,800,000
7	400kV shunt Capacitor bay	"	1	1,100,000	1,100,000
8	400 kV Bus coupler bay	"	1	1,300,000	1,300,000
9	400kV 3x90/1x45 Mvar Shunt Capacitor	MVA	315	22,000	6,930,000
10	Substation Basics	lot	1	4,200,000	4,200,000
11	General civil work	lot	1	1,300,000	1,300,000
		Total			153,130,000

No.	*Description*	*Unit*	*Qty.*	*Unit Cost(USD)*	*Total Cost(USD)*
1	Two Double Ckt,Steel Tower from Mellinnium-5000 to Dedesa	km	344	1,200,000	412,800,000
2	Two Double Ckt,Steel Tower from Dedesa to Menagesha	km	230	1,200,000	276,000,000
	Total Transmission Line Cost				688,800,000
	Total Substation cost				442,690,000

Total Cost				1,131,490,000
Engineering & Administration cost			5.0%	56,574,500
TOTAL PROJECT COST				1,188,064,500
Physical Contingency			5.0%	59,403,225
Price Contingency			10.0%	118,806,450
GRAND TOTAL PROJECT COST				1,366,274,175
Grand Total Project. Cost (Birr) @1USD=17Birr				23,226,660,975